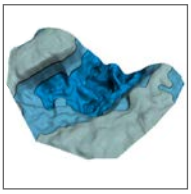

Reconstructing human-landscape interactions through multi-receiver electromagnetic induction survey

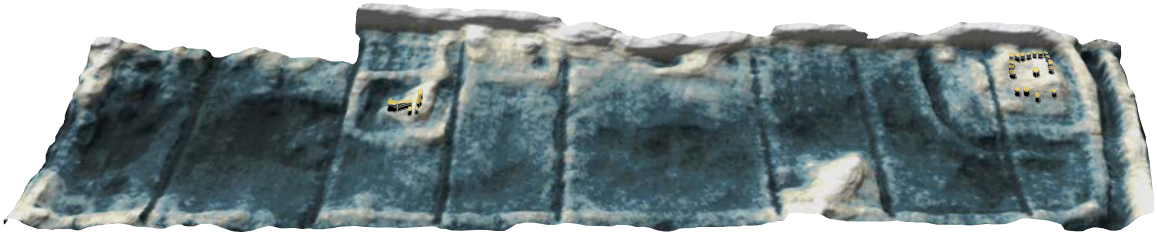

Philippe De Smedt

UNIVERSITEIT GENT

FACULTEIT BIO-INGENIEURSWETENSCHAPPEN

PhD supervisor	**Prof. dr. ir. Marc Van Meirvenne** Department of Soil Management, Faculty of Bioscience Engineering Ghent University
Dean	**Prof. dr. ir. Guido Van Huylenbroeck**
Rector	**Prof. dr. Paul Van Cauwenberge**

Philippe De Smedt

Reconstructing human-landscape interactions through multi-receiver electromagnetic induction survey

Thesis submitted in fulfilment of the requirements
for the degree of Doctor (PhD) in Applied Biological Sciences: Land and Forest Management

Dutch translation of the title:
De reconstructie van interacties tussen mens en landschap door meerspoelige elektromagnetische inductiesurvey.

Illustrations on the cover:
From top to bottom: detail from the profile of the Moervaart Palaeolake sequence (© Machteld Bats, Ghent University), rear view of the mobile multi-receiver survey setup (© Wim De Clercq, Ghent University), depth model based on multi-receiver EMI data of a palaeochannel section at the Daknamse Meersen, 3D reconstruction of a medieval reclaimed wetland at Boudelo, Klein-Sinaai (see Chapter 5).

Citation:
De Smedt, P. 2013. *Reconstructing human-landscape interactions through multi-receiver electromagnetic induction survey*, PhD thesis, Ghent University.

ISBN-number: 978-90-5989-611-6

Dankwoord

In de eerste plaats wil ik mijn promotor, prof. dr. ir. Marc Van Meirvenne, bedanken om me de kans te geven doctoraatsonderzoek uit te voeren aan de Vakgroep Bodembeheer van de Faculteit Bio-Ingenieurswetenschappen, en om voor een wetenschappelijk kader en steun te zorgen om dit tot een succesvol einde te brengen. Ik dank hem in het bijzonder om me aan te leren hoe je op een efficiënte manier aan onderzoek doet; hoe je realistische onderzoeksdoelstelling vooropstelt en vervolmaakt.

Het grootste deel van mijn doctoraatsonderzoek werd verricht in het kader van een interdisciplinair onderzoeksproject geleid door prof. dr. Philippe Crombé. Hem bedank ik eveneens voor de kans om bij te dragen aan dit project, en voor het vertrouwen en de steun die ik van hem, reeds als masterstudent, kreeg. Eveneens bedank ik prof. dr. Jacques Verniers, prof dr. Peter Finke, prof. dr. Jean Bourgeois, prof. dr. Philippe De Maeyer, en prof dr. em. Marc Antrop voor hun hulp en advies bij het werk op en naast het veld, tijdens vergaderingen en bij de gegevensverwerking in het kader van dit project.

Als archeoloog instappen in een onderzoeksgroep aan een Bio-Ingenieursfaculteit is niet altijd een evidentie. Ik dank daarvoor de collega's van de vakgroep Bodembeheer voor hun hulp en geduld, en om me niet telkens te wijzen op de ongetwijfeld bizarre uitdrukkingen op mijn gezicht bij mijn introductie tot bepaalde analyse- en onderzoeksmethodes die me voordien volledig vreemd waren. In het bijzonder bedoel ik hiermee de verschillende – vroegere en huidige – teamleden van ORBit, David Simpson Timothy Saey, Eef Meerschman, Mohammad Monirul Islam, Liesbeth Cockx, Ellen Van De Vijver en Samuël Deleforterie. Hen bedank ik om me in te wijden in de 'geheimen' van het geofysische bodemonderzoek, de wondere wereld van Matlab en geostatistiek. Zonder jullie steun, advies en zin voor discussie had dit doctoraat er nooit geweest. Tenslotte ben ik enorm veel verschuldigd aan Valentijn Van Parys, voor zijn hulp op en naast het veld, en om er steeds, met de nodige zin voor relativering en humor, voor te zorgen dat werkdagen positief startten en ook zo eindigden.

Ook dank ik de collega's van de vakgroep archeologie met wie ik doorheen de voorbije jaren op een bijzondere wijze kon samenwerken. Dit zijn prof. dr. Wim De Clercq, Machteld Bats, Jeroen De Reu en Davy Herremans. Ook de meer geofysische discussies met de Lieven Verdonck en Jeroen Verhegge zullen me steeds bijblijven.

Ook de aardwetenschappers van de Sterre en daarbuiten, niet in het minst Ann Zwertvaegher, Vanessa Gelorini en Ilke Werbrouck als mede-GOA'ers, Koen Verhoeven, Tim Debacker (voor de introductie in het omgevingsmagnetisme en, natuurlijk, de huisvesting).

I would like to thank the fellow geophysicists and archaeologists from the International Society of Archaeological Prospection for all the encouraging discussions, the opportunities and the motivation. I'm thankful to have wound up in such an open scientific community, governed by mutual respect and support.

Verder dank ik alle collega's/onderzoekers die op de een of andere bijgedragen hebben aan dit doctoraat en het onderzoek daarbuiten. Ondanks de druk om tegen een sneltempo A1-artikels te produceren, is het me een genoegen geweest te kunnen werken met mensen waarbij de kwaliteit van het onderzoek en hun deontologie, het aantal te produceren artikels steeds oversteeg. Hopelijk kunnen we dit volhouden...

Bijzonder belangrijk doorheen de voorbije doctoraatsjaren zijn steeds mijn familie en vrienden geweest. De grenzeloze steun en het vertrouwen dat ik van mijn ouders kreeg, is van onschatbare waarde. Ik hoop dat dit doctoraat hetgeen ik de voorbije jaren in binnen- en buitenland allemaal heb uitgespookt, concretiseert. Ik bedank ook mijn meter voor al haar hulp doorheen mijn traject aan de unief, en om er steeds voor me te zijn. Ook bedank ik nonkel Jean, die er met hand en tand voor gezorgd heeft dat dit doctoraat te combineren viel met een verbouwing.

Marjolein, jij hebt me doorheen de doctoraatsjaren het meest intens moeten verdragen. Je hebt gedeeld in mijn enthousiasme, begrip gehad voor alle uit de hand gelopen werkuren, en me gesteund in de minder aangename momenten. Ik bedank je voor alles wat je bent en wat je doet. Ik kijk al uit naar het vervolg…

Contents

List of abbreviations and acronyms

3-D	three-dimensional
B	magnetic induction (magnetic field associated with all currents)
cal BC	calibrated date before Christ
cLHS	conditioned Latin hypercube sampling
DEM	Digital Elevation Model
DOE	depth of exploration
E	electric field
EMI	Electromagnetic Induction
ERT	electrical resistivity tomography
$\mathbf{F}_{electric}$	electric force
$\mathbf{F}_{magnetic}$	magnetic force
GPR	Ground Penetrating Radar
H	magnetic field strength
HCP	horizontal coplanar coil pair geometry
Hp	primary magnetic field (emitted by an EMI sensor)
Hs	secondary magnetic field (induced and received by an EMI sensor)
I	electric current
IP	In-Phase electromagnetic signal response
kHz	kilohertz
LIN	Low Induction Number
LMA	Levenberg-Marquardt algorithm
M	magnetization (magnetic dipole moment per unit volume)
MHz	megahertz
msu	magnetic susceptibility units

NRM	natural remanent magnetization
PRP	perpendicular coil pair geometry
Q	electric charge
QP	Quadrature-Phase electromagnetic signal response
RMSE	Root Mean Squared Error
TRM	thermoremanent magnetization
V	electric potential difference
VCP	vertical coplanar coil pair geometry
β	induction number
δ	skin depth
ε	dielectric permittivity
κ	magnetic susceptibility
κ_a	apparent magnetic susceptibility
μ	magnetic permeability
ρ	electrical resistivity
σ	electrical conductivity
σ_a	apparent electrical conductivity
ω	angular wave frequency

Summary

To study the interaction between humans and their environment, researchers rely on geoarchaeological, palaeoenvironmental and – for historic periods – documentary information. Hence, detecting the ephemeral traces of human occupation at a landscape scale along with information about past landforms, is an invaluable asset in understanding past human-landscape interactions. Geophysical methods have been used since the beginning of the 20th century to aid archaeological research, but their use has been primarily aimed at uncovering archaeological features. Detailed mapping of buried landforms and soil variation, however, remains rare in archaeogeophysics. Throughout this thesis, the author explores how simultaneous mapping of multiple physical soil properties enables reconstructing past human environments with non-invasive geophysical surveying. The primary method of investigation is multi-receiver electromagnetic induction (EMI) survey, used in a mobile configuration. EMI sensors allow simultaneously mapping the apparent electrical conductivity (σ_a) and magnetic susceptibility (κ_a) of the soil. When a multi-receiver instrument is used, these electrical and magnetic properties can be mapped for different soil volumes simultaneously. While the electrical conductivity offers straightforward information on soil textural variations and changes in organic matter content, changes in magnetic susceptibility can often be related to anthropogenic soil disturbances.

The first chapter of this thesis focusses on the use of multi-receiver EMI instruments for reconstructing past landforms. The research reported in this section is an integral part of an interdisciplinary research project entitled "*Prehistoric settlement and land-use systems in Sandy Flanders (NW Belgium): a diachronic and geoarchaeological approach*", which was funded by the Special Research Fund (BOF) of Ghent University (BOF08/GOA/009). The focal point of this project was the prehistoric occupation in and around a Late Glacial palaeolake (Moervaart palaeolake) in the north of Belgium. To grasp the relationship between these occupation phases and their Late Glacial to Early Holocene environment, detailed information about the palaeotopography of the area needed to be obtained.

For understanding the land-use of past societies, alluvial and lacustrine environments are of particular importance as these are often key areas with both a high archaeological and palaeoecological potential. However, the often deep stratification of these sites, the

high water table and the complex sedimentological variations can hamper a detailed reconstruction of the spatial relationship between prehistoric settlement and their environment. Therefore, in the first chapter, specific focus lies on the 3-D modelling of predefined soil layers in such complex pedological environments at a landscape scale. Conventional field methods to map and reconstruct the morphology of past landforms are highly dependent on spatial interpolation. Standard survey techniques such as borehole survey, allow a detailed vertical reconstruction of the shallow subsurface, but leave lateral connections between sample locations open to interpretation.

An integrated approach is presented for reconstructing the morphology of a known palaeochannel segment by modelling the depth to the sandy substrate. In addition, a calibration method based on a limited number of auger data is proposed. The modelling procedure was evaluated along two transects on a 0.45 ha test site, showing palaeochannel depths ranging from 1 to > 4 m beneath the surface. Afterwards, the morphology of the entire test site was reconstructed. These three resulting depth models were then compared with auger observations and electrical resistivity tomography data. The high correlation coefficients between observed and modelled depths showed that even in complex pedological environments, palaeochannel morphology could be predicted accurately using multi-receiver EMI data.

Next, the EMI depth modelling procedure was combined into an integrated approach for mapping and modelling prehistoric landscapes and river systems in and around the Moervaart palaeolake. Based on filtered and unfiltered digital elevation models, a survey area of 60 ha was selected, in which detailed mobile multi-receiver electromagnetic induction survey was conducted. The results allowed for the delineation of palaeochannels in the area and enabled modelling the depth of these features in the survey area, providing insight into their flow characteristics. ^{14}C sampling enabled the dating of the evolving river system to the transition between the Late Glacial and the Early Holocene. Through additional coring, this river system could be traced further through the palaeolake area. Based on these results, a detailed reconstruction was made of the palaeotopography that harboured the Final Palaeolithic and Early Mesolithic occupation of the survey area.

In the second chapter, focus lies on mapping anthropological soil variation. While most archaeogeophysical surveys employ magnetometer instruments, electrical resistance survey or ground penetrating radar, the use of EMI sensors remains limited. The studies presented in this chapter were conducted in the framework of a research project aimed at developing a non-invasive survey methodology for detecting the ephemeral archaeological traces of rural occupation in Flanders. Therefore, the use of different non-invasive survey

methods was evaluated on a test site. Through comparison with magnetometry data, it was shown that multi-receiver EMI allowed for a clearer reconstruction of the layout of the site, and allowed a more straightforward delineation of the subtle archaeological features. Subsequently, the potential of a multi-receiver EMI survey to detect weak magnetic anomalies was evaluated. Most surveys in archaeogeophysical prospection use magnetic properties to detect archaeological features. Such magnetic surveys are usually conducted with magnetometers and, to lesser extent, with magnetic susceptibility meters and EMI sensors. Although the latter are the only instruments that allow mapping multiple physical soil properties simultaneously, EMI remains the odd-one-out in archaeogeophysical prospection. Nevertheless, by simultaneously recording the electric and magnetic soil variability, EMI survey can be beneficial in early archaeological evaluation stages as detailed pedological and archaeological information is gathered at the same time. Furthermore, by using multi-receiver EMI instruments vertical soil variation can also be integrated into the survey. However, while the potential of EMI for mapping electric soil variations is well known from advances in soil science, magnetic susceptibility measurements have been less investigated. Here, apparent magnetic susceptibility data of a multi-receiver EMI instrument is investigated. The shallow κ_a-data were compared to topsoil susceptibility measurements with a magnetic susceptibility loop sensor survey, and to magnetic profiling for evaluating the deeper κ_a data. Through this comparison it was found that the multiple magnetic susceptibility-measurements allowed for a straightforward discrimination of the natural and anthropogenic magnetic variations of shallow and deeper soil volumes, and allowed visualising weak magnetic anomalies.

In the final chapter of the thesis the understanding of the relationship between past anthropological and natural soil variations, acquired through the previous chapters, is integrated to create a full 3-D reconstruction of a buried archaeological environment. The underlying hypothesis of this approach is that studies of past human-landscape interactions rely upon the integration of archaeological, biological and geological information within their geographical context. Geophysical methods can help bridging the gap between point finds and the surrounding landscape in such studies, but these surveys often solely target archaeological features. Here it is shown how simultaneous mapping of multiple physical soil properties with a multi-receiver EMI survey permits a reconstruction of the 3-D layout and pedological setting of a medieval reclaimed landscape. Combined with limited and directed excavations, the results offer a unique insight into the way such marginal landscapes were reclaimed and occupied during the Middle Ages. This integrated approach

provides a robust foundation for unravelling complex historical landscapes and will enhance our understanding of past human-landscape interactions.

As a conclusion, the presented research has proven the potential of multi-receiver EMI instruments to reconstruct different aspects of past human environments. Such instruments facilitate the composition of these human landscape reconstructions and allow gathering information in 3-D and over wide areas in an efficient manner.

Samenvatting

Om de interactie tussen vroegere beschavingen en hun omgeving te bestuderen, zijn onderzoekers afhankelijk van geoarchaeologische en paleoecologische gegevens, en – voor historische periodes – van, schaarse en soms onvolledige, geschreven bronnen. Hierdoor is de detectie van de vaak subtiele menselijke bewoningssporen op een landschapsschaal van onschatbare waarde. Sinds het begin van de 20e eeuw worden geofysische technieken toegepast binnen archeologisch onderzoek, het gebruik ervan is echter vooral gericht op het blootleggen van archeologische kenmerken. Het gedetailleerd in kaart brengen van begraven landschappen en bodemvariatie, daarentegen, gebeurt slechts zelden bij archeogeofysisch onderzoek. In dit proefschrift onderzoekt de auteur hoe het gelijktijdig in kaart brengen van meerdere fysische bodemkenmerken met niet-invasieve methodes, kan gebruikt worden om vroegere interacties tussen mens en landschap op een holistische manier te reconstrueren.

De toegepaste methode vertrekt van het gebruik van meerspoelige elektromagnetische inductie (EMI) sensoren in een mobiele configuratie. Zulke sensoren kunnen gelijktijdig de schijnbare elektrische geleidbaarheid (σ_a) en schijnbare magnetische susceptibiliteit (κ_a) van de bodem in kaart brengen. Door een meerspoelig instrument te gebruiken, kunnen deze fysische bodemeigenschappen van verschillende bodemvolumes gelijktijdig worden gekarteerd. Terwijl de elektrische geleidbaarheid rechtstreekse informatie biedt over textuurvariaties en veranderingen in het organische stofgehalte van de bodem, kunnen veranderingen in magnetische susceptibiliteit vaak gerelateerd worden aan menselijke bodemingrepen.

Het eerste hoofdstuk van dit proefschrift richt zich op het gebruik van meerspoelige EMI instrumenten voor de reconstructie van begraven landschappen. Het onderzoek dat in dit hoofdstuk wordt voorgesteld, is een integraal onderdeel van een interdisciplinair onderzoeksproject, getiteld "*Prehistoric settlement and land-use systems in Sandy Flanders (NW Belgium): a diachronic and geoarchaeological approach*", dat werd gefinancierd door het Bijzonder Onderzoeksfonds (BOF) van de Universiteit Gent (BOF08/GOA/009). Het zwaartepunt van dit project was de prehistorische bewoning in en rond het Laat-Glaciale Moervaart paleomeer (de huidige Moervaartdepressie) in het noorden van België. Om de relatie tussen de gekende prehistorische occupatie van het

gebied en de Laat Glaciale en Vroeg Holocene omgeving te begrijpen, diende gedetailleerde informatie over de paleolandschap van dit gebied te worden verzameld.

Bij het bestuderen van het landgebruik van vroegere beschavingen, zijn alluviale en lacustrine omgevingen van bijzonder belang. Zulke landschappen zijn vaak sleutelgebieden met een enorm potentieel aan archeologische informatie en informatie over vroegere vegetatie en klimaatsvariaties. De dynamische sedimentatiegeschiedenis, alsook de vaak hoge watertafel en dikke afdekkingspakketen van deze gebieden, bemoeilijken echter gedetailleerde ruimtelijke analyses van de relatie tussen (pre-)historische bewoning en zijn omgeving. In dit hoofdstuk ligt de focus daarom op het modelleren van specifieke bodemlagen in drie dimensies (3-D), en op een landschapsschaal. Traditionele methodes om de morfologie van begraven landschappen te karteren vertrekken voornamelijk van puntdata, en hoewel deze een hoge verticale resolutie bieden, zijn deze daardoor sterk afhankelijk van ruimtelijke interpolatietechieken.

Hier wordt een aanpak voorgesteld om de morfologie van een deel van een paleorivier te reconstrueren door de diepte tot de onderliggende zandlaag te modelleren. Daarbij wordt een kalibratiemethode, waarbij een beperkt aantal boringen in het model worden geïntegreerd, toegepast. De modelleertechniek werd langsheen twee transecten geëvalueerd op een testsite van 0.45 ha. Nadien werd de paleotopografie van de volledige testsite gemodelleerd. De drie resulterende dieptemodellen werden vervolgens vergeleken met validatieboringen en elektrische resistiviteitstomografie. De sterke correlatie tussen de geobserveerde en gemodelleerde dieptes, toonde aan dat zelfs in omgevingen met een complexe lithologie de morfologie van het paleolandschape nauwkeurig kon worden voorspeld op basis van meerspoelige EMI sensordata.

Vervolgens werd deze EMI modelleerprocedure gecombineerd in een integrale aanpak om het prehistorische landschap in en rond de Moervaartdepressie te reconstrueren. Met behulp van digitale hoogtedata werd een gebied van 60 ha geselecteerd waar EMI survey werd uitgevoerd. Hierbij werden verschillende paleokanalen gedetecteerd waarvan de diepte kon worden gemodelleerd. Op deze manier werd inzicht verkregen in de stroomkenmerken van het riviersysteem. Radiokoolstof datering van de geulsedimenten plaatste het dynamische riviersysteem binnen het Laat-Glaciaal en het Vroeg Holoceen. Met behulp van bijkomende boringen, kon dit riviersysteem getraceerd worden doorheen het paleomeer. Op basis van deze resultaten, werd een gedetailleerde reconstructie opgemaakt van het paleolandschap waarin de Finaal Paleolithische en Vroeg Mesolithische bewoning plaatsvond.

In het tweede hoofdstuk ligt het accent voornamelijk op het karteren van antropogene ingrepen in de bodem. Daar waar archeogeofysische surveys hiervoor hoofdzakelijk gebruik maken van magnetometer toestellen, elektrische resistiviteitsmetingen en grondradar, blijft de toepassing van EMI sensoren hiervoor eerder beperkt. De studies die hier worden gepresenteerd kaderen in een onderzoeksproject gericht op de ontwikkeling van een efficiënte methode om de subtiele sporen van rurale bewoning in Vlaanderen op niet-invasieve wijze te detecteren. Hiervoor werden verschillende prospectietechnieken vergeleken op een testsite. Vergelijking met magnetometriedata toonde in een vroege onderzoeksfase aan dat meerspoelige EMI survey een duidelijke en meer rechtlijnige reconstructie van de layout van de site toeliet. Vervolgens werd het potentieel van EMI onderzocht om subtiele magnetische bodemvariaties op te sporen. In archeogeofysisch onderzoek is het karteren van magnetische bodemeigenschappen immers de meest toegepaste surveytechniek. Dit gebeurt in hoofdzaak met magnetometer sensoren, en in mindere mate met magnetische susceptibiliteitsmeters. EMI toestellen blijven echter een buitenbeentje bij dit type prospecties. Het potentieel om met EMI gelijktijdig magnetische en elektrische bodemkenmerken te karteren kan echter een grote meerwaarde betekenen bij archeologische evaluaties, doordat samen met magnetische info, gegevens worden verzameld over de natuurlijke bodemkundige variaties. Wanneer een meerspoelig EMI toestel wordt gebruikt, wordt dit potentieel aangevuld met het vermogen om verticale bodemvariaties te registreren. Echter, daar waar het gebruik van EMI om elektrische bodemkenmerken te karteren door toepassingen in de bodemkunde reeds wijd verspreid is, blijft het karteren van magnetische variaties met EMI een weinig onderzocht onderzoekstopic. In deze studie wordt daarom ingegaan op de magnetische susceptibiliteitsdata van een meerspoelige EMI sensor. De meest ondiepe κ_a-data werden vergeleken met magnetische susceptibiliteitsmetingen van de ploeglaag met een hoge resolutie magnetische susceptibiliteitssensor. De diepere κ_a metingen werden vergeleken met magnetische sonderingen. Hieruit kon worden afgeleid dat de meerdere κ_a-metingen van de EMI sensor een eenduidige detectie toelieten van de natuurlijke en antropogene magnetische bodemvariaties in diepe en ondiepe bodemvolumes. Tevens konden zelfs zeer zwakke magnetische variaties in kaart worden gebracht.

In het laatste hoofdstuk van deze thesis worden de inzichten in het karteren van natuurlijke en antropogene bodemvariaties, verworven in de voorgaande secties, gecombineerd om een integrale 3-D reconstructie van een archeologisch landschap op te stellen. De onderliggende hypothese van deze aanpak is dat studies van landgebruik in het verleden vertrouwen op de integratie van archeologische, biologische en geologische

informatie binnen hun geografische context. Naast geografische analyses, kunnen geofysische methoden hierbij helpen om individuele sites in een meer landschappelijke context te plaatsen. Zulke technieken richten zich vaak echter enkel op archeologische landschapsvariaties. De voorgestelde aanpak toont hoe het gelijktijdig in kaart brengen van meerdere fysische bodemeigenschappen met een meerspoelige EMI-sensor, de 3-D reconstructie van de lay-out en bodemkundige context van een middeleeuwse wetlandsite mogelijk maakt. In combinatie met beperkte en gerichte opgravingen, geven de resultaten een unieke en wetenschappelijke kijk op de manier waarop dergelijke marginale landschappen werden ontgonnen en geëxploiteerd tijdens de Middeleeuwen. Deze methode biedt een solide basis voor het ontrafelen van complexe historische landschappen en kan sterk bijdragen tot nieuwe inzichten in de interactie tussen mens en landschap in het verleden.

Als besluit kan gesteld worden dat dit onderzoek het potentieel van meerspoelige EMI sensoren om verschillende aspecten van vroegere leefomgevingen in 3-D te reconstrueren, aantoont. Samen met de toegepaste verwerkingsprocedures, vereenvoudigen zulke instrumenten de integrale reconstructie van archeologische landschappen, en laten ze toe om op een efficiënte manier, op grote schaal, archeologische en landschappelijke informatie te verzamelen.

Chapter 1

Introduction

1.1 Environmental archaeology and the reconstruction of past landscapes

Over the past decades, the historical perception of archaeology as the study of material remains of past humans and societies (Bockheim et al., 2005), has shifted to a more holistic view whereby humans are an integral part of their environment. This changing perception has led to a set of subdisciplines of archaeology that are combined in geoarchaeology. Hereby, the focus lies on the environmental rather than the cultural aspects of past societies. Following the now widespread apprehension over the impact of human activities on the biosphere and atmosphere, environmental scientists have in their turn started using archaeology as a source of information on the human-environment interactions that have shaped Quaternary and Holocene landscapes (Goldberg and Macphail, 2006; Williams et al., 1993).

Whereas geoarchaeology was initially aimed at understanding the context of archaeological remains, i.e. their pedological matrix and the taphonomical processes related to the location, formation and preservation of an archaeological site (Renfew and Bahn, 2004), it now entails all issues on the cross-section between environmental sciences and archaeology (Goldberg and Macphail, 2006). The study of soils, however, takes up a particular place in geoarchaeology. Societies live on soils and rely on them for subsistence, and, evidently, most archaeology is buried in them.

Along with the emphasis on environmental factors, researches have increasingly started approaching archaeology on a landscape level. From insights into hunter-gather mobility, derived from ethnographic studies (Binford, 1983), to advanced spatial analyses,

archaeologists and environmental scientists aim to understand the complex relationship between past societies and their environment by looking at regional variations (French, 2010).

By using an array of prospection methods, researchers try to reconstruct the archaeology of entire landscapes. Traditional archaeological approaches have now been complemented by geoarchaeological methods that take into account the physical variations of landscapes to identify areas with increased archaeological potential (i.e. areas that are assumed to be of particular interest to past societies) and to evaluate interconnectivity between known sites (e.g. De Reu et al., 2010). A large part of this methodology is derived from geographical landscape analysis whereby digital elevation data is used as a guiding variable. At this level, standard soil survey methods have also been integrated into geoarchaeological prospection methods. Through lithological coring, stratigraphic information is gathered, which allows reconstructing past landforms and detecting archaeology in sedimentation areas. However, when looking at a landscape scale, the problem of resolution arises. While at a site level, the resolution of environmental records is often very high (e.g. (sub-)centimetre thick occupation deposits), the resolution diminishes severely when these 'point finds' are put into a wider spatial context. While remote sensing data often renders grid data at rather high resolutions (e.g. elevation data with a 2 m by 2 m grid cell size), these are mainly informative on current landscape variations. On the other hand, coring information offers a high vertical resolution but the spatial resolution of these surveys is rarely finer than a 50 m by 50 m sampling grid.

During the past decades, standard landscape survey methods are being complemented by geophysical techniques. Such methods use the physical characteristics of the subsurface to detect soil discontinuities and anthropogenic disturbances, and to map variations in soil composition. These techniques were initially developed for geological mapping and mineral exploration, but have been gradually been adapted for investigating the shallow subsurface. Termed 'near surface geophysics', the geophysical exploration of the shallow layers of the lithosphere mainly focusses on the top 10 m below the soil surface (Butler, 2005; Reynolds, 1997). When zooming in on the first three metres, the term 'soil sensing' is sometimes used to underline the focus of these surveys on the biologically active part of the lithosphere. Since all of these methods are non-destructive and in some cases do not even require contact with the soil, these enable fast mapping of soil variations at high resolutions (up to 0.08 m by 0.08 m measurement grids (e.g. Trinks et al., 2010)). But, even though the application of these techniques in archaeology has rapidly grown over the

past 60 years, the focus has been mainly on detecting and describing archaeological features.

As with traditional archaeological research before the introduction of geoarchaeological methods, there now seems to be a discrepancy in how geophysical methods are applied in archaeology. Although the array of geophysical methods used for archaeological research is often categorized within the geoarchaeological toolbox, the incorporation of environmental variations into such surveys remains rare.

Geophysical methods are becoming an indispensable part of large scale landscape studies. However, to fully understand past interactions between humans and their environment it is pivotal to integrate more than just the anthropogenic landscape variation. To grasp the complex interaction between humans and their environment we need to go beyond the archaeology and reconstruct multiple aspects of past landscapes. Bridging this gap will again require input from other disciplines.

More or less at the same time as the onset of the use of near surface geophysical methods in archaeology, came the application of these techniques in soil science. In the search for high resolution information on soil variability, the use of ‘proximal soil sensors’ has been welcomed into soil science and is now frequently applied in agricultural studies. However, while in archaeogeophysical survey emphasis lies mainly on anthropogenic features, soil scientists target natural variations. Hereby, one of the primary physical soil properties that is used to map and characterize soil variability is electrical conductivity. While there are different methods that allow gathering this information, electromagnetic induction (EMI) is the most frequently used technique. On the other hand, in archaeology surveyors mainly use magnetic properties of the subsoil to detect anthropogenic disturbances. In most cases, such prospections are conducted with magnetometers. Primarily instigated by pedological research, considerable effort has been invested into correlating electrical variations to specific soil properties such as soil texture or moisture content. Mapping magnetic variability, on the contrary, has been less applied in soil studies.

As specific types of electromagnetic induction sensors allow for mapping electric and magnetic soil variations simultaneously, these instruments offer the potential to target different types of natural and anthropogenic features at the same time. In this thesis, the application of EMI instruments for integrated reconstructions of past landscapes will be investigated.

1.2 Research hypothesis and objectives

1.2.1 General research hypothesis

The main research hypothesis of this thesis is that through mapping electrical and magnetic soil variations simultaneously, detailed and continuous information can be gathered about the natural and anthropogenic variations of the subsurface. In a mobile configuration, measurements can be obtained efficiently at fine resolutions, and over large areas. Furthermore, by using a multi-receiver EMI instrument this information can be gathered in three dimensions. Collecting such information at very fine resolutions should allow reconstructing several environmental aspects of past human landscapes. The research conducted in this thesis builds on the foundations for high-resolution, mobile and multi-receiver EMI survey laid out in the PhD theses of David Simpson (2009) and Timothy Saey (2011).

As all the work presented in this thesis deals with mapping soil variations and detecting objects within the soil matrix, it is important that the reader is informed of the definition of soil upheld throughout the thesis. For this, the definition of soil as formulated by Jacob S. Joffe in 'Pedology' (1936, p. 37) is taken:

> *"Soil is a natural body, differentiated into horizons, of mineral and organic constituents, usually unconsolidated, of variable depth, which differs from the parent material below in morphology, physical properties and constitution, chemical properties and composition, and biological characteristics."*

The author is aware that differences persist when it comes to defining 'soil', especially at the cross-section of multiple disciplines such as archaeology, geoarchaeology, geophysics and soil science. However, as stated by Jenny in his 'Factors of Soil Formation' (1994, p. 4):

> *"It is problematic whether any definition of soil could be formulated to which everyone would agree. Fortunately there is no urgent need for universal agreement."*

Following Jenny's rationale, a discussion of the different definitions of soil across disciplines has not been included in this work. Throughout the following chapters, the applied terminology, used, for example, for defining soil model variables in chapters 3 and 4, will be clarified.

The research questions that will be taken on in this thesis to test the main research hypothesis can be divided into the following topics:

1. reconstructing past landscapes in 3-D;
2. mapping detailed magnetic variations with multi-receiver EMI;
3. composing an integrated reconstruction of a past human environment.

1.2.2 Reconstructing buried landscapes in 3-D

Before targeting archaeological features, the first research objective is to reconstruct buried landforms in three dimensions (3-D), over a large area. At present, standard ways to compose large scale palaeotopographical reconstructions include methods such as auger survey. However, the low sampling density of these methods leaves interpreting the lateral expression of the targeted subsurface deposits to depend on interpolation. Therefore, multi-receiver EMI survey, whereby electrical conductivity measurements are taken at very small sampling intervals, and of different soil volumes, is proposed as a primary survey tool for mapping past landscape variations.

Areas of particular interest for the study of past human-landscape interactions are alluvial and lacustrine environments. However, the often complex genesis and sedimentological evolution of these environments poses specific challenges to geophysical surveys. As different soil properties and constituents influence EMI measurements, it can be difficult to compose a straightforward relationship between the measured electrical conductivity and specific soil components or soil layers needed to compose 3-D reconstructions of these past landscapes.

In a first stage, the potential of multi-receiver EMI for discriminating vertical soil variations in areas with a complex lithology will be investigated. The composition of a straightforward relationship between gathered electrical conductivity data and the depth of a predefined soil layer will be taken on. The inversion of multi-receiver EMI data will then be evaluated and compared to other geophysical survey methods. Subsequently, it will be tested whether it is possible to construct past landscapes in 3-D over a wider area with a complex lithology.

1.2.3 Mapping subtle anthropogenic soil variations

A second objective is to evaluate the use of multi-receiver EMI instruments for detecting weak anthropogenic soil variations. Here, specific focus was on mapping subtle magnetic variations of the subsurface. While, particularly in soil science, the use of EMI sensors for mapping soil electrical conductivity has been studied intensively, mapping magnetic soil variations with EMI sensors remains largely unexplored. In this part of the thesis, the aim is to explore the potential of multi-receiver EMI sensors for detecting different types of magnetic anomalies. Whereas the magnetic component of the EMI instrument output signal is considered to be representative for the soil magnetic susceptibility, there can sometimes be interference between the electrical and magnetic signal components. Therefore, it will be investigated if, within boundary conditions, the magnetic variations detected with an EMI sensor can in fact be considered independent from the electrical soil variations. Furthermore, the vertical discrimination potential, added by mapping different soil volumes at the same time, is discussed. Throughout this section, multi-receiver EMI data will be compared to magnetometry measurements, lithological information, and detailed analyses of vertical and lateral magnetic variations at test sites.

1.2.4 Reconstructing human environments in 3-D

The final research objective is to reconstruct the anthropogenic and natural soil variations simultaneously, and in 3-D, through multi-receiver EMI survey to compose a high-resolution reconstruction of past human-landscape interaction. By combining the results and insights gained from solving the previous research topics, it should be possible to simultaneously reconstruct the natural and archaeological variations of a study area. Here, a major challenge is to differentiate between which variations, detected through EMI survey, are related to man-made structures and which are natural variations. When this relationship can be established, and the available inversion procedures can be applied, an integrated 3-D reconstruction can be composed of a past human environment based primarily on multi-receiver EMI data.

1.3 Structure of the thesis

This thesis consists of six chapters (Fig. 1). The second chapter explains the governing principles of EMI survey and the characteristics of electric, magnetic and electromagnetic fields. Furthermore, the spatial sensitivity of EMI sensors is discussed along with some practical considerations of EMI fieldwork. Chapter 3 deals with the application of multi-

receiver EMI sensors for reconstructing past landscapes in 3-D. This chapter is divided into two segments. Firstly, the methodology for reconstructing the depth to predefined soil layers with multi-receiver EMI data is evaluated in a sedimentation area with a complex stratigraphy. Therefore, a number of field experiments were conducted and comparative surveying was conducted using electrical resistivity tomography. In the second part, this methodology is applied to reconstruct the palaeotopography of a 60 ha area, which was occupied during the late Glacial and the early Holocene. This part further describes how through integrating additional soil sampling, digital elevation data and radiocarbon dating, a detailed reconstruction is made of a prehistoric environment. The fourth chapter describes how multi-receiver EMI can serve as a tool for detecting anthropogenic soil disturbances. In this chapter, specific focus lies on mapping magnetic soil variations. While in a first segment multi-receiver EMI is compared to magnetometry and aerial photography, the second part focusses specifically on variations in soil magnetic susceptibility. The potential for detecting weak magnetic anomalies is discussed, along with the influence of natural soil variations. In the fifth chapter, the integrated reconstruction of human environments is examined. By combining the landscape reconstruction methodology discussed in Chapter 2, with multi-layered magnetic susceptibility data, a detailed 3-D reconstruction is composed of a medieval reclaimed wetland. Finally, a general discussion and conclusions of the thesis are given in Chapter 6, along with future research perspectives.

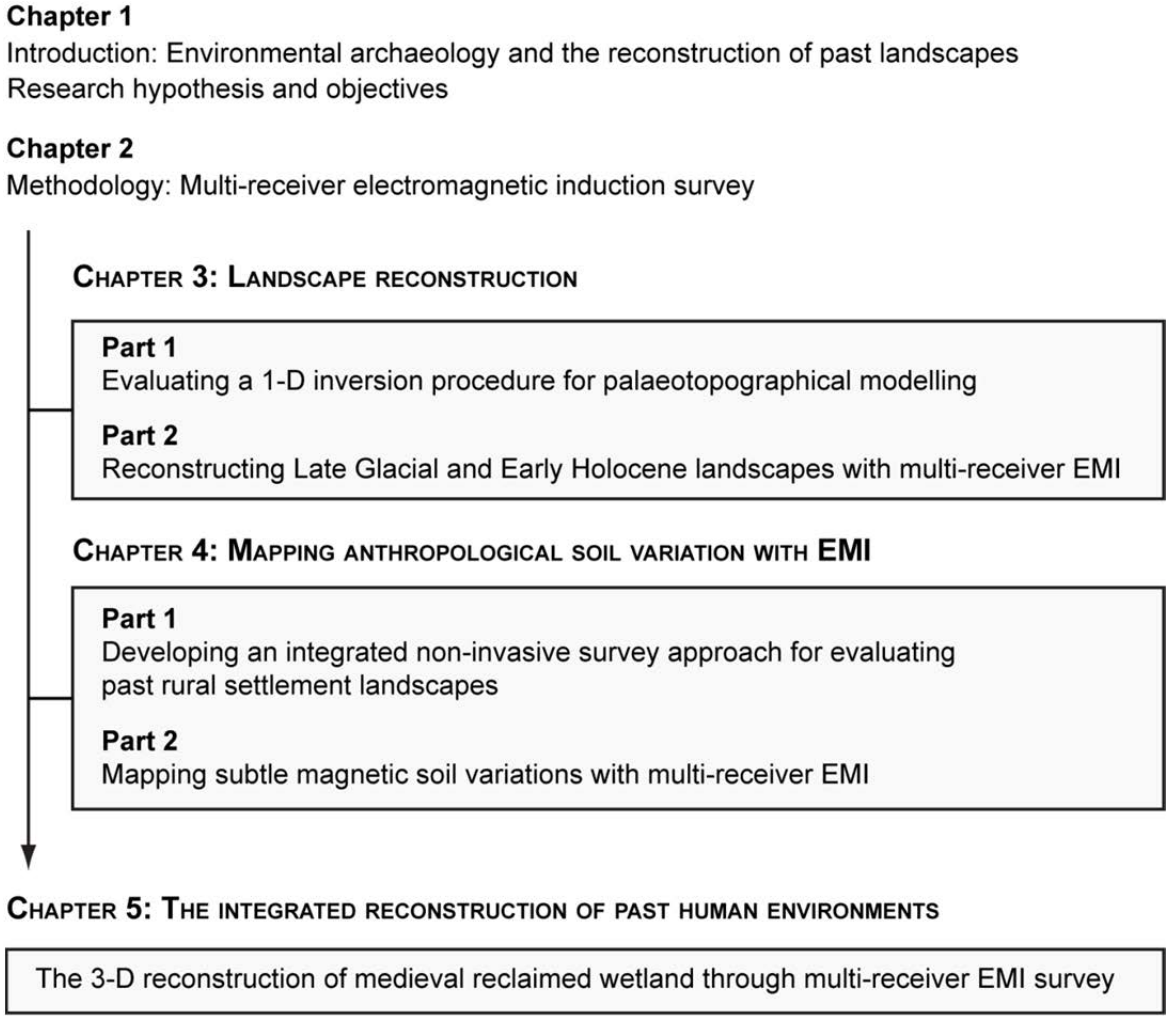

Fig. 1 Structure of the thesis

Chapter 2

Multi-receiver electromagnetic induction survey

2.1 Principles of frequency domain EMI survey

EMI instruments can operate either in the frequency or the time domain. Time domain systems emit electromagnetic pulses with a specific intensity and at given time intervals, while frequency domain systems make use of continuous waves in one or more frequencies (Fig. 2).

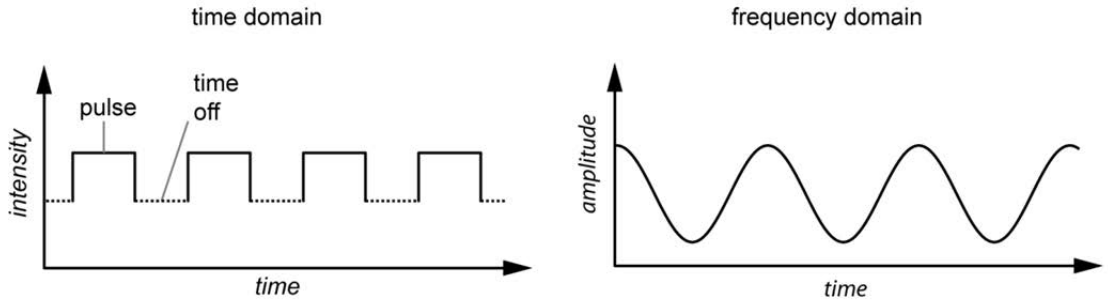

Fig. 2 Transmitted electromagnetic signal in the time-domain with alternations between an emitted pulse with a given intensity and zero-emission moments (time off) (left), and a transmitted electromagnetic signal in the frequency domain with a given frequency and amplitude (right).

Time domain systems are often used for metal detection. However, in archaeology, mainly frequency domain EMI sensors are used that operate at frequencies in the kHz range (generally around 10 kHz), whereas electromagnetic waves applied in ground penetrating radar (GPR) survey are in the MHz range, causing the GPR signal to refract and reflect on

soil discontinuities. The lower frequency range of EMI sensors induces a field of influence around the sensor that allows evaluating the soil composition within this field. To grasp the principles of EMI sensors it is important to understand some fundamental concepts and properties of electric and magnetic fields.

2.1.1 Electric and magnetic fields and properties

Electric and magnetic fields result from movements of electrically charged objects. The most direct expression of the distribution of electric charge (**Q**), expressed in Coulomb, is the Coulomb law that, in differential form, is:

$$\nabla \times \varepsilon_0 \mathbf{E} = \mathbf{Q} \tag{2.1}$$

with $\nabla\times$ the curl operator and ε_0 the dielectric permittivity of free space (West and Macnae, 1991). The dielectric permittivity ε of a material, expressed in Farads per meter (F/m), is the potential of that substance to diminish an electric field **E**, and in free space ε = 8.85.. × 10^{-12} F/m or ε_0 (also known as the dielectric constant).

E, expressed in Volts per meter (V/m), diverges from any distribution of **Q** in free space and can be defined as a vector field surrounding the electrically charged particles. Within this field, other electrically charged particles would be subject to an electrical force $\mathbf{F}_{electric}$, expressed in Newtons (N), defined by Coulomb's law as:

$$\mathbf{F}_{electric} = k\frac{\mathbf{Q_1}\mathbf{Q_2}}{r^2}, \tag{2.2}$$

with $\mathbf{Q}_1$ and $\mathbf{Q}_2$ the magnitude of two electrically charged particles, *r* the distance between them and *k* is Coulomb's constant (defined as $1/4\pi\varepsilon_0$ and equal to 8.988×10^9 F/m). In a conductive medium, e.g. a metal wire, the electric charges can flow from one place to another when there is an electrical potential difference *V*, expressed in Volts(V). This flow of charge constitutes an electric current *I*, expressed in Ampère (A). The relationship between the potential difference between two points and *I* is described in Ohm's law:

$$R = \frac{V}{I}. \tag{2.3}$$

The electrical resistivity ρ quantifies how strongly the conductor opposes the electrical current and is expressed in Ohms meter (Ωm):

$$\rho = R\frac{a}{l}, \tag{2.4}$$

with *l* the length of the conductor in metres and *a* the cross-sectional area in units of metres squared. Electrical conductivity (σ), which is mainly used when working with EMI sensors, is the reciprocal of ρ (i.e. 1/ρ) and expresses how easily current can pass through a material. Its unit is Siemens per meter (S/m).

When in motion, charges generate another type of field in an electrical conductive medium. This is the induced magnetic field **B**, expressed in Tesla, and can again be defined as a vector field surrounding the electrically charged particles. **B** results from the moving electrical charges and the magnetic moment and 'spin' of elementary particles (i.e. particles without any substructure), and is commonly referred to as the *magnetic induction* or the *magnetic flux density*. Within this magnetic field **B**, electrically charged particles are subject to a magnetic force $\mathbf{F}_{magnetic}$ (expressed in N):

$$\mathbf{F}_{magnetic} = \mathbf{Q}v \times \mathbf{B}\,. \tag{2.5}$$

Whereas an electric force depends only on the value of the total charge **Q**, the magnetic force also depends on the velocity *v* (expressed in meters per second (m/s)) of the charge. However, ambiguities arise when defining the induced magnetic field outside of a vacuum, where magnetic materials themselves contribute internal magnetic fields to the total magnetic field. This makes it difficult to interpret which part of the total magnetic field comes from the external charges and current, and what the material itself contributes. Therefore, it is common to talk about the *magnetic field strenght* **H** (expressed in ampère per meter (A/m)), which is independent of the medium in which the magnetic field is located and is given by:

$$\mathbf{H} = \frac{\mathbf{B}}{\mu}, \tag{2.6}$$

whereby μ is the magnetic permeability of the medium, expressed in Newton per ampère squared (N/A^2), and quantifies how well a material supports the formation of a magnetic field within itself. Based on μ, materials can be classified into diamagnetic, paramagnetic and ferromagnetic substances (Dearing, 1999). While *diamagnetic* materials have a permeability μ less than the permeability of free space (μ_0; also known as the magnetic constant), and are repelled by magnets, materials that minutely increases **H** are called *paramagnetic*. These have a permeability larger than μ_0. When a substance has a permeability hundreds or thousands times larger than that have a permeability larger than μ_0, it is classified as *ferromagnetic*. In practice, diamagnetic substances are repelled by magnets, whereas para- and ferromagnetic materials are attracted by them (see section 2.2.2 for additional information).

The contribution of materials to an applied external magnetic field is called the *magnetic susceptibility* κ, which is dependent on **H** and the strength of the magnetization **M** (or magnetic dipole moment per unit volume), both expressed in A/m:

$$\kappa = \frac{\mathbf{M}}{\mathbf{H}}. \tag{2.7}$$

As both **M** and **H** have the same unit, κ is dimensionless and expressed as the volume magnetic susceptibility or magnetic susceptibility per unit volume. Commonly SI is written after the magnetic susceptibility value, referring to the international system of units (Système International d'Unites). The relationship between κ and μ can be further described through:

$$\mu = \mu_0(1 + \kappa). \tag{2.8}$$

2.1.2 Electromagnetism

Electromagnetic fields are a manifestation of the interaction between electric charges. From the previous section, we have seen that moving charges generate electric and magnetic fields, which exert an electrical and magnetic force on charged particles within their field of influence. Combined, these forces lead to the total electromagnetic force $\mathbf{F}_{magnetic}$, acting on a particle of electric charge **Q** as defined by the Lorentz force law:

$$\mathbf{F}_{magnetic} = \mathbf{Q}v \times \mathbf{B}. \tag{2.9}$$

How electric charges act as a source for electromagnetic fields and how electric and magnetic fields affect each other, is described in Maxwell's equations. For EMI survey, Maxwell's interpretation of Ampère's law and Faraday's law are of particular importance.

Maxwell-Ampère's law describes how a magnetic field circulates around an electric current flux, i.e. how an electrical field **E** induces a magnetic field **H**. In a homogeneous, isotropic medium with an electrical conductivity σ and an electrical permittivity ε this can be shown by the following equation (in differential form):

$$\nabla \times \mathbf{H} = \sigma\mathbf{E} + \varepsilon\frac{\partial \mathbf{E}}{\partial t}, \tag{2.10}$$

with ∂t the partial derivative with respect to time. The right hand side of the equation represents the total current, which is the sum of the ohmic current flow ($\sigma\mathbf{E}$) and the displacement current ($\varepsilon\partial\mathbf{E}/\partial t$). This is particularly relevant to frequency-domain EMI instruments as at low frequencies any magnetic field generated by the displacement current

can usually be neglected. In GPR survey, where higher frequencies are used, these displacement currents remain important.

The Faraday law describes how an electric field is created by a time-varying magnetic field. For a homogeneous, isotropic medium, with a magnetic permeability μ, this is given by:

$$\nabla \times \mathbf{E} = -\mu \frac{\partial \mathbf{B}}{\partial t}. \tag{2.11}$$

As the magnetic permeability of soils and rocks is generally nearly equal to the magnetic constant μ_0, ferromagnetic exceptions aside, by approximation, their permeability can be assumed to be that of free space.

2.1.3 Operating principles of frequency domain EMI sensors: the Slingram method

In their most basic form, EMI instruments consist of a transmitter and a receiver. Hereby, the response of the ground to the propagation of induced electromagnetic waves is used to describe the electric and magnetic properties of the measured volume (Reynolds, 1997).

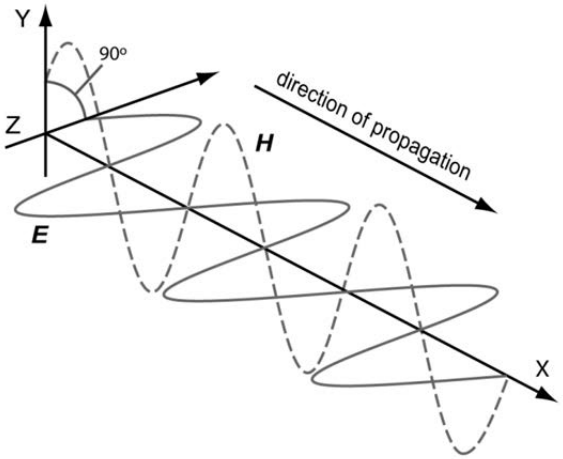

Fig. 3 Basic elements of an electromagnetic wave with the two principal electric (**E**) and magnetic (**H**) components. After Beck (1981).

Electromagnetic waves are made up of two orthogonal vector components; an electric and a magnetic component (Beck, 1981) (Fig. 3). The main EMI sensors that are applied in archaeological prospecting use magnetic dipoles in the form of wire coils for transmitting and receiving induced electromagnetic waves, and are often referred to as Slingram-type EMI instruments based on the original development of this method in Sweden in the 1930s. These sensors combine one or more receiver coils at a certain distance from the transmitter. By sending an alternating current through the transmitter coil, a continuously oscillating magnetic field of the same frequency is generated around the coil according to the Ampère law (Fig. 4). When the transmitter coil is placed near the soil, this *primary magnetic field* (*Hp*) will interact with the conductive particles of the soil. According to Faraday's law, the primary magnetic field induces electrical currents (eddy currents) in the conductive parts of the soil, which then induce a *secondary magnetic field* (*Hs*). In addition, magnetic particles in the

soil become magnetized, or magnetically polarized by the primary field (Keller and Frischknecht, 1966), whereby the intensity of magnetization **M** is determined by κ, following eq. 2.7.

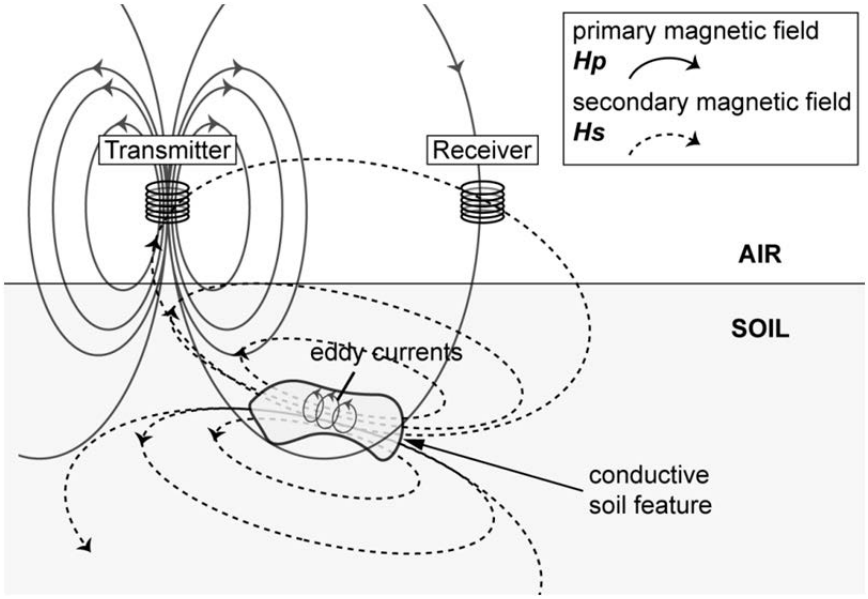

Fig. 4 Schematic representation of the basic principle of EMI soil survey.

Consequently, the magnetic polarization also contributes to the characteristics of the secondary magnetic field. When a receiver coil is placed near the transmitting coil and the measured medium, both the magnetic fields induce currents in the receiver, which can be measured. The magnitude of the voltage of these induced currents is directly proportional to the rate of change of the induced magnetic fields.

To deduce electric and magnetic properties of the measured soil volume, the characteristics of the primary and secondary magnetic fields are compared. In frequency domain EMI survey, the primary magnetic field is a time-varying signal with the form of a sine wave. As it takes a finite amount of time to generate eddy currents and induce magnetic polarization in the soil with the primary magnetic field, a time difference occurs between the primary and secondary magnetic field at the receiver coil. This time difference can be described by a phase lag between both magnetic fields (Beck,

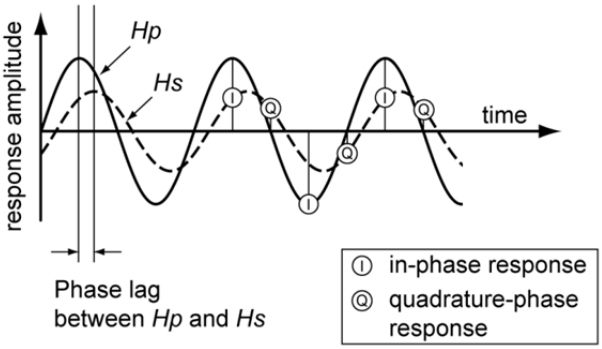

Fig. 5 Relationship between the primary (*Hp*) and secondary (*Hs*) magnetic field, with indication of the in-phase and quadrature response.

1981). This phase lag, together with the amplitude difference between the primary and secondary magnetic field, is influenced by the electromagnetic properties of the soil. In the vector diagram (Fig. 5) the in-phase (IP) and quadrature-phase (QP) response of the secondary magnetic field are shown. While the in-phase response is the amplitude of the secondary field when the primary field reaches its maximum amplitude, the quadrature-phase response is measured when the primary field is equal to zero. The sensor output is given by the ratio of the secondary over the primary magnetic field for the in-phase and quadrature-phase response; i.e. $(Hs/Hp)_{IP}$ for the in-phase and $(Hs/Hp)_{QP}$ for the quadrature-phase response. These sensor outputs are dimensionless and usually expressed in parts per thousand.

2.1.4 Instrument output to electrical conductivity and magnetic susceptibility

Slingram EMI instruments are designed to produce a direct measurement of the electrical conductivity of the measured soil volume. This direct relationship is achieved by applying an approximation of the complex analytical equations that describe the IP and QP response obtained from the electrical conductivity and the instrument configuration when measuring a homogeneous soil (Keller and Frischknecht, 1966; Wait, 1982). However, this approximation is only valid under certain conditions, commonly referred to as the "low-induction number" (LIN) conditions (Callegary et al., 2007; McNeill, 1980b; Nabighian, 1991). The induction number β is dependent on the separation *s* between the transmitter and the receiver coil of the instrument and on the skin depth δ, which is expressed in metres. The skin depth is defined as the depth at which the amplitude of a wave diminishes to 1/e or 37% of its initial amplitude (Sheriff, 1991) and can be expressed as:

$$\delta = \sqrt{\frac{2}{\omega\mu\sigma}}, \tag{2.12}$$

with ω the angular wave frequency ($2\pi f$), expressed in radians per second, μ the magnetic permeability and the electrical conductivity σ. In other words, the skin depth indicates the penetration depth of the electromagnetic signal, and is relative to the frequency and electrical conductivity of the soil. The induction number can then be defined as:

$$\beta = \frac{s}{\delta} \tag{2.13}$$

or the ratio of the coil separation *s* over the skin depth. If this number is small enough, the quadrature-phase signal response is directly proportional to the electrical conductivity of the measured soil volume following the equation:

$$(Hs/Hp)_{\mathrm{QP}} = \frac{\omega\mu_0\sigma s^2}{4}. \tag{2.14}$$

The electrical conductivity of the measured soil volume can then be calculated through:

$$\sigma = \frac{4}{\omega\mu_0 s^2}(Hs/Hp)_{\mathrm{QP}}. \tag{2.15}$$

When the same LIN conditions are met (i.e. when the induction number is sufficiently low), the IP signal response is proportional to the magnetic susceptibility of the soil and can be calculated with:

$$\kappa = 2(Hs/Hp)_{\mathrm{IP}}. \tag{2.16}$$

The ratio of the secondary to the primary magnetic field is hereby multiplied by two to account for measuring a half-space (i.e. the soil being the half-space and the air being the other half of the space).

For EMI operating at low induction numbers, the following issues need to be considered.

1. The operating frequency of the instruments needs to be <100 kHz (usually in the 10 kHz range) (Tabbagh, 1986a). When operating at such frequencies, the measurements are independent of the signal frequency (McNeill, 1996).
2. The electrical conductivity of the soil needs to be ≤ 100 mS/m (Callegary et al., 2007; McNeill, 1980b).
3. In very electrically conductive environments, the IP response can be influenced by the electrical conductivity of the soil (e.g. in saline environments) (Beamish, 2011).
4. When the electrical conductivity is very low (e.g. between 0 – 1 mS/m) the QP response can be influenced by magnetic particles with a 'viscous magnetization' (Tabbagh, 1986a).

2.2 Measuring electrical conductivity and magnetic susceptibility with multi-receiver EMI instruments

2.2.1 Soil electrical conductivity

When certain constraining conditions, discussed in the previous section, are met, the QP and IP signal response from EMI sensors can be directly related to electric and magnetic soil properties. The QP response is directly proportional to the electrical conductivity σ of the soil, which represents how easily an electric current can pass through a material. Electrical conductivity is usually expressed in Siemens per meter (S/m), but as the conductivity of soils is generally very low, milliSiemens per meter (mS/m) is used in soil surveys. In the soil, current is mainly electrolytic, which means that current is transported through fluid in the pores (McNeill, 1980a). The mineral components of soil mostly have a very low conductivity (exceptions include conductive minerals such as magnetite and pyrite). Therefore, the main factors that influence soil electrical conductivity are; soil texture, soil moisture content and the amount of dissolved ions in the soil moisture. The latter is particularly important in soils with a high salt content (saline soils). In these cases, the conductivity is primarily influenced by salt content. However, in this section, saline soils will not be considered.

In non-saline environments, soil texture, and particularly clay content, has the largest influence on the conductivity. As clay particles usually have a negative charge at their surface, these attract positive ions. These ions can guide electrical current through the soil, which means that an increase in clay content causes an increase in soil electrical conductivity. Furthermore, the geometry and distribution of soil pores, following from the soil texture, influence the conductivity. While large pores are less conductive than smaller ones, connected pores have a potentially higher conductivity than closed pore distributions. When water content in the soil pores increases, more potential pathways become available for current flow, which again increases the conductivity. In clayey soils, this effect is enhanced by the increased water retention capacity of the clay particles.

As soil moisture can potentially have a significant effect on soil electrical conductivity, it is advisable to have a general understanding of the soil water content in survey areas (Brevik et al. 2006). However, this effect is only deemed to have a significant effect in low conductive environments with a small variation in soil electrical conductivity. As in non-saline environments, soil texture has the largest effect on the QP EMI signal response, especially in clay-rich environments the effect of soil moisture will not mask the electrical variation related to soil texture variations (see for example Islam et al. 2011).

Contrasts in electrical conductivity can allow discerning anthropogenic or archaeological features within the natural soil. For example, if a ditch, dug into a sandy soil, is filled up with organic and clayey sediments, it will contrast as an anomaly with a high electrical conductivity (the clayey and organic infilling) within its environment (the low conductive sand). Other examples include a sandstone wall (low conductivity) within a loamy environment (higher conductivity).

2.2.2 Soil magnetic susceptibility

The in-phase component of the EMI signal response is a measure for the volume magnetic susceptibility κ of the soil. Based on the way materials are magnetized by an external field **H**, and by their general magnetic behaviour, they can be classified into; diamagnetic, paramagnetic and ferromagnetic (Dearing, 1999; Evans and Heller, 2003; Smith, 1999). The latter can be subdivided into ferromagnetic, ferrimagnetic, and antiferromagnetic materials[1].

Materials that cannot obtain any magnetization, or in which **H** in some cases even causes a slight negative magnetization, are diamagnetic. In soils, these are mainly minerals that do not contain iron (e.g. quartz, calcite, feldspars) along with water and organic matter. Paramagnetic materials obtain a weak magnetization when subjected to **H**, but without this field, these materials lose their magnetization. Paramagnetic minerals are common in soils, and usually contain iron. For example, most clay minerals (except for kaolinite) are paramagnetic, along with pyrite and biotite.

Ferromagnetic materials, such as iron, have the highest magnetic susceptibility, but these are rarely found in the environment. The most prominent category of magnetic substances in soil studies are the ferrimagnetic materials. These include magnetite, maghaemite and a number of other iron minerals with high susceptibility values. When such minerals are present in the soil, they often dominate the measured magnetic susceptibility. Lastly, antiferromagnetic materials have a rather weak magnetization, which is slightly higher than in paramagnetic materials. In the soil, this group consists of iron oxides such as haematite and goethite. It is important to mention that such minerals can lead to the formation of more magnetic particles under certain environmental conditions.

[1] Throughout the thesis, the term ferromagnetic will be used in reference to all these types of ferromagnetic behaviour, unless otherwise stated.

In soils, increased susceptibility is mainly concentrated in the upper, and biologically active, layer (i.e. the topsoil). The increase in magnetic susceptibility in this layer is mostly caused by ferrimagnetic minerals. A number of processes can initiate the formation or enrichment of ferrimagnetic minerals in the topsoil (Dearing, 1999; Dearing et al., 1996; Evans and Heller, 2003), including microbial activity, general soil formation processes (pedogenesis) and thermal transformation of weakly magnetic particles (Le Borgne, 1960). When the topsoil is disturbed, so is the magnetic susceptibility measured at the surface. For example, when a pit is dug, the more susceptible topsoil material is removed. Later infilling of the same pit with magnetically susceptible material, can then cause a magnetic contrast with its environment, which can be detected through magnetic surveying. As such, many anthropogenic disturbances of the topsoil result in a magnetic anomaly, which explains the popularity of magnetic survey methods (e.g. magnetometry). A more detailed description of the properties and genesis of magnetic minerals in the soil related to magnetic archaeological prospection has been given by Fassbinder (1994).

2.3 The difference between EMI and magnetometer instruments for magnetic survey

Although EMI instruments and magnetometers both allow detecting magnetic variations in the subsurface, there are a number of fundamental differences between the working principles of these instruments. Consequentially, EMI and magnetometer results differ significantly and should be approached as such. Furthermore, it is crucial that the different nature of these methods is taken into account when developing a specific survey strategy, or when comparing results of these two techniques.

2.3.1 Induced and remanent magnetization

The terms induced and remanent magnetization can easily lead to misunderstandings about the underlying nature of a magnetic variation, and about the way these variations are recorded during surveys. In section 2.2.2, magnetic susceptibility was discussed as one of the physical soil properties that can be recorded with EMI sensors. As shown in equation 2.7, magnetic susceptibility is the ability of material to become magnetized under the influence of an external magnetic field **H** (Evans and Heller, 2003). The obtained magnetization **M**, induced by **H** is therefore called the *induced magnetization*. With diamagnetic and paramagnetic materials, the magnetization disappears after the external magnetic field **H** is removed, i.e. for such materials, without **H**, **M** = 0. For example, many

ferromagnetic substances[2] keep a certain level of magnetization without an external magnetic field. For these substances without **H**, **M** > 0. This remaining, or permanent magnetization, is called *remanent magnetization.*

2.3.2 Basic principles of magnetometry

While EMI sensors offer a direct measurement of a magnetic property, i.e. the magnetic susceptibility κ (see section 2.1.4), magnetometer instruments record the effect of changes in magnetic soil properties on the Earth's magnetic field (Aspinall et al., 2008; Dalan, 2008; Gaffney and Gater, 2003). These 'distortions' of the geomagnetic field are primarily caused by substances with a remanent magnetization, which can locally influence the geomagnetic field, and can be picked up by a magnetometer. Some substances, such as antiferromagnetic materials, do not possess a permanent magnetization (Evans and Heller, 2003; Smith, 1999), but under the influence of the Earth's magnetic field, a magnetization can be induced that is strong enough to cause a disturbance that can be detected with a magnetometer.

While EMI and GPR are active methods, magnetometry is a 'passive' geophysical method. This means that no signal, such as the primary electromagnetic field in EMI survey, is emitted into the measured medium (i.e. the soil) before conducting a measurement. The already present local disturbances of the geomagnetic field are picked up by the magnetometer. The way these minute local changes of the Earth's magnetic field are detected with magnetometry, differs based on the instrument type that is used. These can be classified into instruments that measure a scalar quantity or a vector quantity. Scalar instruments, such as proton magnetometers or alkali-vapour magnetometers[3] measure the intensity of the magnetic field influencing the sensor. Vector instruments, such as fluxgate and SQUID magnetometers[3], measure a directional component of the magnetic field that influences the instrument.

2.3.3 Magnetic susceptibility vs. induced and remanent magnetization

The different working principle of EMI sensors and magnetometer instruments can sometimes lead to confusion when comparing the two methods, and discussing the induced

[2] Ideal antiferromagnetic substances, which have a zero net magnetization (Evans and Heller, 2003; Smith, 1999), not included.
[3] As the working principles of these different sensor types surpass the scope of this section, the reader is referred to Aspinall et al. (2008), who provide an elaborate overview of magnetometry instrumentation.

or remanent nature of the detected magnetic anomalies. As EMI sensors induce a relatively strong magnetic field in the soil, the resulting magnetic susceptibility is, evidently, a measure of the induced magnetization **M** (see equation 2.7). Discriminating between induced and remanent magnetization is irrelevant as the measured magnetic variations are based on the presence of dia-, para- and ferromagnetic substances in the subsurface. Furthermore, remanent magnetization is not recorded with an EMI sensor. Although substances that possess remanent magnetization, usually also have a high magnetic susceptibility, the effect of their magnetic remanence does not influence the EMI measurement. Only the induced magnetization, caused by the primary magnetic field *Hp*, is recorded.

For magnetometry, the distinction between induced and remanent magnetization is mainly based on the spatial signature of the detected substance in a magnetometry data plot. Remanent magnetic anomalies, whereby the magnetic field of the substance 'defies' the Earth's magnetic field, often show up as magnetic dipoles that are oriented irrespective of the Earth's magnetic field (i.e. not north-south oriented). The second group are referred to as induced magnetic anomalies, as the change in the Earth's magnetic field that is detected, is induced by the Earth's magnetic field itself. As stated above, this is also what happens when antiferromagnetic substances are detected through magnetometry, where the Earth's magnetic field induces a magnetization that can be picked up with a magnetometer.

2.3.4 A practical example: heating of soil

As one of the most cited examples of magnetic anomalies in archaeogeophysical prospection, the heating of soil can serve as an illustration to show the different mechanisms behind the detection of these features with EMI and magnetometer instruments.

There are two pathways that each can lead to an alteration of the magnetic characteristics of soil when subjected to heath. The first occurs at a mineralogical level and is commonly referred to as *magnetic enhancement* or *ferrimagnetic enrichment* (Dearing et al., 1996; Evans and Heller, 2003). Hereby, weakly magnetic iron oxides, hydroxides and carbonates, in the presence of organic matter, are transformed to ferrimagnetic magnetite or maghemite under the influence of fire. An example of such a thermal transformation is the reduction of haematite to magnetite when heated. The degree of magnetic enhancement obtained through thermal transformation varies, and depends on the organic matter content, the burning temperature, the presence and nature of iron minerals, and the porosity of the

soil (Evans and Heller, 2003). This thermally induced ferrimagnetic enrichment causes a higher magnetic susceptibility of the influenced soil.

The second pathway occurs at the level of the magnetic domains and the magnetization of soil. While ferromagnetic substances can have an inherent magnetization, called the *natural remanent magnetization* (NRM), heating and subsequent cooling of a substance or soil can also cause remanent magnetization. This *thermoremanent magnetization* (TRM) arises by cooling a substance from a very high temperature, more specifically from that particular substance's Curie temperature. The Curie temperature is the temperature at which the orientation of the atomic magnetic moments in the substance changes. Above this temperature, ferromagnetic substances become paramagnetic, and their magnetic moments are oriented randomly. Under the influence of the Earth's magnetic field, magnetic moments align with this field. Subsequent cooling 'freezes' this newly obtained orientation of the magnetic moments to the Earth's magnetic field, resulting in TRM.

A quick comparison of these two pathways shows that there can be an overlap between them. While in the soil, firing easily causes ferrimagnetic enrichment, this does not necessarily mean that the influenced soil also obtains TRM. This only occurs when the Curie temperature, which is material-dependent, is surpassed. Ferrimagnetic enrichment through thermal transformation can occur regardless of passing the Curie point.

The consequences of these different pathways are different when working with EMI than with magnetometry. With EMI, it is the first pathway, leading to ferrimagnetic enrichment that influences the measurements. At locations where such enhancement has taken place, a higher magnetic susceptibility can be measured. For magnetometry, thermally induced ferrimagnetic enrichment at moderate temperatures (i.e. below the Curie point) can be picked up when the enrichment is allows for a strong enough induced magnetization (induced by the geomagnetic field) to cause a local distortion of the Earth's magnetic field. However, when the Curie temperature has been reached, the TRM will strongly influence the magnetometer reading and show the remanent magnetic field of the feature, independent from the geomagnetic field. In other words, when TRM is present, EMI sensors will pick up the higher susceptibility caused by the ferrimagnetic enrichment, while a magnetometer instrument will detect the remanent magnetization.

In Fig. 6 the difference between the influence of these two pathways as detected with both survey methods is illustrated with a practical example. Both data plots show a magnetic anomaly picked up with and EMI sensor and a magnetometer of the fluxgate gradiometer type. The feature causing this anomaly is a small brick foundation. As brick is

heated clay, the two discussed pathways can be seen are responsible for its particular magnetic characteristics.

The higher magnetic susceptibility of this structure, measured with the EMI sensor, is caused by the ferrimagnetic enrichment of the clay used to produce the bricks. The highly magnetic anomaly, visible as a magnetic dipole with a proper orientation in the magnetometry data, is caused by the TRM of the bricks. In this case, the two pathways allow detecting the structure with both EMI and magnetometry. While the increased magnetic susceptibility of the structure is detected with EMI, the magnetometer also picks up the TRM of the feature.

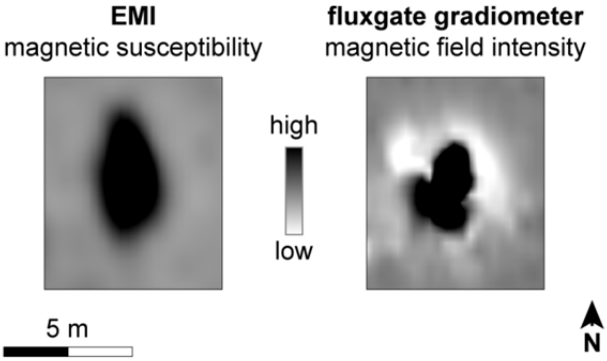

Fig. 6 Two magnetic measurements over the same brick structure. Left: a measurement of the magnetic susceptibility of the feature with EMI, right: a measurement of the disturbance in the geomagnetic field detected with a fluxgate gradiometer.

2.4 Measuring a soil volume

Soil often consists of thin horizontal layers, caused by a number of soil formation processes, with different electrical conductivities and magnetic susceptibilities (Fig. 7). While the conductivities and susceptibilities of these individual soil layers do not influence each other, they all contribute to signal responses obtained with an EMI instrument. EMI measurements are thus a result from the heterogeneous mixture of soil components with varying electrical conductivity and magnetic susceptibility. For the measured bulk soil volume, the terms apparent electrical conductivity (σ_a) and apparent magnetic susceptibility (κ_a) are therefore preferred. The magnitude of this contribution, or relative weight of each layer, to the sensor measurement is a function of the depth *z* of such a layer (Keller and Frischknecht, 1966; McNeill, 1980b; Wait, 1962). This implies that the depth-weight relationship is

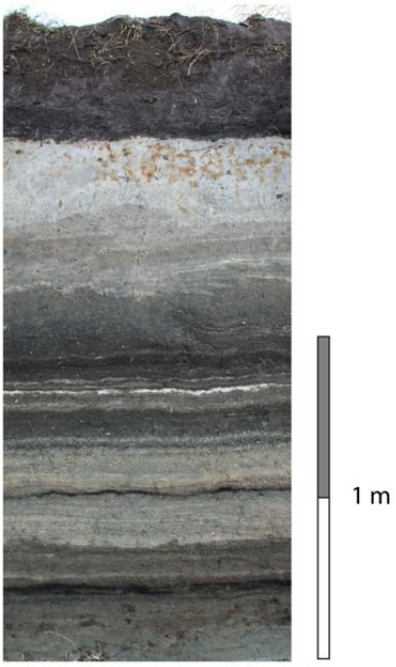

Fig. 7 Soil as a heterogeneous medium: an example of a strongly layered soil.

independent from the conductivity of susceptibility of the layers. This relationship is, however, dependent on the separation between the transmitter and the receiver coil and on their respective orientation towards each other. In other words, the spatial sensitivity of EMI measurements depends on the distance between the transmitter and the receiver coil and their respective orientation. Common coil orientations, or geometries, are the horizontal coplanar (HCP), the vertical coplanar (VCP) and the perpendicular (PRP) orientation (Fig. 8).

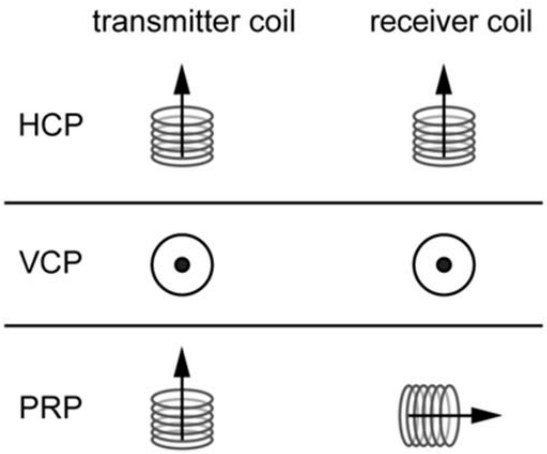

Fig. 8 Schematic representation of frequently used coil configurations. HCP: horizontal coplanar configuration, VCP: vertical coplanar configuration and PRP: perpendicular coil configuration.

For each coil configuration, the relative weight of a soil layer to the sensor measurement can be expressed as a function of its depth *z* (Table 1) given that the restraining LIN conditions are honoured. By integrating the relative weights of all soil layers from an infinite depth to the EMI instrument, the cumulative weight of all layers within the measured soil volume can be calculated (Table 1). The resulting relative and cumulative response functions can be plotted as a function of depth to evaluate the depth sensitivity of a specific coil configuration (Fig. 9).

Plotting the relative signal response of a coil pair as a function of depth shows which part of a one-layer soil renders most of the signal response. In Fig. 9 the relative QP response of HCP, VCP and PRP coil configurations with a 1 m separation between transmitter and receiver coil are plotted. This plot shows that while VCP and PRP orientations obtain most influence in the upper part of the measured medium, the influence of the upper 30 cm in HCP coil configuration is rather negligible. The HCP coil orientation

thus takes into account more of the deeper soil variability, whereas the VCP and PRP orientations have more potential for discerning topsoil variations.

	Relative weight *R*	Cumulative weight *C*
HCP	$\frac{4\frac{z}{s}}{s(4\left(\frac{z}{s}\right)^2+1)^{\frac{3}{2}}}$	$\frac{1}{(4\left(\frac{z}{s}\right)^2+1)^{\frac{1}{2}}}$
VCP	$\frac{2}{s}-\frac{4\frac{z}{s}}{s(4\left(\frac{z}{s}\right)^2+1)^{\frac{1}{2}}}$	$(4\left(\frac{z}{s}\right)^2+1)^{\frac{1}{2}}-2\frac{z}{s}$
PRP	$\frac{2}{s(4\left(\frac{z}{s}\right)^2+1)^{\frac{3}{2}}}$	$1-\frac{2\frac{z}{s}}{(4\left(\frac{z}{s}\right)^2+1)^{\frac{1}{2}}}$

Table 1 Relative and cumulative depth weight equations for the most common coil configurations with a coil separation *s* and to a depth *z* based on McNeill (1980b) and Wait (1962).

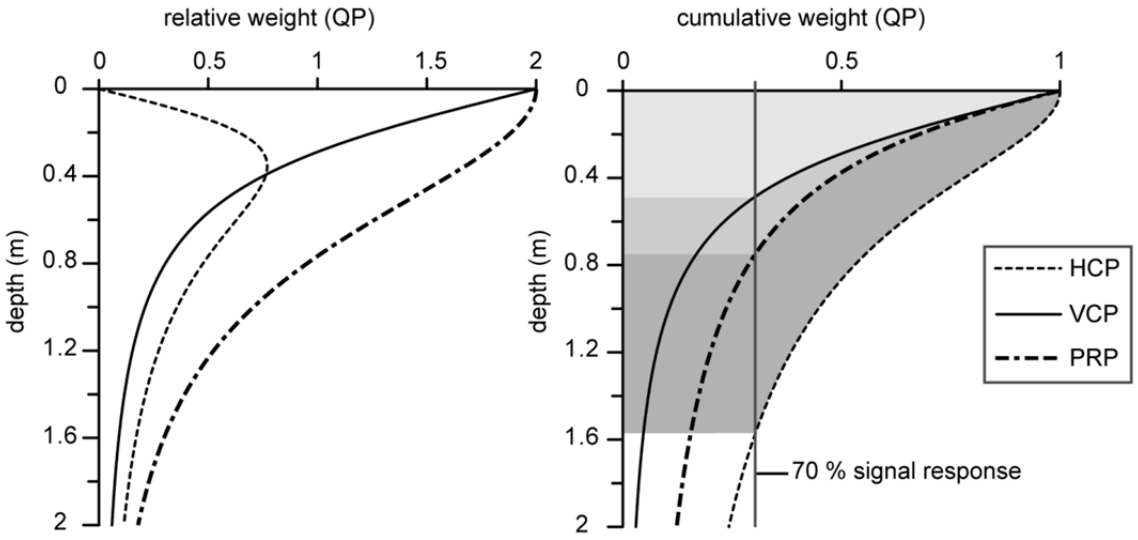

Fig. 9 Relative (left) and cumulative (right) response functions for the QP signal response of the HCP, VCP and PRP coil orientations with a 1 m separation between the transmitter and receiver coil. On the cumulative response function plot, the 70% signal response is indicated. The shaded areas represent the volume that contributes most to the signal response of each of respective coil configurations.

The cumulative QP signal response (Fig. 9, right) allows determining the depth sensitivity of a certain coil pair in a layered soil. For this, the 70% signal response is conventionally used as the point above which most of the signal response is obtained (see for example Abdu et al. 2007, Allred et al. 2006, and Saey et al. 2009). This area is

indicated by the shaded zones in Fig. 9. The 70% signal response boundary is often referred to as the signal penetration depth or the depth of investigation of a certain coil pair, and is indicative of a certain coil pair's depth sensitivity. In the presented example, with a 1 m coil separation, the depth of investigation of the HCP coil pair is 1.58 m, for the VCP coil pair it is 0.75 m and it is 0.5 m for the PRP coil pair.

Analysis of the cumulative IP signal response shows that the IP depth sensitivity of a certain coil pair is shallower than its QP depth sensitivity. In Fig. 10 the cumulative response functions of the QP and IP signal components of a 1 m VCP coil pair are shown. While the 70% depth response for the QP response is obtained at 0.75 m depth, 70% of the IP response is obtained above 0.55 m below the sensor. The intricacies of the IP signal response will be discussed further in Chapter 4.

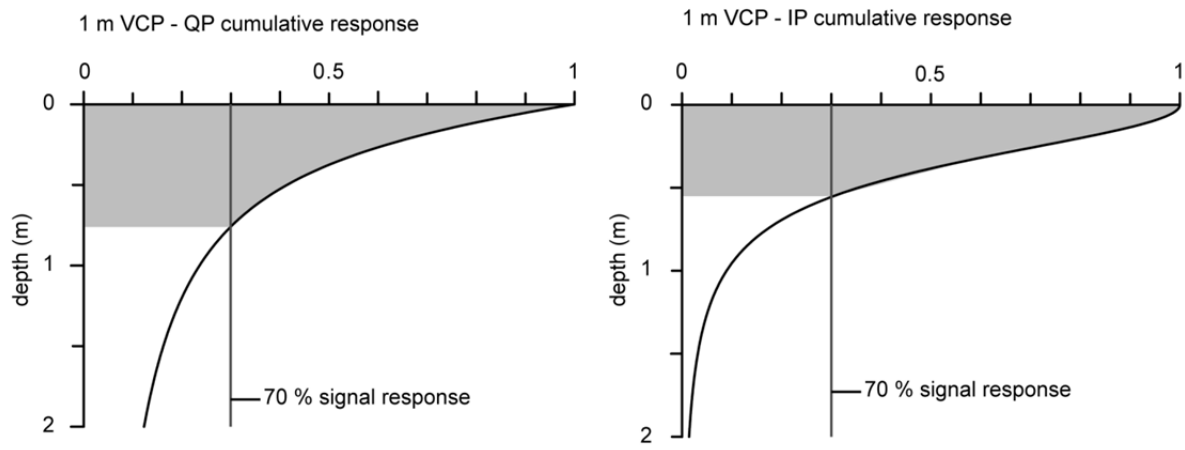

Fig. 10 Cumulative depth response of the QP (left) and IP (right) signal component of a the 1 m VCP coil configuration, with indication of 70% signal response. The shaded areas represent the volume that contributes most to the signal response.

As each coil configuration has a specific depth sensitivity, combining multiple coil pairs in one instrument can significantly increase the level of information that is gathered in one survey run. The introduction of such multi-receiver instruments has made it possible to record electromagnetic characteristics of multiple soil volumes simultaneously. This way, vertical soil variations can be taken into account as well. Most of these multi-receiver instruments combine one transmitter coil with a number of receiver coils in one or more orientations (Fig. 11). Along with the introduction of multi-receiver instruments, it is now possible to record both the IP and QP signal response with one coil pair (e.g. the instruments shown in Fig. 11).

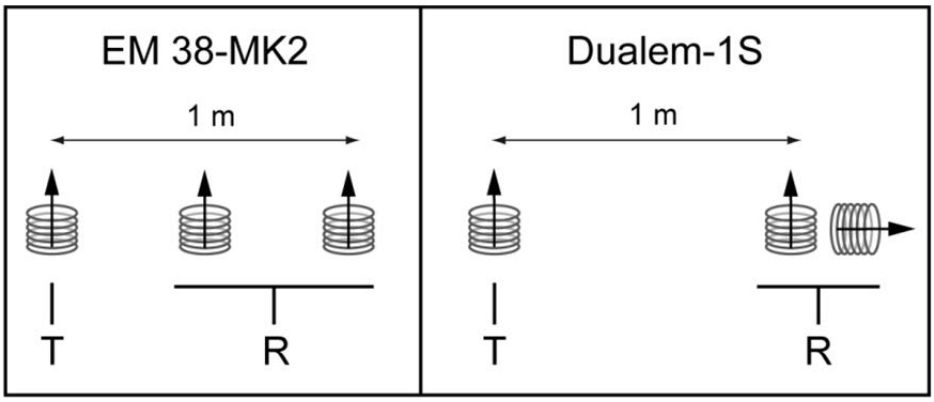

Fig. 11 Two examples of multi-receiver EMI sensor configurations; the EM38-MK2 (Geonics, Canada) with two receiver coils (R) in HCP orientation but at different distances (0.5 m and 1 m) from the transmitter coil T, and the Dualem-1S (Dualem, Canada) with one receiver coil in HCP orientation (at 1 m from T) and one in PRP orientation (at 1.1 m from T) towards T.

2.5 Mobile survey with a multi-receiver EMI sensor

2.5.1 Instrumentation: the Dualem-21S sensor

The EMI sensor that was used in the presented research is the Dualem-21S sensor. This multi-receiver EMI instrument combines one transmitter coil with four receiver coils in a 2.41 m long tube. With each coil pair, the σ_a and κ_a can be measured simultaneously. The four receiver coils are placed at distances of 1 m, 1.1 m, 2 m and 2.1 m from the transmitter coil. The receiver coils at 1 m and 2 m separation are placed in HCP orientation, while the remaining receiver coils are in PRP orientation Fig. 12A). The cumulative depth response functions of the Dualem-21S coil configurations, show signal penetration depths of 0.5 m (1.1 m PRP), 1 m (2.1 m PRP), 1.5 m (1 m HCP) and 3.2 m (2 m HCP) below the instrument (Fig. 12 B). The in-phase signal response has a more shallow depth penetration, resulting in a maximum depth of exploration of approximately 1.5 m below the Dualem-21S (Simpson et al., 2010). This will be discussed in more detail in Chapter 4.

For large-area surveys with the Dualem-21S, a mobile setup was used (Fig. 13). In this configuration, the sensor was put in a polyethylene sled, placing the inter-coil centre line 0.16 m above the soil surface, and towed 3 m behind a quad bike. Measurements were recorded on an Allegro field computer (Juniper Systems, Inc., USA) with HGIS software (Starpal, Inc., USA) and georeferenced with a Trimble AgGPS332 (Trimble, Inc., USA) with OmniSTAR differential correction (Omnistar, Inc., USA), which was mounted on the quad.

The GPS was also used in combination with a Trimble EZ-guide 150 lightbar guidance system to ensure straight survey lines. With the guidance system, the interval between survey lines can be fixed. By using a standard survey speed of 5 to 7 km/h and an instrument sampling rate of 8 Hz, one measurement cycle (i.e. one σ_a and one κ_a measurement with each coil configuration) was conducted approximately every 0.25 m. The spacing between survey lines varied from 0.75 m to 2 m, based on the size of the targeted features. During each EMI survey, soil temperature was recorded at 0.3 m below the surface for temperature correction between individual survey days.

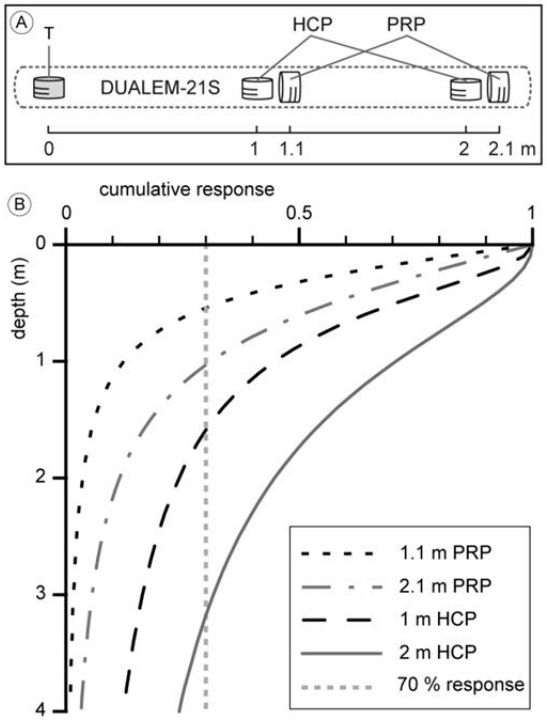

Fig. 12 Schematic representation of the Dualem-21S sensor with the transmitter (T) and the four receiver coils (A) with the depth response functions for the QP signal component of each coil pair (B).

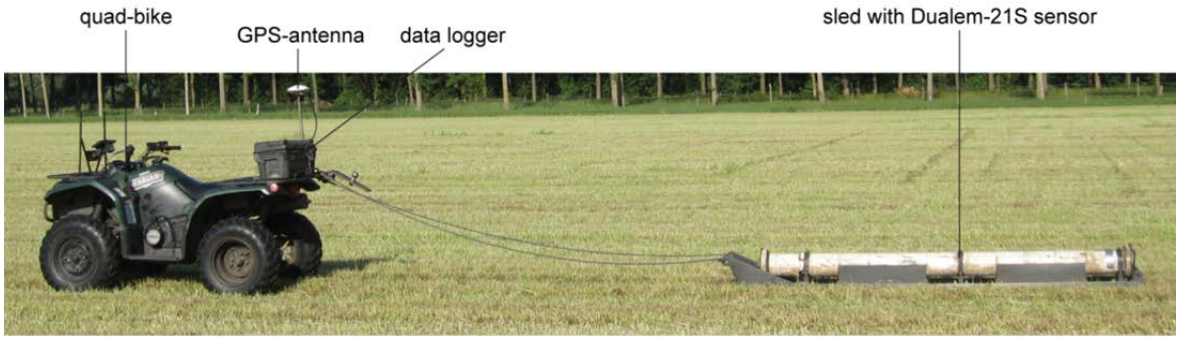

Fig. 13 Mobile survey configuration with the sled holding the Dualem-21S towed by the quad-bike with data logger and GPS antenna. From De Smedt et al. (2013a).

2.5.2 Sensor calibration, drift and temperature correction

The Dualem-21S sensor is a factory-calibrated instrument and therefore does not require additional calibration on the field prior to surveying. However, upon start-up the sensor performs a number of internal tests to identify its current state and strong external electromagnetic fields that can interfere with this process (Dualem, 2007). Therefore, sensor start-up has to be performed at an electromagnetically 'quiet' location; i.e. away

from objects with a high electrical conductivity, a high magnetic susceptibility or sources of electromagnetic interference.

During prolonged surveying, instrument drift can occur, which is mainly due to temperature variations within the instrument, caused by ambient temperature and sunlight. To compensate for this time-varying drift, calibration measurements are taken by driving a diagonal or W-shaped line over the study area at the beginning of each EMI survey following Simpson (2009). The subsequent survey lines then cross the calibration line so that these can be compared. This comparison allows defining and removing the trend of the drift in each data layer (Simpson, 2009; Simpson et al., 2009a).

During each survey, soil temperature needs to be taken into account to correct for the influence of temperature variations on the measured σ_a between survey days. Based on the measured soil temperature, each σ_a measurement is converted to a reference temperature of 25°C, following the method of Sheets and Hendrickx (1995):

$$\sigma_{a\_25} = \sigma_{a\_obs}\left(0.4470 + 1.4034e^{-T/26.815}\right) \quad (2.16)$$

whereby σ_{a_25} refers to the measured standardized σ_a at a soil temperature of 25°C and T refers to the measured soil temperature during the survey whereby the original σ_a data (σ_{a_obs}) were obtained. In this thesis, all σ_a measurements have been standardized to the 25°C reference temperature.

2.5.3 Data interpolation: variography and kriging

Even though the mobile survey configuration allows very fine sampling grids, survey data needs to be interpolated to produce continuous maps. To fill the gaps between sampling points, interpolation techniques start from the assumption that data values that lie closely together are more likely to be similar that data values that are farther apart. To interpolate the EMI data, ordinary kriging was used as the main interpolation technique (Goovaerts, 1997). Contrary to other common interpolation methods, such as ‘inverse distance weighting’ or ‘nearest neighbour interpolation’, kriging takes into account the spatial distribution of the data. This is particularly beneficial when dealing with sensor measurements obtained with a mobile survey setup. Firstly, the survey setup induces a striping effect on the data as the measurement density is higher within survey lines than between the lines. Secondly, as sensor measurement are time-triggered, slowing down can cause data clustering. By attributing less weight to clustered measurements, kriging accounts for such unevenly spaced data (Goovaerts, 1997; Webster and Oliver, 2001). Furthermore, the structure of the spatial variability of the measured values is described by

modelling a theoretical variogram. The rationale behind the characterization of the spatial variability of a variable is the assumption of the intrinsic hypothesis. Hereby, the variance between data points is considered, and mathematically expected difference between two observation points is seen as dependent on the distance vector (or lag) **h** between the two locations **x** of the data points. This allows composing the variogram function $\gamma(\mathbf{h})$:

$$\mathrm{Var}[\{Z(\mathbf{x})-Z(\mathbf{x}+\mathbf{h})\}]=\mathrm{E}[\{Z(\mathbf{x})-Z(\mathbf{x}+\mathbf{h})\}^2]=2\gamma(\mathbf{h}) \tag{2.17}$$

The variogram thus considers the squared difference between two data points separated by a distance **h** (Matheron, 1962). The practical formula to calculate the variogram can be derived from Eq. 2.17 as:

$$\gamma(\mathbf{h})=\frac{1}{2N(\mathbf{h})}\sum_{\alpha=1}^{N(\mathbf{h})}\{z(\mathbf{x}_\alpha+\mathbf{h})-z(\mathbf{x}_\alpha)\}^2 \tag{2.18}$$

with observations $z(\mathbf{x}_\alpha)$ and $z(\mathbf{x}_\alpha+\mathbf{h})$, and $N(\mathbf{h})$ the total number of data pairs separated by a lag **h**.

A plot of the obtained $\gamma(\mathbf{h})$ values in function of h is the experimental variogram, which describes how the sampled data are correlated spatially (Fig. 14). Following the spatial dependency between observation points, the variogram function increases as **h** increases. The function often reaches a maximum, called the sill, C_1, at a larger distance, which represents the total variance of the variable. The distance or lag h where the sill is reached is known as the range *a*, and represents the maximal extent of the correlation between data values at the observation points. Near the origin of the variogram, one would theoretically assume the variogram to be zero. However, in practice there always exists a minimum separation between the two most adjacent observations. The variation that exists within distances closer than the smallest sampling interval induces a so-called micro-variance. This can result in a value greater than zero at **h** = 0. Such a positive intercept on the y-axis is called the nugget effect C_0. All measurement or sampling errors, such as the instrument signal-to-noise ratio, contribute to the nugget effect as error variance.

Before integrating the structure of spatial variability characterized by the experimental variogram into an interpolation sequence, a theoretical variogram model needs to be fitted to the experimental one to fully describe the $\gamma(\mathbf{h})$ relationship (Fig. 14). Different theoretical models exist, but the most common types in geostatistical analysis of soil data are spherical and exponential models (Webster and Oliver, 2001).

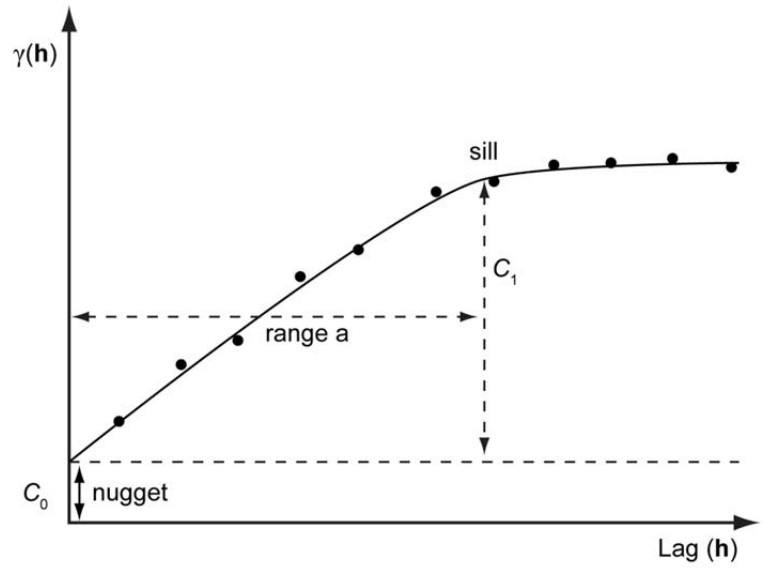

Fig. 14 Example of a typical experimental variogram (black dots) and a fitted theoretical model (black curve), with indication of the three model parameters; nugget, range and sill.

To model the theoretical variogram, one can choose to focus on variation within short distances (i.e. between close lying data points) or take into account the variation at a larger spatial scale by determining a small or larger maximum lag **h**. As a rule of thumb, the maximum lag must be smaller than half the length of the longest side of the study area. With densely scattered data, such as the sensor data presented throughout this thesis, defining a very small maximum lag **h** aids in visualizing small scale features. Hereby, the theoretical variogram can be composed with particular focus on the variation at small lag distances.

When comparing the experimental variograms of different EMI survey datasets, specific tendencies can be observed that characterize the spatial behaviour of the different densely sampled EMI data. The resulting variograms often display a distinct linear behaviour, which starts near the origin and indicates a more gradual underlying variation. This is commonly caused by the within field soil variability, and can be observed in the example presented in Fig. 15. Contrary to the variogram behaviour of σ_a datasets, variogram analysis of κ_a – data shows that these data display a much larger impact of the small scale variations on the experimental variogram. This is a consequence of the absence of large underlying trends in magnetic soil variation on most surveyed areas, combined with the smaller soil volume that is taken into account with the IP component of a certain coil pair. Furthermore, the larger nugget effect in κ_a data demonstrates the smaller signal to noise ratio and larger microvariance of this data type.

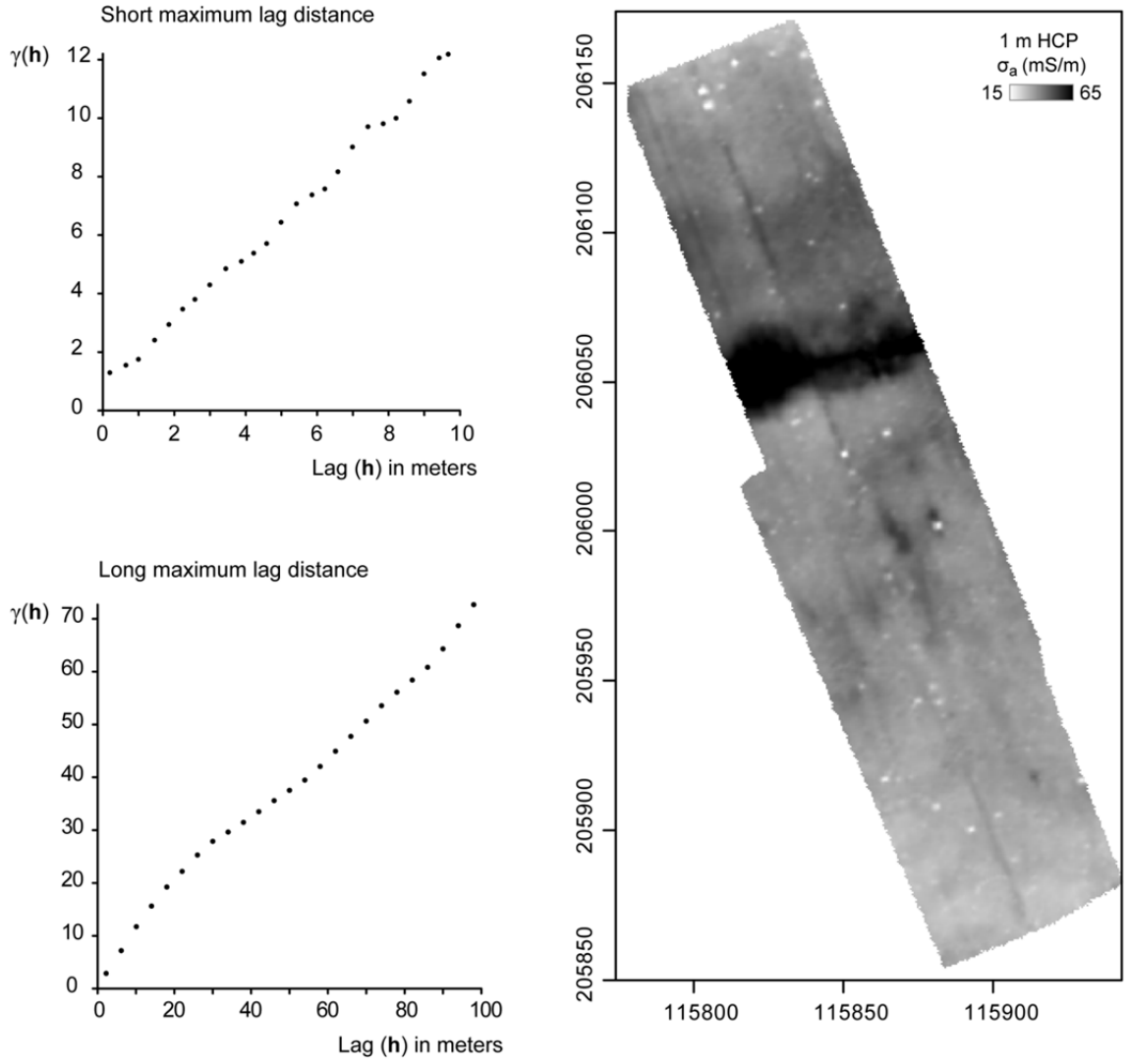

Fig. 15 Experimental variograms (left) with a maximum lag distance of 10 m (top) and a maximum lag distance of 100 m for the σ_a dataset shown on the right. The σ_a data, collected in a 2 m by ca. 0.25 m grid, has been interpolated to a 0.5 m by 0.5 m grid through ordinary kriging with the upper left variogram, and a search window of 8 m by 8 m. Coordinates are in Belgian Lambert 72.

In Fig. 16 the experimental variograms are shown for a σ_a and κ_a data of a survey site, simultaneously collected with the Dualem-21S sensor. While the σ_a data displays the typical linear variogram behaviour, starting near the origin of the variogram, the variogram of the κ_a data displays a stronger nugget effect. Additionally, a larger impact of the small scale variation can be seen in the κ_a data, causing the experimental variogram to deviate from a purely linear curve.

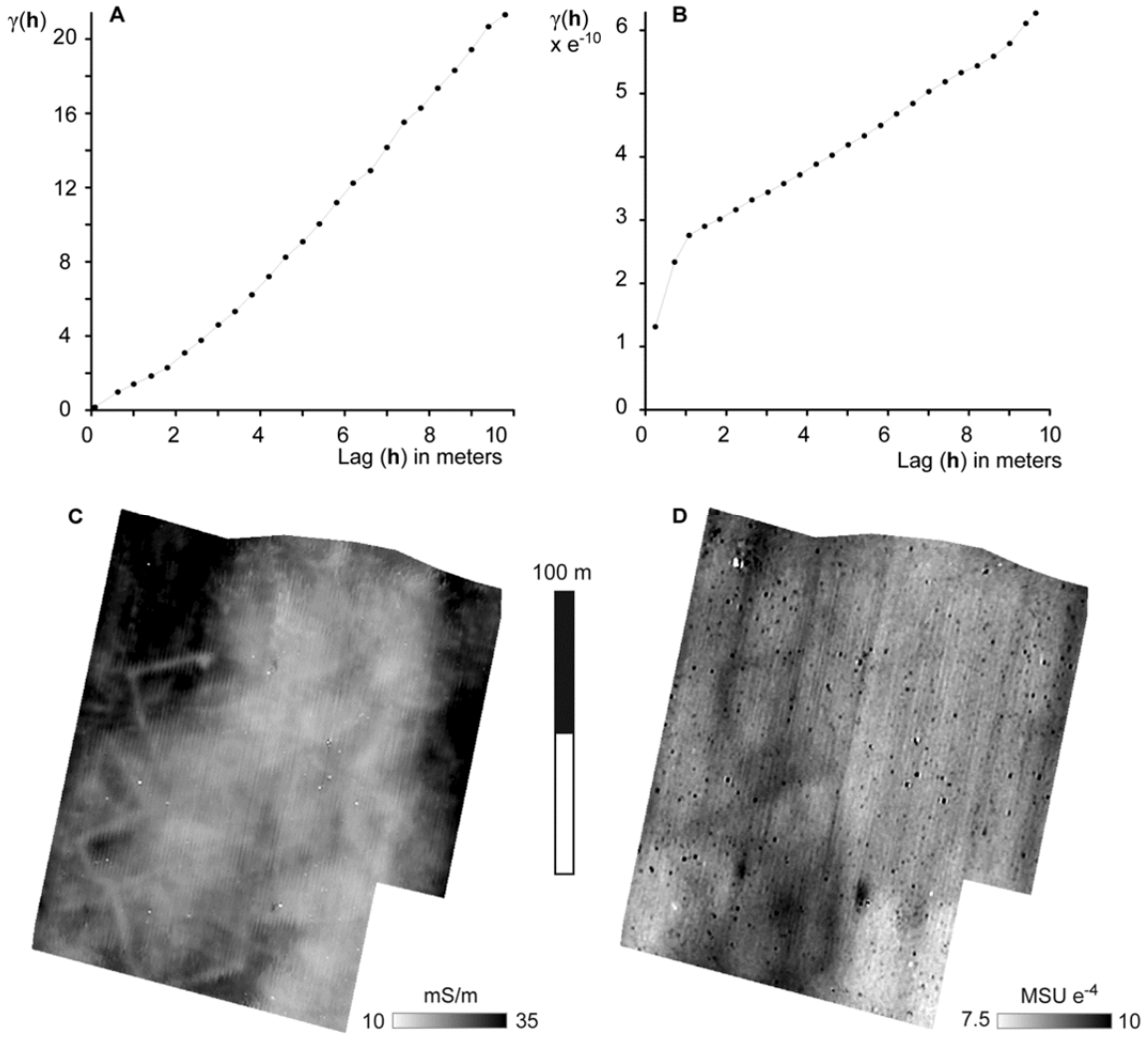

Fig. 16 Experimental variograms for the simultaneously gathered σ_a (A) and κ_a (B) from the 1 m HCP coil configuration along with the data plots for these σ_a (C) and κ_a (D) data. These data were interpolated to a 0.1 m by 0.1 m grid using ordinary kriging based on the experimental variograms in A and B, with a 3 m by 3 m search neighbourhood.

Ordinary kriging was performed in Surfer (Golden Software), whereby theoretical variogram models were fitted to the experimental variograms prior to interpolation. With kriging, the predicted values are calculated as weighted linear combinations of adjacent measurements. The weights are hereby obtained through minimizing the squared difference between true and predicted values whilst taking the distance between sampling locations into account, along with clustering of data points (Webster and Oliver, 2001). The kriging predictor at an unsampled location $\mathbf{x}_0$, with n sampling locations $\mathbf{x}_\alpha$ (α = 1, …, n) can be expressed as:

$$Z^*(\mathbf{x}_0) - m(\mathbf{x}_0) = \sum_{\alpha=1}^{n(\mathbf{x}_0)} \lambda_\alpha \cdot [Z(\mathbf{x}_\alpha) - m(\mathbf{x}_\alpha)] \tag{2.19}$$

whereby $Z^*(\mathbf{x}_0)$ is an prediction of the data value at location $\mathbf{x}_0$, based on the neighbouring observed values $Z^*(\mathbf{x}_\alpha)$, measured at *n* locations. λ_α are the weights that are assigned to the observed data values. $m(\mathbf{x}_0)$ and $m(\mathbf{x}_\alpha)$ are the expected values at $\mathbf{x}_0$ and $\mathbf{x}_\alpha$, respectively. These weights are calculated through minimizing the prediction error, or prediction variance, under the constraint of unbiasedness:

$$E[Z^*(\mathbf{x}_0) - Z(\mathbf{x}_0)] = 0, \tag{2.20}$$

which allows classifying kriging as an exact interpolation method.

The most common type of kriging is ordinary kriging (OK), which has been used throughout this thesis. In OK, the mean of the observations is considered unknown, but locally stationary. As a result, within the search window used for data interpolation, the mean is constant. The most common type of kriging is ordinary kriging (OK), which has been used throughout this thesis. In OK, the mean of the observations is considered unknown, but locally stationary. As a result, within the search window used for data interpolation, the mean is constant. This allows defining the ordinary kriging equation as:

$$Z^*_{OK}(\mathbf{x}_0) = \sum_{\alpha=1}^{n(\mathbf{x}_0)} \lambda_\alpha \cdot Z(\mathbf{x}_\alpha) \quad \text{with} \quad \sum_{\alpha=1}^{n(\mathbf{x}_0)} \lambda_\alpha = 1 \tag{2.21}$$

To determine the weight of each available observation the theoretical variogram model, with the three model parameters (nugget, range and sill) is incorporated into the OK system through:

$$\begin{cases} \sum_{\beta=1}^{n(\mathbf{x}_0)} \lambda_\beta \gamma(\mathbf{x}_\alpha - \mathbf{x}_\beta) + \Psi = \gamma(\mathbf{x}_\alpha - \mathbf{x}_0) \quad \text{with } \alpha = 1, ..., n \\ \sum_{\beta=1}^{n(\mathbf{x}_0)} \lambda_\beta = 1 \end{cases} \tag{2.22}$$

where $\gamma(\mathbf{x}_\alpha - \mathbf{x}_\beta)$ is the variogram between sampled locations $\mathbf{x}_\alpha$ and $\mathbf{x}_\beta$, and $\gamma(\mathbf{x}_\alpha - \mathbf{x}_0)$ is the variogram between sampled locations $\mathbf{x}_\alpha$ and the unsampled locations $\mathbf{x}_0$. Ψ is the Lagrange multiplier, introduced to optimize the minimization of the OK variance under the constraint of unbiasedness (Eq. 2.20) whereby the sum of the weights must be equal to one (see Eq. 2.21).

Even though the sensor data presented throughout this thesis has a very high sampl;ling density, the use of OK remains beneficial. Taking into account the spatial variation through variogram analysis along with the intrinsic declustering effect of kriging, particularly contribute to its importance for producing continuous data plots. A comparison to inverse distance weighting (IDW), a widely used deterministic interpolation method shows the advantages of kriging when working with densely sampled sensor data. IDW uses a weighted average of observed data values occurring within a search neighbourhood to calculate the value at unsampled locations. To increase the weight of nearby points (i.e. points close to an unsampled location $\mathbf{x}_0$), the inverse of the calculated weights is raised by a power *r*. In most cases, a power of two is used resulting in the name inverse squared distance weighting (ISDW).

In Fig. 17 the same σ_a data plot is shown, interpolated through ISDW (Fig. 17 A) and interpolated through OK (Fig. 17 B). These data were collected by using a 2 m by ca. 0.25 m survey grid. With each interpolation, an 8 m by 8 m search neighbourhood was used to create a 0.5 m by 0.5 m grid. For the OK interpolation, a theoretical linear variogram model was fitted to the experimental variogram with the 10 m maximum lag distance shown in Fig. 14 (top left). More specifically, a nugget effect of 0.847 was used along with a linear variogram model with a slope of 1.14.

Cross-validation of the obtained interpolated grids shows the slightly better performance of OK in predicting sample values. OK rendered a root mean squared error (RMSE) of 0.615 and a Pearson correlation coefficient of 0.996. Cross-validation of the ISDW data gave a RMSE of 0.863 and a Pearson correlation coefficient of 0.995. A visual comparison of the two resulting grids (Fig. 17) further shows the consequence of using kriging interpolation. As the survey method results in a denser sampling within survey lines (approximately one sample per 0.25 cm), this causes a strong striping effect in the ISDW data plot (Fig. 17 A and C). On the other hand, the declustering effect of kriging, along with the incorporation of a nugget effect that takes microvariance and error variance into account, allows compensating for the effects such as data striping.

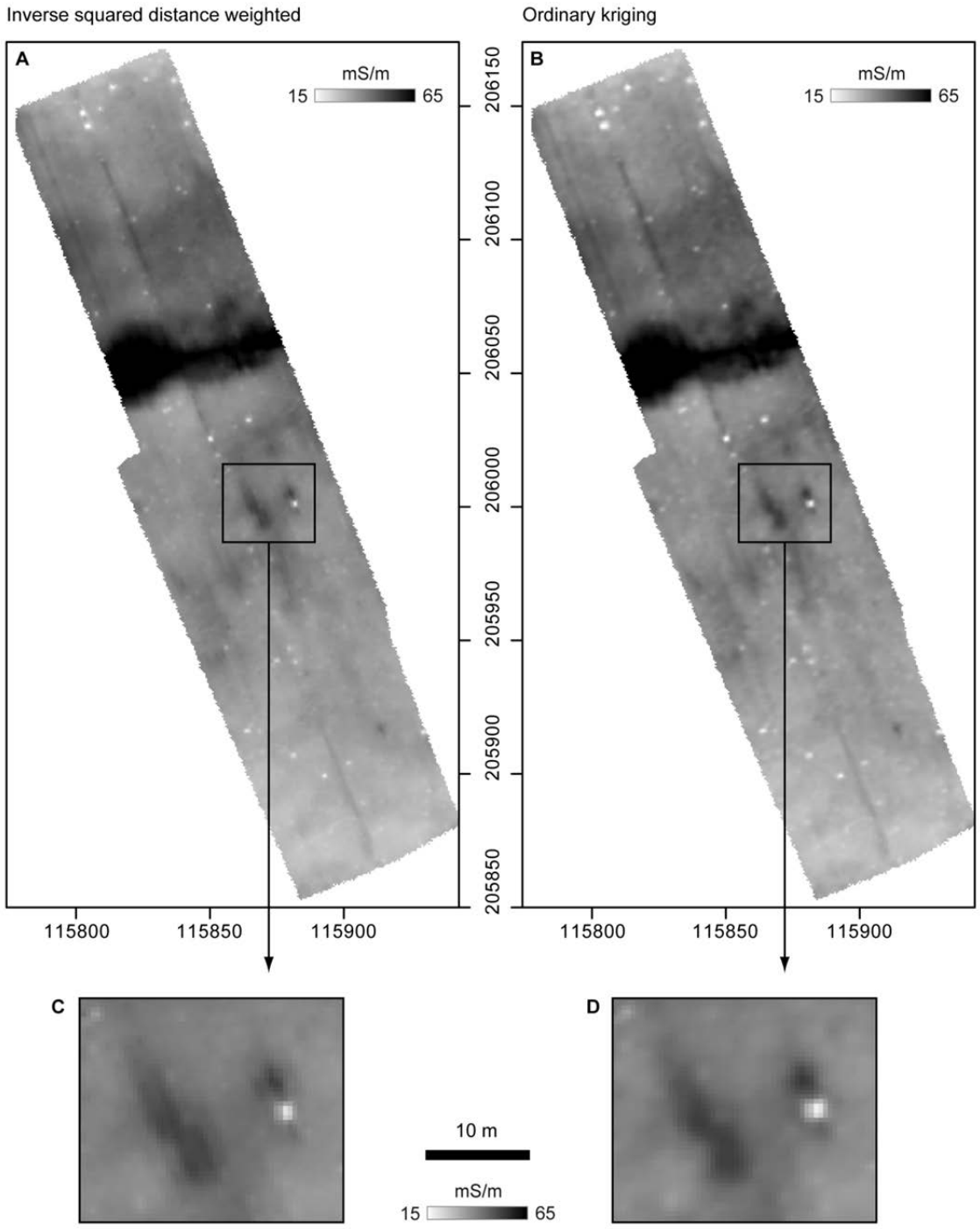

Fig. 17 Plot of σ_a data gathered with an EMI sensor over a palaeochannel segment (high values), interpolated through ISDW (A) and through OK (B). Below two details of the survey area are plotted, showing the different effect of small scale variation and the sampling strategy when using different interpolation techniques (C = IDW, D = OK).

When comparing ISDW and OK interpolation for a κ_a dataset, similar observations can be made. For the OK interpolation of the κ_a dataset, the theoretical variogram shown in Fig. 18 was used, which was modelled with a nested variogram combining a spherical and a linear model. The slope of the linear component was 3.7 e^{-11} [4]. The scale of the spherical component was 1.65 e^{-10} with a range of 1.1. A nugget effect of 7 e^{-11} was also incorporated into the variogram. For both interpolations, a search neighbourhood of 3 m by 3 m was used. Visual comparison of the interpolated results (Fig. 20) again shows how OK allows compensating for the linearity of the sampling grid, and aids in producing a more straightforward continuous data plot. Cross-validation of the interpolation data resulted in a RMSE of 2.371 e^{-5} for the ISDW interpolation, with a Pearson correlation coefficient of 0.90. Again a slightly better result was obtained with OK, which rendered a RMSE of 1.152 e^{-5} and a correlation coefficient of 0.968.

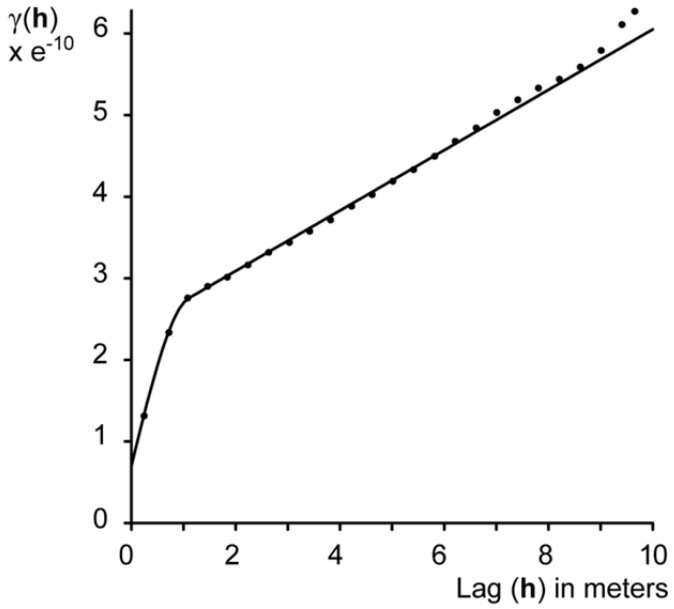

Fig. 18 Experimental (dots) and modelled theoretical variogram (curve) used in the OK interpolation shown in Fig. 20.

[4] Throughout this thesis the letter 'e' will be used to express 'times ten raised to the power of'. For example, $1e^{-3}$ can be noted as 1×10^{-3} or 0.001.

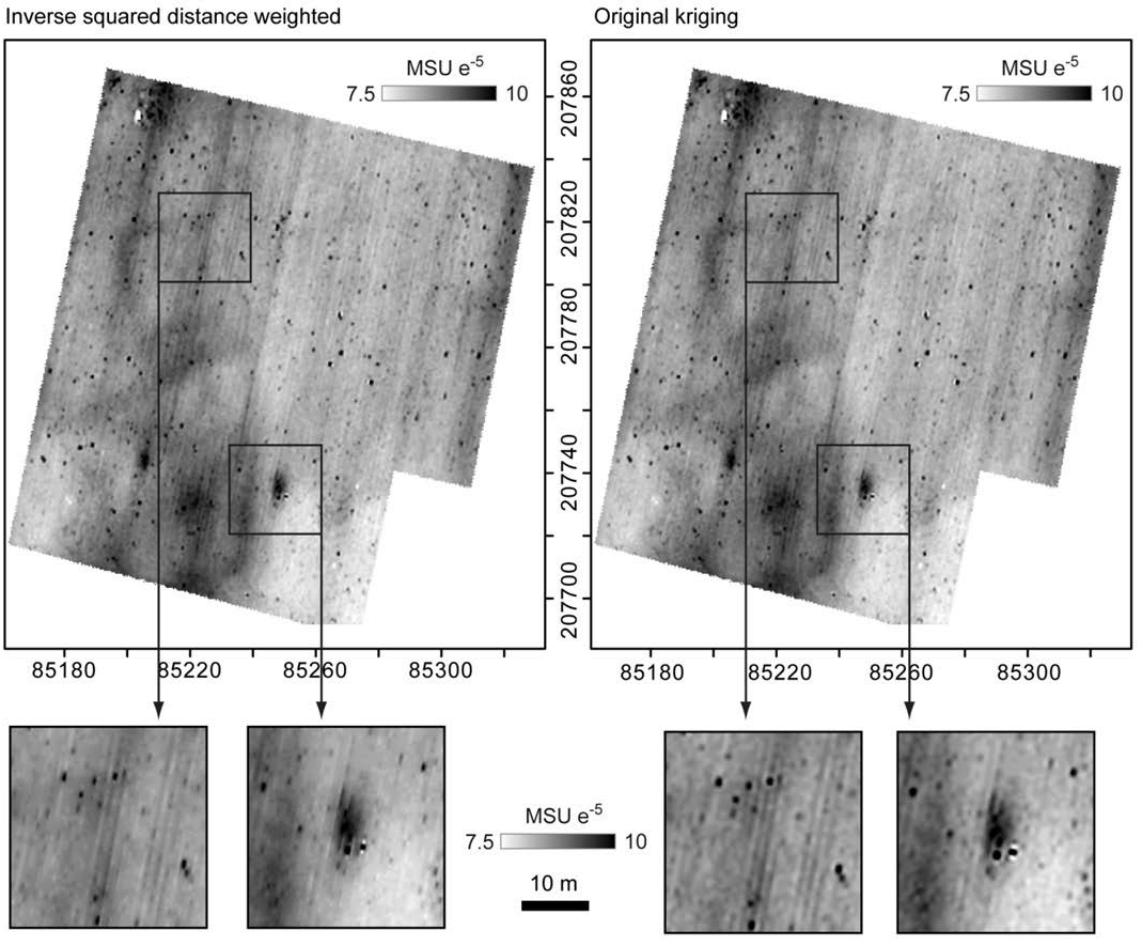

Fig. 19 ISDW and OK interpolated κ_a dataset (top), with detailed comparison on to locations (bottom)

Chapter 3

Landscape reconstruction

The content of this chapter was published as:

1) De Smedt, P. et al., 2011. Reconstructing palaeochannel morphology with a mobile multicoil electromagnetic induction sensor. *Geomorphology*, 130, 136-141.

2) De Smedt, P. et al., 2013. A multidisciplinary approach to reconstructing Late Glacial and Early Holocene landscapes. *Journal of Archaeological Science*, 40, 1260-1267.

3.1 Introduction

3.1.1 Mapping subsurface deposits

Mapping the lithology and morphology of Quaternary deposits continues to challenge researchers studying the geomorphological and environmental characteristics of the palaeolandscape. To obtain thorough understanding of the genesis of the studied environments, information about the internal structure and subsurface expression of past landforms is often pivotal (Van Dam, 2012). In geoarchaeological research, such geomorphological mapping programmes can form the basis for understanding human-landscape interactions and aid evaluating the archaeological value of research areas (De Clercq et al., 2011).

Commonly, airborne sensing data (e.g. LIDAR-derived digital elevation models) and satellite imagery are employed as guiding tools in order to understand palaeotopographical

variety at a larger scale. However, detailed palaeolandscape analyses with these data can be hampered by historical and more recent anthropogenic alterations in the landscape such as urbanisation, terrain levelling or peat extraction. In addition, remote sensing data can be largely ineffective in areas with increased sedimentation, which makes it difficult to assess the palaeotopography based on elevation data. In these areas, sediment cover can create unique preservation potential for archaeological and palaeoenvironmental remains (Challis and Howard, 2006) but unfortunately it can also mask past landscape features.

As a complement to these data, detailed lithostratigraphic information can be added by manual or mechanical coring (Bates et al., 2000), or by trenching and the description of profiles. The latter allows a detailed description of the various stratigraphical units and can serve as a robust foundation for further palaeotopographical and geomorphological studies. But, when it comes to tracing the surface expression of these different deposits throughout the landscape, their use is restricted by the length and number of the available sections. Furthermore, their applicability is mainly confined to short sequences (Bates et al., 2007). Here, borehole data provide a valuable addition to the geomorphological dataset, as these have the benefit of offering detailed insight into stratigraphical variability at sampling locations, have a larger depth range and, aided by interpolation methods, allow reconstructing their lateral extent (Bates and Bates, 2000). However, whereas remotely sensed data can be heavily influenced by anthropogenic disturbances and are of limited use in areas of sedimentation, the generally low sampling density of coring survey restricts lateral accuracy. This limited lateral resolution may prevent a correct reconstruction of the buried topography, especially in areas with a more complex hydrological evolution.

Near surface geophysical techniques are increasingly being applied in geoarchaeological research (Baines et al., 2002; Bates et al., 2007), however, they are still rarely used to conduct large scale and high-resolution palaeotopographical surveys. While surveying large areas at very fine resolutions is becoming common practice in purely archaeological geophysical prospection (e.g. Gaffney et al., 2012; Keay et al., 2009; Neubauer et al., 2002), a similar approach is rare when mapping past landscapes, as in most cases, surveys are primarily conducted along transects (e.g. Gourry et al., 2003). A commonly employed technique for geomorphological studies is electrical resistivity tomography (ERT). Although this transect-wise survey method incorporates more of the lateral variation along the survey transects, a high measurement density across the entire survey area is rare. The interpretation of continuous lateral variations again remains dependent on interpolation methods used for producing maps. Combined approaches, whereby coring is used alongside geophysical and geotechnical data have already been

proposed (Bates et al., 2007; Conyers et al., 2008), but these are still mainly aimed at revealing local sedimentological variability and less directed towards creating high-resolution palaeotopographical models of larger areas.

Non-invasive methods such as GPR and methods based on EMI do enable a more continuous mapping of the lithological variation by generating a higher sampling density in a mobile configuration, but, these also have some limitations (Schrott and Sass, 2008). Clay layers and a high level of water saturation can lead to a stronger attenuation of GPR signals, which especially restricts the application of this technique on alluvial deposits (Howard et al., 2008; Moorman, 1990; Schrott and Sass, 2008). On the other hand, EMI prospection is not hampered by water and clay content but sometimes does not produce sufficient information about vertical facies changes (Conyers et al., 2008). This lack of vertical discrimination potential particularly applies to EMI systems such as the EM31 (Geonics, Toronto, Canada) that only have one single coil pair (transmitter-receiver) determining the depth of exploration (McNeill, 1980b). When a frequency-domain EMI system with a multi-receiver configuration is integrated into a mobile field setup, two major mapping limitations can be avoided. Lateral soil variability can be continuously mapped at a high resolution by measuring changes in σ_a, thus eliminating the possible interpolation error caused by a low sampling density (Saey et al., 2009; Simpson et al., 2008). Furthermore, the integration of multiple coil pairs with different vertical sensitivities generates conductivity measurements of different sediment volumes. If the measurements resulting from each coil pair are then compared, soil conductivity can be accurately modelled at different depths (Saey et al., 2009).

3.1.2 Human landscape interactions in alluvial and lacustrine environments

Understanding palaeotopographical variability forms the basis for understanding prehistoric societies. Alluvial and lacustrine environments, in particular, are the focal point of many geoarchaeological studies (Howard and Macklin, 1999). These dynamic environments are often the key to understanding human settlement patterns and subsistence strategies, especially when considering prehistoric societies during the Late Glacial and at the onset of the Holocene. As the visibility of prehistoric hunter-gatherers is largely influenced by taphonomy and the interpretative potential of excavated assemblages (Zvelebil and Moore, 2006), detailed insight into landscape morphology and palaeotopography provides an invaluable asset to the study of these societies.

The current study is part of a project that aims to construct the geomorphological, pedological, and environmental evolution of Late Glacial palaeolake against the background of its archaeological importance throughout prehistory (more detailed information about the project can be found in Bats et al., 2009). An important part of this research project is the detection and geomorphological investigation of palaeoriver systems. The general aim of the geophysical fieldwork is to map these river systems and describe their morphology, enabling an evaluation of their impact on the former landscape.

3.2 Study Area

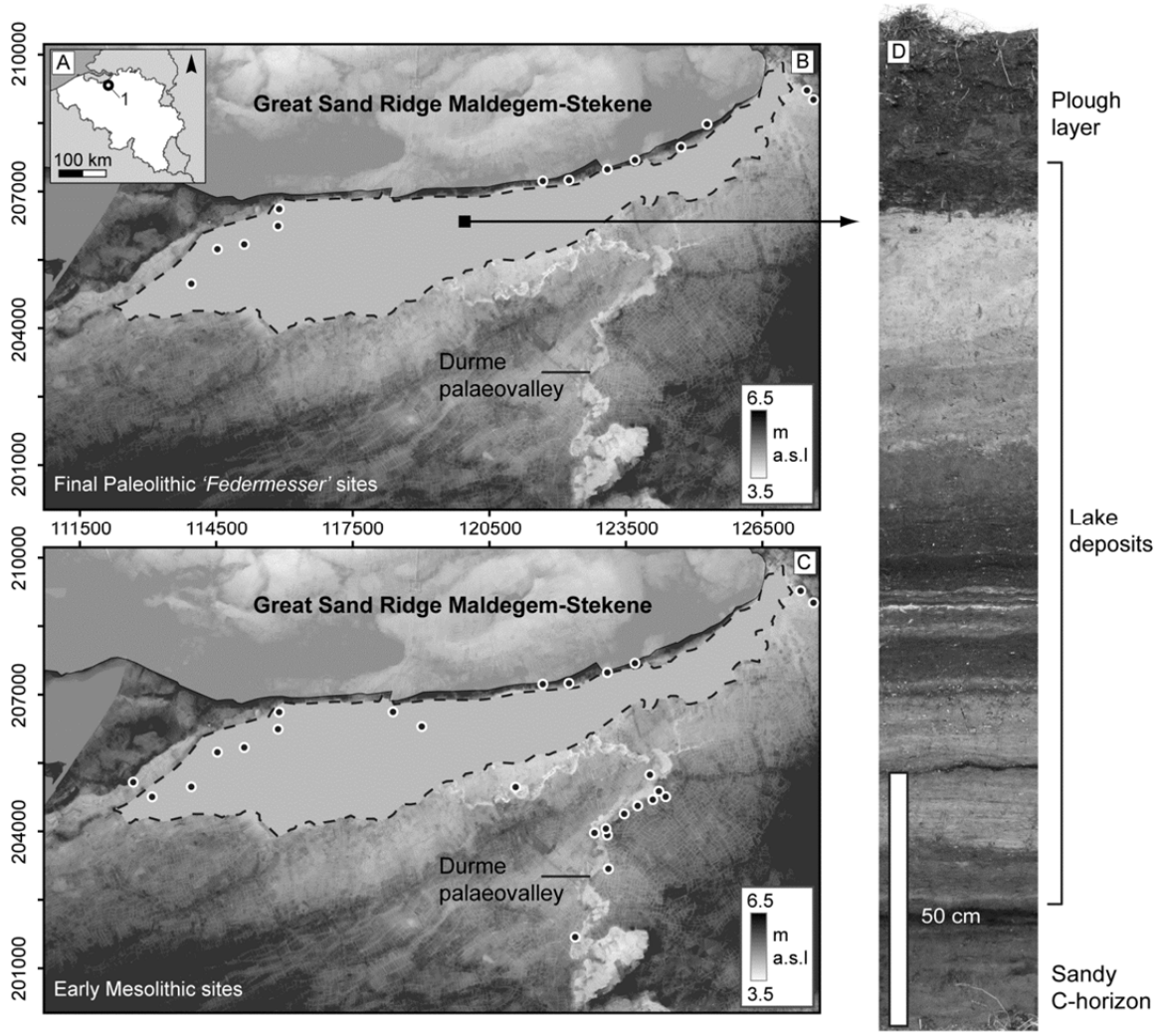

Fig. 20 Location of the Moervaart palaeolake (1) in Belgium (A) and digital elevation models of the study area showing the Moervaart palaeolake (grey area/dashed line) delineated by the coversand ridge in the north (B, C) (coordinates are according to the Belgian metric Lambert 72 projection). The known Final Palaeolithic sites (B) and the Early Mesolithic sites (C), given by Van Vlaenderen et al. (2006), are indicated by dots. In D, a type section of the lake's stratigraphy is shown, taken in the deepest part of the lake indicated by the arrow on B.

Most of the fieldwork in this thesis was conducted in and around the Moervaart palaeolake, which covers an area of ca. 25 km^2 in the north-western part of Belgium (Fig. 20). The dune barrier, called the Great Ridge of Maldegem-Stekene (Fig. 20A, B), gradually dammed the northward draining Pleniglacial river system, triggering the palaeolake formation on top of the coversands. At the end of the Allerød or the onset of the Younger Dryas, the lake dried out, changing the drainage network of the area.

Today, lacustrine deposits containing up to 45% $CaCO_3$ dominate the centre of the palaeolake (Fig. 20D). Throughout the area, palaeochannels can be found that have been filled in with silty to clayey sediments, intercalated with gyttja and peaty layers. Often peat layers covering the deposits can still be found, usually amidst a clayey alluvium. During the Allerød (~12.1 - 10.7 ka cal BC), Final Palaeolithic *Federmesser* groups started occupying this dynamic landscape (Crombé et al., 2011; Crombé and Verbruggen, 2002). Traces of occupation are mainly found on the northern bank of the palaeolake, which exhibits a Final-Palaeolithic site density unique for the region (Fig. 20B) (Crombé et al., 2011; Van Vlaenderen et al., 2006). This distribution pattern was maintained throughout the Early Mesolithic (~8.8 - 7.4 ka cal BC), however, as by then the lake had largely disappeared, there was already an occupational shift towards the banks of the Durme river (Fig. 20C). Afterwards, site density greatly decreased during the Middle and Late Mesolithic (~7.4-6.5 ka cal BC and ~6.5 - 4.5 ka cal BC, respectively), although river banks remained the preferred settlement location. Site complexes were replaced by widely dispersed settlements, installed at important nodal positions between the most dominant features in the landscape. The shifting settlement pattern suggests a strong correlation between the (palaeo-)hydrological features in the area. In order to understand in detail the driving mechanisms behind these prehistoric settlement systems, a thorough understanding of the palaeohydrology of the area was required.

3.3 Evaluating a 1-D inversion procedure for reconstructing palaeochannel morphology

3.3.1 Research objective

In this study, the focus lies on the vertical sensitivity of the applied geophysical technique. Multi-receiver EMI data will be used to model the depth of a palaeoriver segment on a test site in the Moervaart palaeolake (Fig. 21). More specifically, a two-layer model will be composed to reconstruct the depth to the sandy substrate through which the palaeoriver segment has been cut out. In addition, a calibration method based on auger data will be introduced to adjust the modelling parameters and increase the model's accuracy.

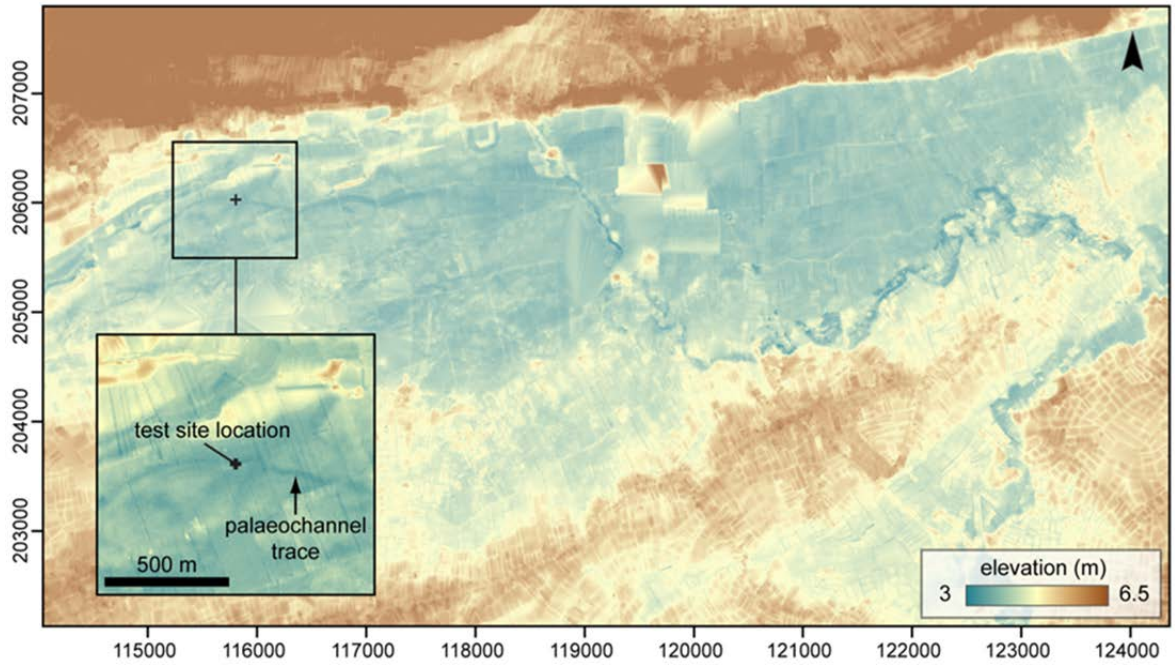

Fig. 21 Filtered digital elevation model of the Moervaart palaeolake, visible as the east–west oriented depression, with localisation of the test site indicated with a cross and on the enlarged inset (coordinates are according to the Belgian metric Lambert 72 projection).

3.3.2 Soil layers and soil horizons

Throughout the following chapters the term 'soil layer' is used to define the different parts of the geophysical soil models that are composed with multi-receiver EMI data. The term 'soil layer' is used instead of 'soil horizon' as the respective soil layers are in most cases a combination of different soil horizons (or surpass the level of a soil horizon). For example, in this chapter a two-layered soil model will be composed. In this model, the first soil layer consists of the plough layer and underlying peat and levee deposits, while the

second layer is made up of the sandy C-horizon. In Chapter five, another two-layered soil model is presented. Here, the upper model layer combines the plough layer, the infillings of a medieval ditch and peat accumulations, while the second model layer combines calcareous lacustrine deposits and the sandy C-horizon.

3.3.3 Test site

Within the Quaternary deposits of the Moervaart palaeolake, traces of several palaeorivers can be found that are related to the Late Glacial and the early Holocene. These traces are mostly located just beneath the plough layer, and sometimes peaty outcrops related to the buried channels can still be seen in the landscape. As with the palaeolake itself, the morphology of these palaeorivers and the sedimentological composition of their infillings show a large variability. With palaeochannel depths ranging from around 1 m to >7 m and river types varying from braided systems to straight and alluvial streams, the area is a testimony of a complex hydrological evolution. The pedological variation of the infillings, often made up of different peat and gyttja layers and laminated silt packages, adds up to the heterogeneity of the system. Based on a filtered digital elevation model (DEM) (Werbrouck et al., 2011), a first test site of 0.45 ha was selected at the boundary of the palaeolake (Fig. 14). Here, DEM data suggested the presence of a branch of the palaeoriver system intersecting the field.

3.4 Methodology

Because of the complex sedimentology of the study area, two types of near-surface geophysical methods were selected: ERT and EMI; GPR was excluded because of the high clay percentages and the frequent water-saturated conditions (Moorman, 1990; Schrott and Sass, 2008). In addition to these methods, hand augering was performed for further interpretation of the geophysical data.

3.4.1 Multi-receiver EMI survey

The EMI surveys were conducted with the Dualem-21S in a mobile configuration (see section 2.5). To combine the vertical discrimination potential of the instrument (offering exploration depths ranging from 0.5 to 3.2 m below the surface) with a high spatial resolution, field measurements were conducted with a mobile setup that enabled recording four bulk conductivity values every 0.20 m, i.e., one measurement with each coil pair every second. By driving over the test site in parallel lines with a 2-m separation, a nearly

complete lateral coverage of the site was achieved. In this configuration and at this resolution it was possible to map 1 ha every hour. Field data were then processed and combined in four σ_a maps (Fig. 22). Based on these maps, two 65-m sections were set up (section 1, S1, and section 2, S2) along which palaeochannel depth would be modelled (Fig. 15A). Section 1 (S1) was set up over the palaeoriver segment's maximum extent as represented in the σ_a maps, whereas in section 2 (S2) a smaller part of the feature would be investigated.

3.4.2 Hand augering and electrical resistivity tomography

Auger locations along both sections that covered the range of σ_a values were selected for model calibration and evaluation. On each transect, seven calibration and eight evaluation hand augerings were drilled with a 2-cm gouge auger (Fig. 22A).

For further evaluation, ERT (Baines et al., 2002; Samouëlian et al., 2005) was performed on both sections. These data were used to detect inconsistencies between the modelled depths and the ERT pseudosection at locations where no auger data were available. We used a Terrameter SAS 1000 LUND imaging system (ABEM instruments AB, Sundbyberg, Sweden). Each ERT transect consisted of 64 electrodes that were connected to a resistivity meter by an electrode selector system, enabling the automatic measurement of the soil apparent resistivity in a Wenner-Schlumberger configuration (Samouëlian et al., 2005).

As the ERT was carried out across a known palaeochannel segment, the electrode spacing was defined based on the auger data to match both the width and the depth of the feature. This resulted in two 63-m ERT sections with a 1-m electrode spacing (Fig. 22A). The inversion of the apparent resistivity data to modelled vertical sections was done with RES2DINV software (Geotomo software, Malaysia), following the method of Loke and Barker (1996).

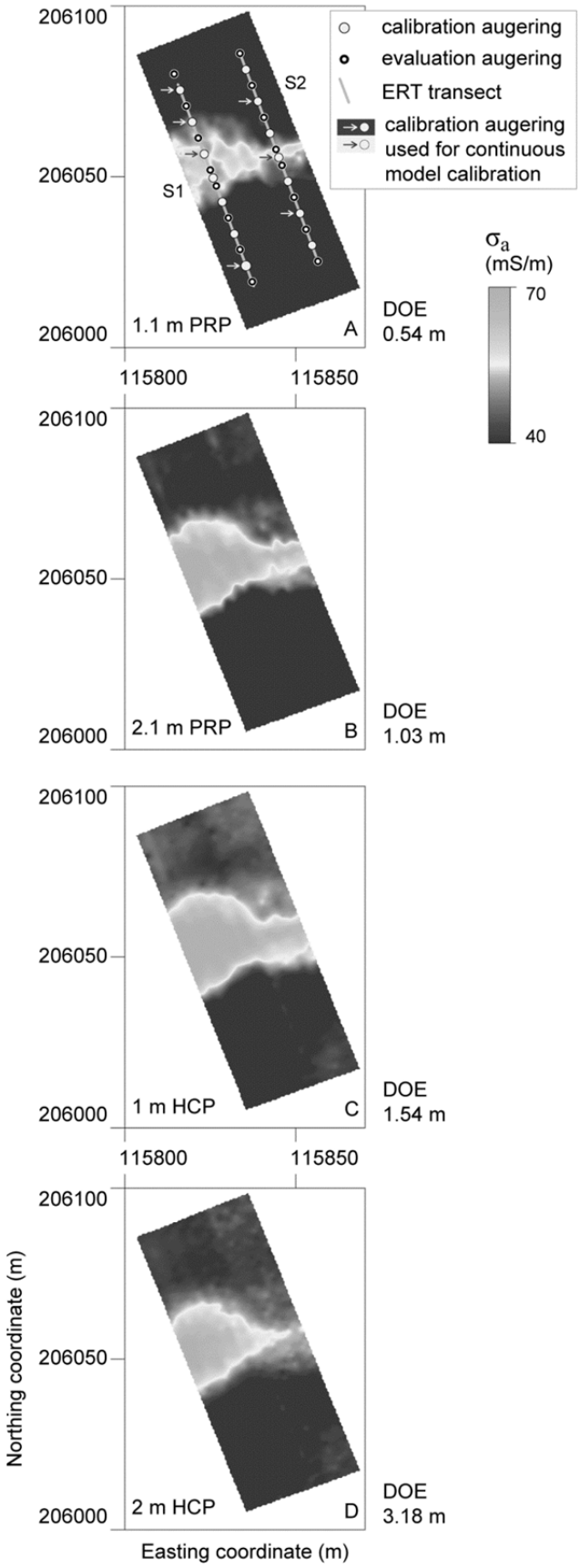

Fig. 22 σ_a maps of each of the four coil configurations of the Dualem-21S EMI sensor. In (A) the auger locations and the ERT transects are also shown.

3.4.3 Modelling the depth of a predefined soil layer

To model the morphology of the palaeochannel, we assumed a two-layered subsurface model. The palaeochannel infillings and the loamy sediments overlaying most of the site were considered as the top layer (i_{top}), while the substrate (i_{sub}) was defined as the Quaternary sand through which the palaeorivers were incised. The objective was to model the depth to i_{sub}, i.e., z_{sub}. Therefore, the contribution of each layer's conductivity to σ_a was considered. Given the conductivity of the top layer (σ_{top}) and the substrate (σ_{sub}), this relationship can be defined by the cumulative response (R) up to z_{sub} for any coil configuration (x) with intercoil separation (s) (McNeill, 1980b; Saey et al., 2009):

$$R_{x,s}(z_{sub}) = \frac{\sigma_a - \sigma_{top}}{\sigma_{sub} - \sigma_{top}} . \quad (3.1)$$

Saey et al. (2008) combined these response functions (equation 3.1), taking the sensor height above the surface (z_α) into account, to predict the depth of a predefined soil layer. For HCP configurations, this predicted depth (z^*_{sub}) can be found with:

$$z^*_{sub} = s\left[\frac{1}{4R_{HCP}(z^*_{sub})^2} - \frac{1}{4}\right]^{0.5} - z_\alpha , \quad (3.2)$$

and for PRP coil configurations with:

$$z^*_{sub} = s\left[\frac{R_{PRP,s}}{\left(2\left(1-R_{PRP}(z^*_{sub})^2\right)\right)^{0.5}}\right] - z_\alpha , \quad (3.3)$$

To obtain z_{sub}, both σ_{top} and σ_{sub} had to be predicted and entered into the modelling equation. A common method to determine these conductivities is EC-probing, but this was impossible because of the high and strongly fluctuating groundwater level at the test site. Therefore, theoretical top layer (σ^t_{top}) and substrate (σ^t_{sub}) conductivity values were modelled by minimizing the difference between the observed z_{sub} and the modelled z^*_{sub} for each coil configuration separately (Saey et al., 2008). To fit the non-linear response curves to the calibration data (i.e. the observed z_{sub}), the Levenberg-Marquardt algorithm (LMA) for non-linear least squares curve-fitting problems was implemented in Matlab (Gavin, 2011; Marquardt, 1963). With LMA, the sum of squares of the error between each of the calibration points and the response functions is minimized. LMA combines the Gradient Descent minimization method, when parameters are far from their optimal value, and the Gauss-Newton method, when the parameters are close to their optimal value, to fit the targeted function to the calibration data (Gavin, 2011).

Next, theoretical response curves were fitted to the calibration data by iteratively adjusting bulk conductivity values (σ^t_a) under the predefined assumptions that σ_{top} is higher

than σ_{sub} and that both layer's conductivity values are homogeneous throughout each section. First, calibration cores were taken over palaeochannel segments to determine z_{sub} (Fig. 23A). For each section, the seven calibration observations were plotted as a function of the measured σ_a at these locations per coil configuration. Next, theoretical response curves were fitted to the calibration data with LMA, by iteratively adjusting the conductivity values under the predefined assumptions that σ_{top} is higher than σ_{sub} and that both layer's conductivity values are homogeneous throughout each section. This way, the smallest sum of squared distance between modelled and observed z_{sub} was obtained (Fig. 23B), and the response functions of each coil pair were fitted to the calibration data (Fig. 23C).

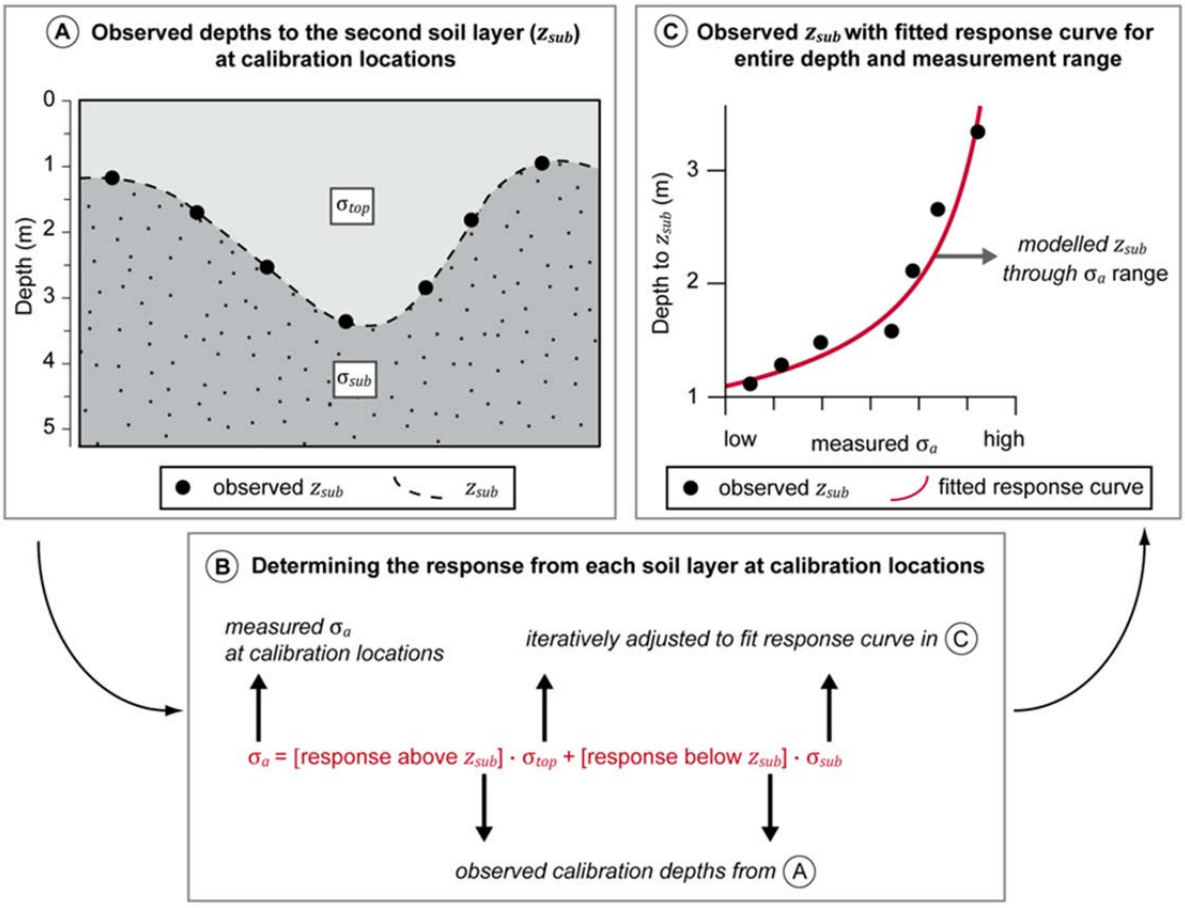

Fig. 23 Schematic representation of the calibration procedure showing the calibration corings used to predict z_{sub} (A), the depth modelling algorithm combined with the obtained calibration depths to determine theoretical σ_{top} and σ_{sub} values (B) and the resulting theoretical response function curve fitted to the calibration data using these obtained σ_{top} and σ_{sub} (C).

These theoretical σ_a were then used to determine z^*_{sub} along both sections. At each measurement location, the four Dualem conductivity values were combined and entered into equation 3.4 per coil pair (x,s) in order to model z^*_{sub}:

$$\sigma_a = \left[R_{x,s}(z_\alpha) - R_{x,s}(z^*_{sub} + z_\alpha)\right] \cdot \sigma^t_{top} + \left[R_{x,s}(z^*_{sub} + z_\alpha)\right] \cdot \sigma^t_{sub} \; . \qquad (3.4)$$

The resulting depth models were then evaluated with auger data from eight locations for each section to determine the correlation coefficient and the RMSE between the modelled and observed substrate depths.

After applying this methodology to both sections, a depth model was composed for the entire test site. Again calibration data from seven locations (Fig 22A) were used to determine σ_{top} and σ_{sub} of the entire site with the same calibration procedure as applied on S1 and S2. The remaining auger data (23 locations) were used for model evaluation.

3.4.4 Results and discussion

The EMI survey revealed the presence of a palaeochannel on all four σ_a maps (Fig. 22A-D). In addition, two lithological profiles were composed based on the auger data (Fig. 24). The laminated deposits of the palaeoriver were made up of silty to loamy sediments overlain with surfacing peat. In S1, these fine-grained infillings were found over a width of 32 m, with a maximum depth to the sandy substrate of 4.6 m. In S2, the palaeochannel's infillings extended over 20 m of the section and were observed to a maximum depth of 1.27 m. Within the channel deposits, marly and organic layers as well as clay bands could be observed. At both sides of the palaeochannel, the slightly silty sand layers that separate the substrate from the loamy plough layer were interpreted as levee deposits. At these locations, the depth of i_{sub} was based on the depth of the levee deposits because of the textural similarities between these deposits and the substrate. In both sections, the transition zone between i_{top} and i_{sub} was marked by a gradual textural change with sand content increasing with depth.

For each section, the seven calibration z_{sub} values were fitted, through the implementation of the LMA non-linear least-squares optimisation in MatLab, to response curves (eq. 3.1) per coil configuration using the modelled σ^t_{top} and σ^t_{sub} (Fig. 23, 25). The resulting depth models were then evaluated with auger data and compared to the ERT pseudosections (Fig. 26). In S1 (Fig. 26, top), model evaluation resulted in a correlation coefficient between z_{sub} and z^*_{sub} of 0.96 and an RMSE of 0.56 m. For S2 (Fig. 26, bottom), a correlation coefficient of 0.97 and an RMSE of 0.11 m were found.

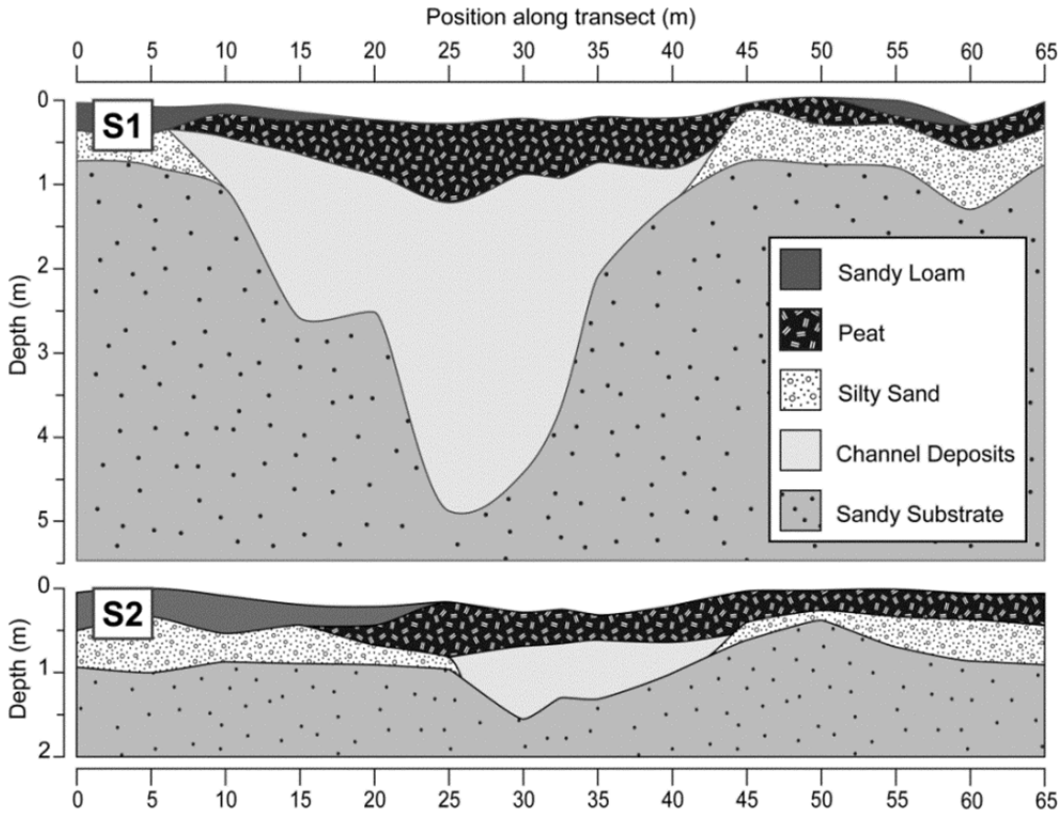

Fig. 24 Schematic lithological profile of the palaeochannel in S1 (top) and S2 (bottom) based on auger data.

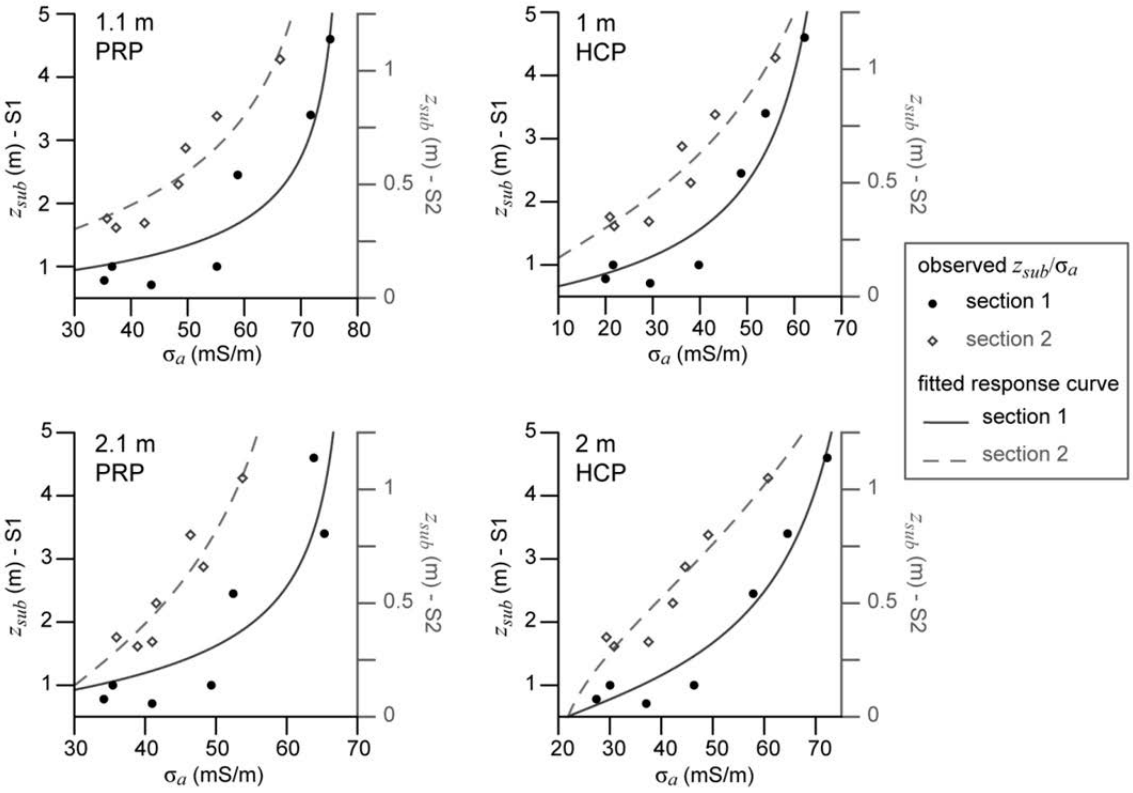

Fig. 25 Observed depths to i_{sub} with observed σ_a at the auger calibration locations with fitted response curves for both sections.

Although the ERT pseudosection for S2 slightly overestimated the palaeochannel depth, ERT data confirmed the modelled morphology for both sections (Fig. 26). However, in S1 the influence of the limited DOE of the sensor could be seen. Compared to the ERT data, this model showed a local deviation around 45-55 m along the transect. In general, local model precision for S1 lessened at increasing depths, but the overall morphology of the palaeochannel was well represented. In S2, depths never surpassed 2 m, which enabled a more precise modelling over the entire depth range. This limitation can be avoided by using multi-receiver EMI sensors with a larger DOE (e.g. Monteiro Santos et al., 2010), but at the cost of a lower measurement resolution.

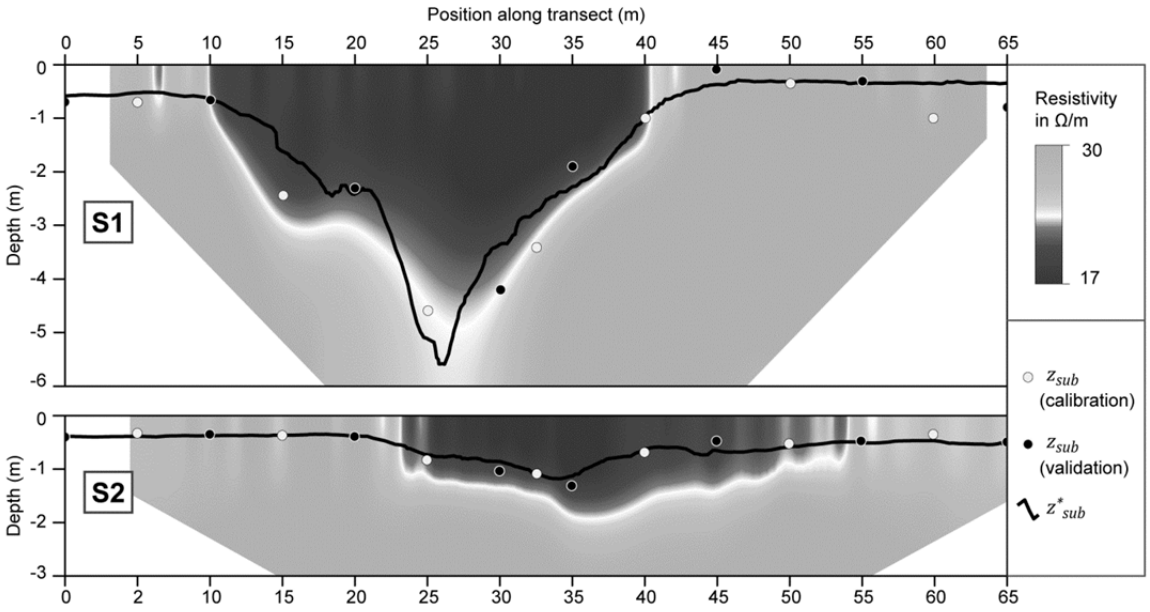

Fig. 26 ERT resistivity profile with observed and modelled palaeochannel depths for S1 (top) and S2 (bottom).

Next we modelled z^*_{sub} for the entire test site. Based on seven calibration values, σ^t_{top} and σ^t_{sub} were determined. The resulting depth model (Fig. 27) was evaluated at the remaining 23 auger locations (Fig. 22A). Fig. 28 shows the correlation between the modelled and the observed depths at these locations. Whereas at small depths z_{sub} was often overestimated in the continuous model, greater depths to the substrate tended to be underestimated, indicating a general smoothing effect of the modelled morphology.

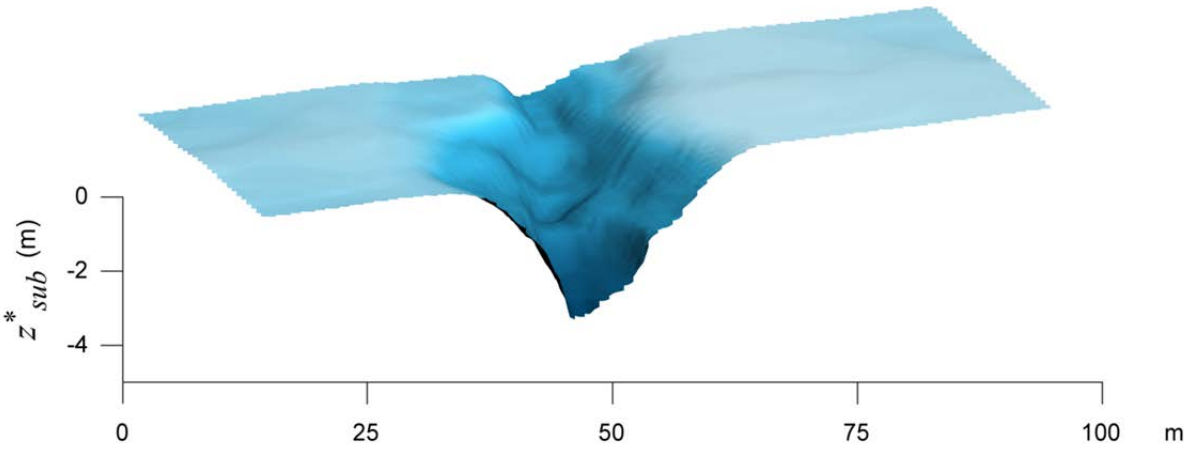

Fig. 27 Continuous depth model of the test site.

Still, a correlation coefficient of 0.93 and an RMSE of 0.41 m between the modelled depths and the evaluation data confirmed the precision of the model in predicting the soil morphology. The model clearly showed the morphology of the site and the width and gradient of the palaeochannel. Even with the sensor's limited DOE, the method allowed to model the depth to predefined soil layers accurately.

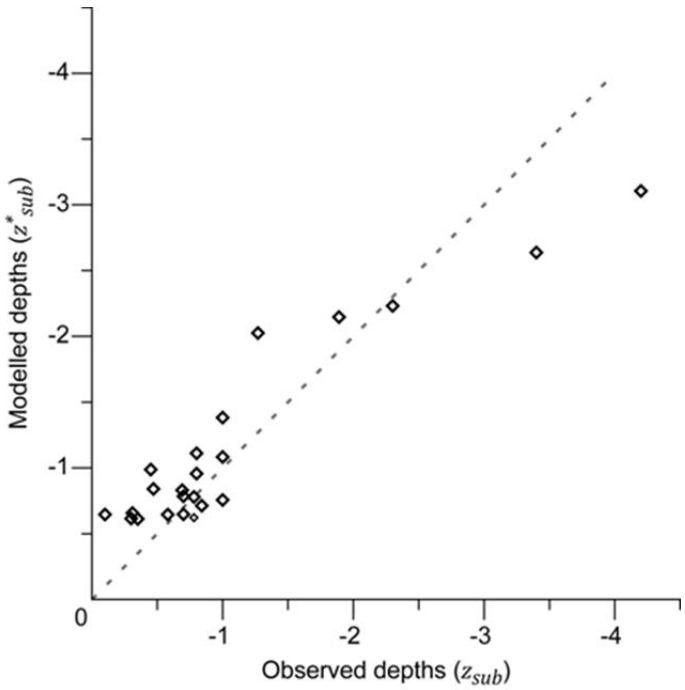

Fig. 28 Scatter plot of the observed and modelled depths for the continuous model.

3.4.5 Evaluation of the inversion procedure in a complex pedological environment

The predicted depth to the substrate along both modelled sections, as well as the continuous model, showed a strong correlation to the evaluation data. Especially by introducing auger data as a calibration method in the modelling process, local precision was added and the accuracy of predicting palaeochannel depths could be extended beyond the instrument's DOE. Combined with the spatial resolution of a mobile survey, multi-receiver EMI allows high-resolution exploration of the shallow subsurface, which is demonstrated by the continuous depth model. However, the general smoothing effect observed in this model hints at the limitations of the method in predicting soil layer depths in complex pedological environments and with depths exceeding the DOE. Despite this drawback, the overall model precision was very good, providing unique insights into the test site's morphology. The presented results show that the mobile multi-receiver EMI survey combined with the proposed modelling sequence can be an efficient tool to map buried sediments and land surfaces. In particular, buried fluvial systems can this way be extensively and accurately traced throughout the landscape.

3.5 Reconstructing late-Glacial and early Holocene landscapes with multi-receiver EMI

3.5.1 Research objective

After evaluating the inversion procedure for reconstructing palaeochannel depth for a small test site, the palaeotopographical reconstruction of a 100 ha area in the Moervaart depression was taken on (Fig. 29). To overcome the limitations of conventional palaeolandscape studies as elaborated in the introduction (section Chapter 3), we propose an integrated methodology combining remote and mobile near surface sensing data with traditional coring. The novelty of this approach lies in the composition of a highly detailed and large-scale geomorphological dataset, whereby a fine lateral resolution is combined with accurate vertical information.

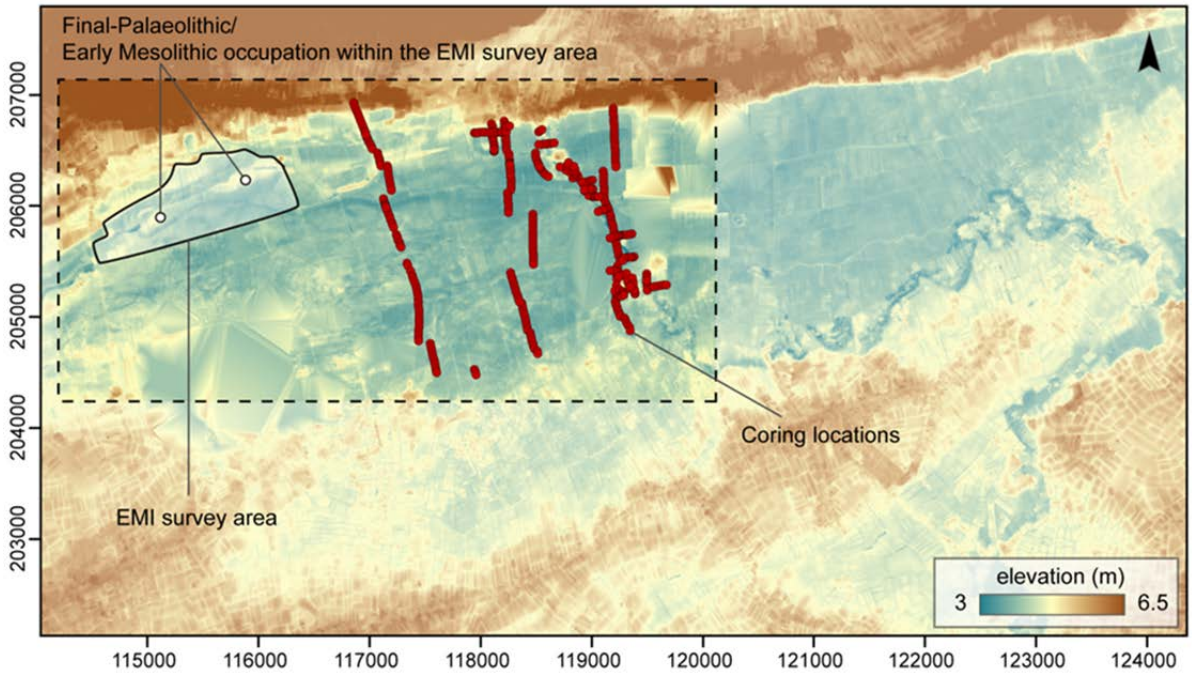

Fig. 29 Filtered digital elevation model of the Moervaart palaeolake (visible as the low-lying area) with indication of the EMI survey area and coring locations (red dots).

The proposed methodology was used in the Moervaart palaeolake in order to gain insight into the overall geomorphological variability and to create high-resolution subsurface models where complex hidden landscapes were expected. Complemented by palaeoecological information, the resulting palaeotopographical data should represent a robust foundation for interpreting prehistoric settlement behaviour.

3.5.2 Survey design and methodology

a. Digital elevation model, historical landscapes and geomorphology.

The basis for the field surveys in the area were high precision airborne LIDAR data, made available by the Flemish GIS agency (AGIV) (Werbrouck et al., 2011), which had an average sample density of 1 point per 2 m^2 and an altimetric accuracy ranging from 7 to 20 cm (AGIV, 2003a). After filtering out artificial features and artefacts by using topographical vector data, manually checking the data, and automatically filtering ditches and field borders through slope analysis, thematic (e.g. soil and geomorphological maps) and historical maps were used as ancillary data in order to estimate the natural pre-19th century topography (Werbrouck et al., 2011). The result was a 2 m x 2 m gridded DEM, excluding the main present-day anthropogenic features (Fig. 21). The data were then used to identify fluvial patterns and large geomorphological features, and to interpret the palaeolake dimensions.

b. Multi-receiver electromagnetic induction survey

The focus of this survey was a zone of approximately 100 ha in the western part of the study area, where the DEM had indicated a braided pattern of small inactive channels (Fig. 29). At two locations, Stone Age assemblages were found, dating to the Final Palaeolithic and the Early Mesolithic (Van Vlaenderen et al., 2006). The high clay content of the area, together with the often water saturated conditions, made geophysical methods targeting electrical resistance or electrical conductivity the most suitable (De Smedt et al., 2011a). As both high lateral resolution and vertical discrimination potential were needed, a mobile configuration with a Dualem-21S sensor was chosen as the primary prospection technique. The mobility of this configuration made it possible to obtain a high sampling density in a time efficient manner by driving across the survey sites along parallel lines, 2 m apart, with an in-line sampling interval of 0.25 cm. This way, over 1 ha was surveyed per hour. After

surveying, the data were interpolated to a 0.25 m by 0.25 m grid using ordinary kriging and plotted in ArcGIS (ESRI) to visualise the lateral soil texture variability.

The multi-layer σ_a dataset enabled the examination of the vertical soil variability. By combining the different σ_a measurements in the depth modelling sequence presented in the previous section, the depth to predefined soil layers can be predicted. To this end, a theoretical two (Saey et al., 2008) or three layered soil model (Saey et al., 2012) can be composed in which the primary contrasting soil layers are isolated in separate model layers. In the palaeolake area, the main objective was to map and trace the depth of different palaeoriver systems. The shallow depth of the channel deposits and overlying peat, which in some cases outcrops in the area, and the difficulty to discriminate between the plough layer and the underlying peat, favoured the use of a two-layered soil model. A two layered soil model was set forth (see section 3.3), combining both the plough layer and the palaeochannel deposits in the first layer (i_{top}), and the sandy substrate in the second (i_{sub}) (Fig. 30).

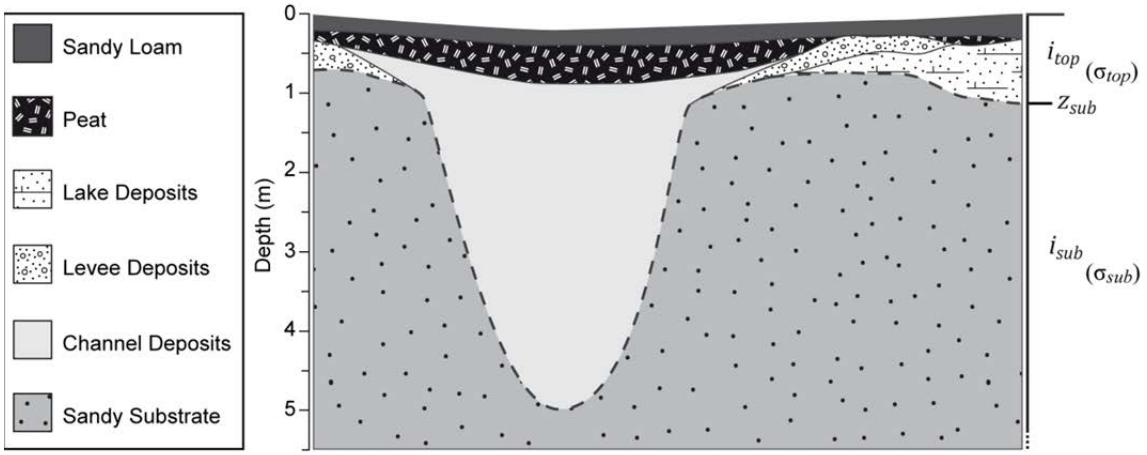

Fig. 30 Example of a two-layered soil model, where the palaeochannel deposits and overlaying soil layers are combined in a first layer (i_{top}) while the sandy substrate is considered as the second layer (i_{sub}).

The combination of the theoretical cumulative response functions of the Dualem-21S coil pairs, derived from McNeill (1980b) and Wait (1962), enabled modelling the depth to i_{sub} (i.e. z_{sub}) (Saey et al., 2008). Using these response functions, the contribution of each layer's σ to the total measured σ_a can be determined. When the conductivity of the first (σ_{top}) and second (σ_{sub}) soil layers are known, z_{sub} can be obtained through equation 3.4.

As discussed in the previous section, the high and strongly fluctuating groundwater level prevented the obtaining of the conductivity values through electrical conductivity-

probing. Theoretical conductivity values for each survey site were therefore modelled through the calibration procedure presented in section 3.4. (De Smedt et al., 2011a; Saey et al., 2008). Based on the theoretical response functions and the obtained σ_{top} and σ_{sub} , z_{sub} could be modelled for the surveyed area. In order to obtain the true depth below the surface, the modelled depths were subtracted from the unfiltered DEM of these areas. The results were filtered using a median filter with a search window of 10 m in diameter, which removed small local variations and outliers.

c. Coring and sampling

To validate and supplement the EMI survey and the proposed depth models, 73 manual coring samples were taken. For validation of the EMI depth models, 23 locations were first set out across a palaeoriver segment so as to evaluate the predicted depths in these sediments (De Smedt et al., 2011a). Secondly, 50 additional validation samples were selected using a conditioned Latin hypercube sampling (cLHS) algorithm (Minasny and McBratney, 2006, 2010). The application of a conditioned selection procedure instead of conventional LHS is preferred as this prevents selecting sample points that do not exist in the real world. LHS allows sampling the full range of the targeted variables through maximally stratifying the distribution. In this process, randomisation is used which can lead to a misrepresentation of the real spatial variability of the targeted variable (Minasny and McBratney, 2006). With cLHS, a selection is made of *n* observations, or sites, from the available dataset that form a Latin hypercube. Subsequently, an optimization problem is solved as formulated by Minasny and McBratney (2006, p. 1381):

> *"… given N sites with ancillary data (x) select n sample sites (n<<N) so that the sampled sites x form a Latin hypercube, or the multivariate distribution of X is maximally stratified."*

This sampling method thus takes into account both the extent of the study area and the variation of an ancillary dataset - the modelled depth. Consequentially, the resulting sample dataset is an efficient replication of the distribution of the modelled depths and their spatial distribution. For further information and examples of the application of cLHS, the reader is referred to Minasny and McBratney (2006 and 2010).

In the deepest part of the palaeochannels, detailed core sampling was performed to enable the dating of the channel deposits. Samples were taken above and below the deposits, dating the sedimentation period. At each sample location, ^{14}C samples were taken from the bottom of the channel lag, in order to obtain a maximum age for the start of the

channel's active phase, and from base of the peat formed above the abandoned channel, dating the end of the sedimentation period.

455 additional core samples were taken east of the EMI survey area (Fig. 29), tracing the different palaeochannels farther through the palaeolake. Here, descriptive coring was conducted every 25 m along north-south oriented transects (Fig. 29) using a 3 cm diameter hand corer or a 7 cm dutch auger, and had a depth range of approximately 1 m to 5 m below the surface (Bats et al., 2009b; Bats et al., 2011; Bats et al., 2010).

3.5.3 Results and interpretation

In the EMI survey area, a total of 60 ha was mapped with the Dualem-21S in 16 days (Fig. 31). The non-surveyed areas were inaccessible due to agricultural activities or forest, leaving a few blind spots in the dataset (Fig. 31B). The overall high σ_a, on average 29 mS/m for the 1 m HCP coil pair, indicating the presence of fine grained, organic and clayey sediments, proved the alluvial nature of the area. While the elevated σ_a values indicated a high organic matter content, slightly clayey deposits and/or calcareous sediments, the lower values indicated more sandy zones. The results confirm the presence of different palaeochannels surrounding small sandy interfluves, as had already been hinted by the DEM results (Fig. 31A). Morphologically, a distinction could be made between the channels in the north and south of the study area. North of the interfluve patches, results indicate that a single-channel fluvial system ran parallel to the southern margin of the Great Ridge of Maldegem-Stekene. This pattern contrasts to that seen in the south, where a system comprised of multiple narrow channels, here interpreted as reflecting an anastomosing fluvial behaviour (cf. Nanson and Knighton, 1996), occurs.

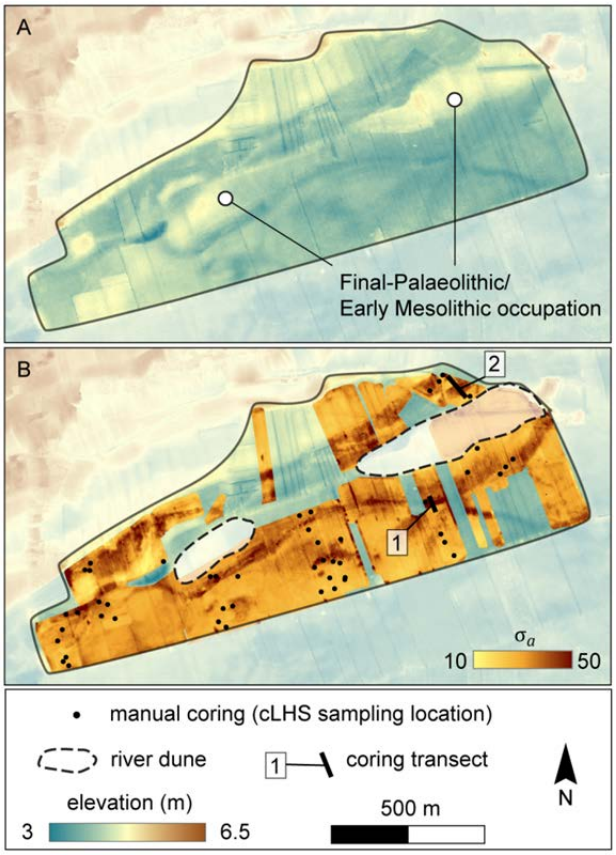

Fig. 31 Digital elevation model of the EMI surveyed area without (A) and with σ_a data from the 1 m HCP coil configuration and indication of further sampling locations (B).

Across palaeoriver segments in the northern and southern palaeoriver channels, 2 x 7 calibration coring locations were set out along transects 1 and 2 (Fig. 31B). These showed that the multiple anastomosing channels to the south (coring transect Fig. 31B) had a laminated sequence with a high silt and $CaCO_3$ content, resembling the palaeolake sediments. The deposits in the northern channels, on the other hand, had a much higher organic matter content with intercalated peat and gyttja layers (coring transect 2, Fig. 31B). Based on this difference in lithology, the geophysical dataset was divided into northern and southern parts. By integrating the coring conducted for initial calibration with the depth modelling procedure, it was possible to predict the depth of the Pleniglacial sand for the entire EMI surveyed area (Fig. 32), rendering modelled depths to the Pleniglacial sand between 0.2 – 4 m below the surface. This procedure was evaluated along a small palaeochannel segment by correlating modelled to observed depths, and proven accurate for modelling the substrate depth below the palaeochannel deposits with a RMSE of 0.41 m (section 3.4.4 and De Smedt et al., 2011a).

The validation with the cLHS selected samples confirmed this accuracy but revealed a larger prediction error outside the palaeochannel deposits, resulting in a RMSE of 0.57 m. This larger error in the area surrounding the palaeochannel segments could be attributed to the configuration of the calibration procedure, which focused on the relationship between the σ_a and z_{sub}. In the surrounding areas, the relationship was altered by the heterogeneity of the lacustrine and alluvial deposits overlaying the sandy substrate, causing a lower model accuracy. A Pearson correlation coefficient of 0.77 was found between the observed and modelled values, confirming the potential of the modelling procedure in reconstructing the distribution of the depth values throughout the survey area. The obtained RMSE of 0.57 m is therefore considered acceptable. Even though the depth variations of the palaeoriver system could be predicted accurately throughout the survey area, a clear description of the flow characteristics of both channel patterns was only partially possible. For one, non-surveyed areas made a detailed discharge analysis impossible, as this requires a continuous dataset. However, based on the depth modelling a distinction could already be made between the northern and the southern palaeochannels. While the individual southern, channels are narrow and shallow, the northern channel is wider and deeper, suggesting a larger drainage capacity of the latter.

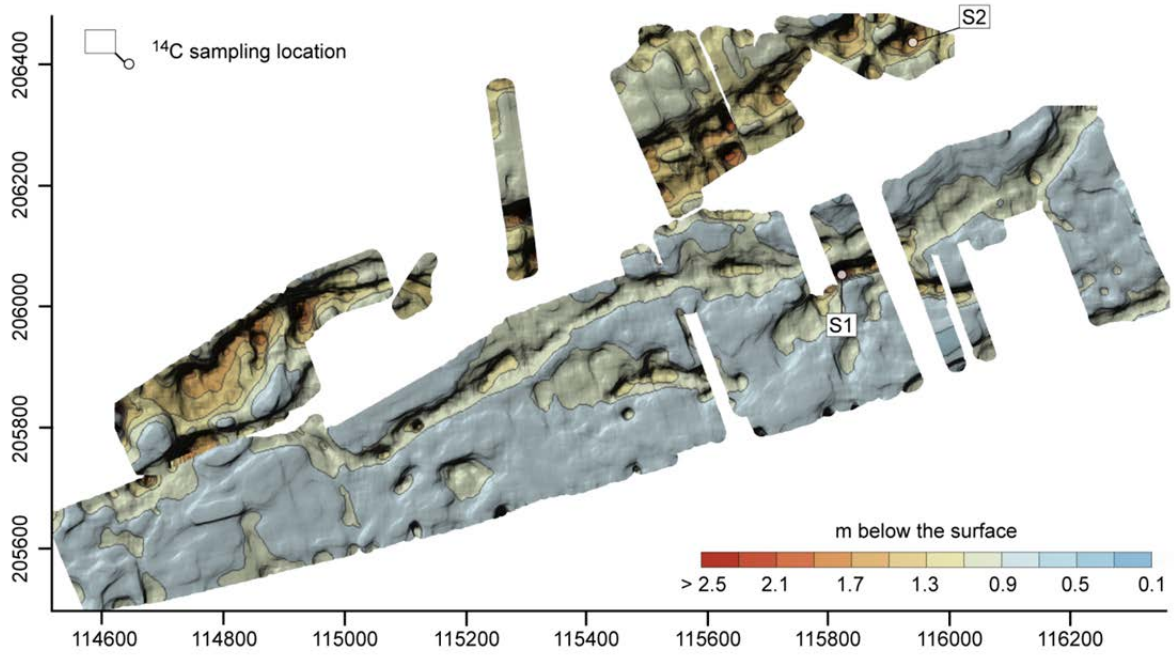

Fig. 32 Depth model of the surveyed area with the ^{14}C sampling locations in the deepest segments of the palaeochannels.

The flow direction of the detected channels was studied by comparing the depth of the different sections of the palaeochannels. Only for the palaeochannels north of the river dunes could an inclination be detected. In the palaeotopographical model (Fig. 32), this was the most visible in the easternmost surveyed fields and indicated a preferential eastward flow for these stream channels. Farther towards the east of the palaeolake, DEM data and coring supported the notion that the straight channels were connected to a meandering palaeoriver, extending to the east and bending towards the south in the central part of the depression (Fig. 33). Here, coring confirmed the eastward inclination as the depth of the channel deposits tilted from around 0.50 m below sea-level in the north to 1.45 m below sea-level in the southeast (i.e. approximately 4.50 m and 5 m below the surface respectively). For the southern palaeochannels, and by extension the anastomosing palaeochannels further south in the area (Fig. 33), a straightforward interpretation of flow direction was more difficult. Apart from a deeper section where two channels of the river system intersected and a westward descent from 1.5 m above to 0.5 m below sea level (2.5 m to 4.5 m below the surface) was detected, no clear declination towards the west or the east was attested.

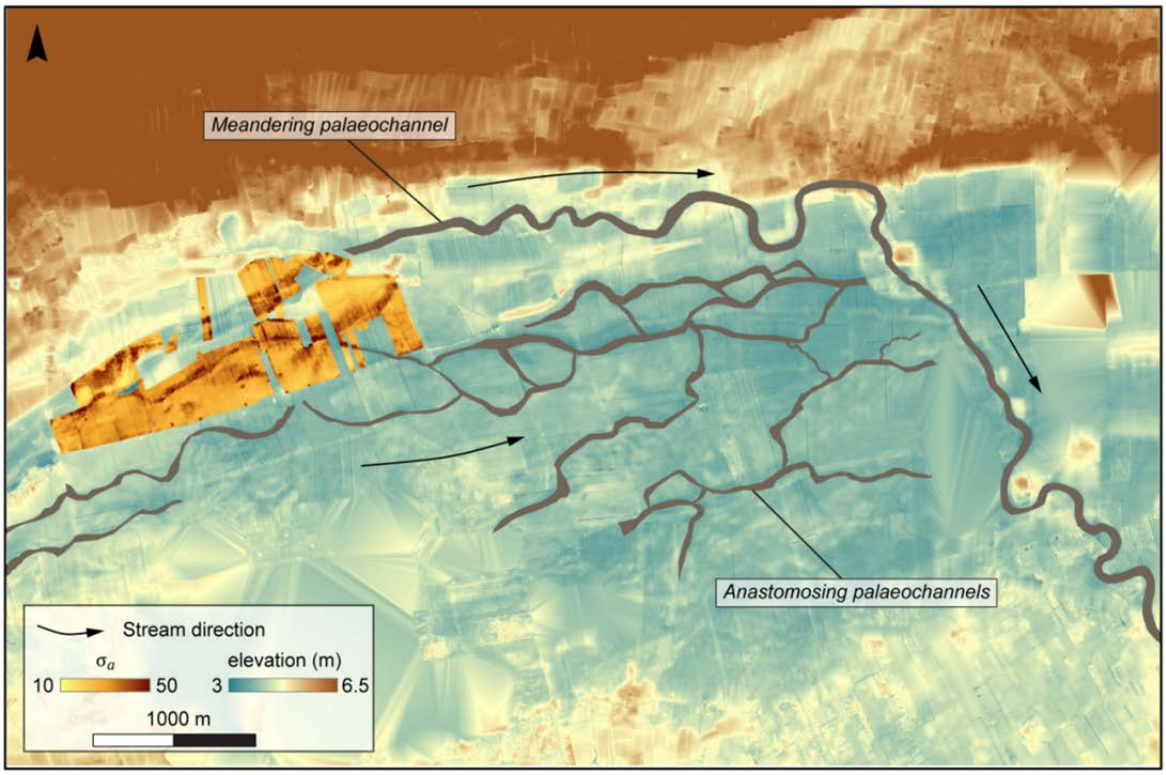

Fig. 33 Overview of the results from the EMI survey (σ_a data from the 1HCP coil configuration) connected to the palaeochannels traced using elevation and coring data, with indication of the stream direction.

Farther east into the area of the palaeolake, this trend was maintained and similar depths of approximately 1.75 m above sea level (1.25 m below the surface) were attested. This negligible slope would have promoted avulsion and aggradation within the multiple-channel system (Richards et al., 1993). However, the palaeotopographical data are unsuitable for detailed reconstructions of palaeoflow direction based on slope alone. Guided by the EMI depth model, ^{14}C dates were obtained from the deepest palaeochannel sections (Fig. 32), which showed a different chronology of both parts of the river system; (Fig. 34) placing the sedimentation of the channel deposits of the anastomosing palaeochannels in the Late Glacial, between the (late) Bølling and the (late) Allerød period (Fig. 34, S1).

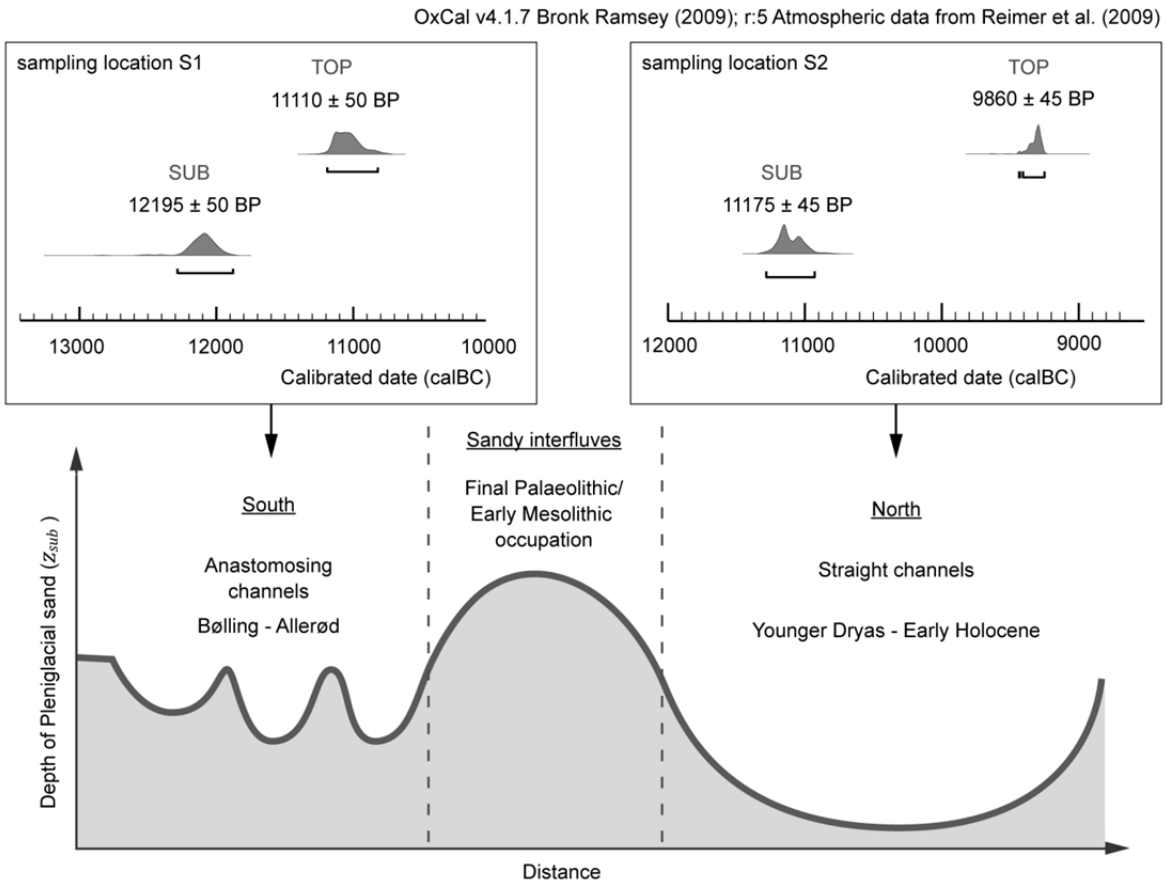

Fig. 34 ^{14}C-dates obtained above (TOP) and below (SUB) the palaeochannel deposits of both the southern (sampling location S1) and the northern (sampling location S2) channels in the surveyed area. Below: Schematic cross-section of the surveyed area showing of the morphology and chronology of the different parts of the palaeoriver system related to the prehistoric occupation of the sandy interfluves.

Channel deposits in the northern palaeochannels were younger, with sedimentation starting in Late Allerød or the Younger Dryas and continuing into the Early Holocene (Fig. 34, S2). Based on these data and the combined results from EMI-survey, coring and DEM analysis, both the channels detected north and south of the sandy interfluve outcrops were interpreted as different stages of channel reorganisation within the same palaeoriver system. The northern channel, with its elevated individual discharge capacity, seems to record the concentration of fluvial flow into a single trunk channel subsequent to the gradual abandonment of the southern anastomosing channels near the end of the Allerød (Fig. 34, bottom). In considering the prehistoric occupation in the survey area, the perpetual Final Palaeolithic to Early Mesolithic occupation phases identified here were contemporary to both phases of the palaeoriver system recorded in the EMI survey data.

3.5.4 Conclusion

A multi-disciplinary approach, combining remote and mobile near-surface sensing techniques with traditional coring, has allowed for a detailed palaeotopographical reconstruction of the study area. The incorporation of a three-dimensional geophysical survey dataset enabled a detailed interpretation of the morphology of the area, whereas coring added lithological information and the digital elevation model offered continuity at a larger scale. However, in very heterogeneous areas where no large depth variations are present in the palaeotopographical record, limitations of the method used become apparent. In this study, this can be seen outside the palaeochannels where the correlation between the modelled and observed depths deteriorates. While the heterogeneity of the areas makes it more difficult to establish a relationship between the palaeotopographical variability and the geophysical data, the palaeotopography itself has limited interpretative potential, especially when dealing with avulsive channel systems. Nevertheless, the use of mobile geophysical techniques with vertical discrimination potential alongside more traditional methods can form a broad basis for interpreting past landscapes and could serve as a guiding tool in covered landscapes where DEM data do not allow a straightforward interpretation of the palaeolandscape. The presented methodology allowed for a detailed reconstruction of the palaeotopography harbouring known Final Palaeolithic and Early Mesolithic occupation sites. Combined with ^{14}C dating, we were able to obtain a detailed view of the changing landscape around these settlements. The simultaneity between the palaeohydrological system and the archaeological remains shows the close relationship between prehistoric settlement locations and the alluvial features in the area. Despite the drastic change in drainage system, from a multi-channel system during the (late) Bølling and the (late) Allerød period to a single deep gully system in the Late Allerød/Younger Dryas and continuing into the Early Holocene, both sandy interfluves remained attractive for human occupation throughout the Final Palaeolithic (*Federmesser*) and Early Mesolithic. In order to develop a deeper understanding of the driving mechanisms for settlement patterns in the entire palaeolake area, a fuller description and reconstruction of its palaeotopographical and hydrological evolution is vital. It is the combination of these new and revisited survey methods, and their integration alongside palaeoecological and chronological techniques, that can offer a more complete foundation for interpreting prehistoric human-landscape interactions.

Chapter 4

Mapping anthropogenic soil variation with EMI

The content of this chapter is based on:

> De Clercq, W., De Smedt, P. et al., 2012. Towards an Integrated Methodology for Assessing Rural Settlement Landscapes in the Belgian Lowlands. *Archaeological Prospection*, 19, 141-145

and

> De Smedt, P., et al., Comparing apparent magnetic susceptibility measurements of a multi-receiver EMI sensor to topsoil and profile magnetic susceptibility data over weak magnetic anomalies. *Submitted to Archaeological Prospection.*

4.1 Introduction

4.1.1 Towards an integrated archaeogeophysical prospection?

The shift from a largely academic framework for archaeological investigations to a developer-led archaeology during the past 20 years, has resulted in an overwhelming increase in archaeological evaluation surveys (De Clercq et al., 2011). Combined with technological advances and their commercialization, this evolution stimulates the application of geophysical techniques as a standard part of site assessment in Western Europe (Jordan, 2009). However, whereas the archaeological and pedological

characteristics of the evaluated sites are seldom alike, the applied geophysical methodologies remain rather uniform.

Today, the three main survey techniques are GPR, electrical resistivity measurements, and magnetometry, which indisputably dominates the archaeogeophysical toolbox (Gaffney, 2008). The almost dogmatic application of magnetometry, has pushed the importance of detailed soil mapping to the background, as in these surveys no significant information is gathered about the pedology of surveyed sites. Nevertheless, especially within a commercial framework exhaustive mapping techniques are needed that can offer insight into archaeological as well as pedological and geomorphological variations. As geophysical techniques are usually deployed during the first phases of a site evaluation, the incorporation of accurate pedological analyses, or the lack thereof, can have a major impact on the entire further evaluation process. Here, the application of different methodologies, e.g. magnetic and electrical techniques, can offer an outcome, but particularly in commercial programmes, multiplying survey runs is not always an option.

The introduction of EMI instruments with 'Slingram' geometry that enabled recording both the IP and QP component of the EMI signal response seemed to offer an efficient solution. Whereas the σ_a measurements record information about the textural variability, soil organic matter content and moisture content, the κ_a measurements enables detecting anthropogenic disturbances comparable to the potential of magnetometry (see section 2.3).

4.1.2 EMI and archaeogeophysical prospection

EMI instruments have a somewhat peculiar place within the archaeogeophysical toolbox. The earliest EMI surveys in archaeology were conducted with so-called soil conductivity meters (Howell, 1966). However, contrary to what the instrument name suggests, these instruments measured mainly changes in magnetic susceptibility (Tite and Mullins, 1970). From the 1980s onwards, it was mainly the research of Prof. Alain Tabbagh that showed the potential of EMI survey in archaeology. Through theoretical studies and field tests different sensor configurations were compared, and the impact of using different coil configurations for recording archaeological features was investigated (Tabbagh, 1984; 1985; 1986b).

Although the initial application of EMI instruments in archaeology started in the 1960s (Scollar, 1962 and 1990), these were quickly overshadowed by the adaptation of magnetometer and electrical resistance surveying (Gaffney, 2008). However, in soil science and exploration geophysics the use of EMI persisted and led to a number of

technological advances (e.g. Abdu et al., 2007; Fraser, 1972; Slavich and Petterson, 1990). The development of instruments allowing to simultaneously record the IP and QP signal response along with the first multi-receiver EMI soil sensors, have increased the potential of these instruments for archaeological prospection. Nevertheless, a number of operational and interpretational difficulties inherent to EMI survey, such as the limited penetration depth (Dalan, 2008; Henry, 2011) and difficult interpretation (Simpson et al., 2010) of the IP response, along with the sometimes capricious calibration procedures of these instruments, have made EMI a rare first choice in archaeological prospections.

Over the past years, research efforts into the application multi-receiver EMI sensors to archaeology have increased substantially. Starting with detailed studies of the detection potential of such instruments (Simpson et al., 2009b) to the integration of multiple, simultaneous electrical conductivity measurements into inversion procedures (see Chapter 3 and De Smedt et al., 2011a; Saey et al., 2011; Saey et al., 2008), these studies showed the potential of EMI to study soil variations in three dimensions. However, the main aim of these studies has been on combining and analysing the multiple σ_a measurements. The added value of multiple κ_a measurements, on the other hand, has been less investigated. Even though ground-breaking work has been conducted on the use of Slingram EMI sensors of mapping magnetic anomalies (e.g. Benech and Marmet, 1999; Tabbagh, 1984; Tabbagh, 1986a), and on the comparison between different magnetic survey techniques (Linford, 1998),the added value of multiple κ_a measurements has been less investigated.

In this chapter, focus will be mainly on the analysis and interpretation of multiple κ_a datasets, gathered with the Dualem-21S sensor. In a first section, results from different survey methods and multi-receiver EMI data will be compared. In the second part, the representativity of multiple simultaneous κ_a-measurements for vertical and lateral variations in soil magnetic susceptibility κ[5] is investigated.

[5] In the following chapter, a distinction is made between apparent magnetic susceptibility measurements (κ_a) from the EMI sensor and magnetic susceptibility (κ) data from the Bartington MS2 meter when used in combination with the MS2H downhole probe whereby 'apparent' is omitted (i.e. the subscript 'a').

4.2 Developing an integrated, non-invasive survey approach for evaluating past rural settlement landscapes

4.2.1 Research context and study area

The north-western part of Belgium is made up of lowlands that were densely occupied throughout history, with a considerable development during the Roman and Medieval periods. With important towns such as Ghent, Ypres and Bruges, the region was in medieval times amongst the most densely populated in Europe between the 11th and the 15th century. This high density of city-dwellers had a profound impact on the landscape surrounding the cities, as is testified by historic text-sources and maps (Verhulst, 1995; 1999), resulting in the creation of farms and the reclamation of forests and waste lands to develop agriculture. Unfortunately, the exact morphology and evolution of this rural settlement pattern as well as the wider natural and cultural landscape in which it was integrated, have remained poorly understood archaeologically. Similarly, earlier forms of rural settlement (e.g. dating from the Roman period), have also remained largely unknown until recently. More and more parts of these historical landscapes have emerged during the last decade, allowing a first synthesis of the Roman period (De Clercq, 2011). However, scientific archaeological study of these landscapes remains rare and important questions relating to their landscape-context and structural evolution remain largely unanswered. From a heritage point of view, assessing and defining settlement areas, and making scientifically based choices as to the strategies needed to map and understand the farm-complexes is often problematic, especially in the framework of making choices for ex-situ preservation by excavation. Moreover, a danger of circular reasoning and the loss of important information emerges when evaluation strategies remain almost solemnly based on densities of features and not on an integrated evaluation of landscape-context, structure, density and quality of the features detected, leaving low-density farms complexes undiscovered. An academic as well as a heritage management challenge lies therefore at the basis of our research. In combining different datasets and methods, our main goal is to develop an efficient integrated archaeogeophysical approach towards the evaluation and characterisation of these rural landscapes, and to reconstruct the evolution of their reclamation and use. In this section, the methodological aspects and first results are discussed.

4.2.2 Methods and research strategy

Previous archaeogeophysical studies in Belgian lowlands focused on smaller phenomena such as a burial mounds or a small castles (Simpson et al., 2009a; Simpson et al., 2009b) or on large-scale landscape-assessment (Bats et al., 2010; De Smedt et al., 2011a). Geophysical techniques such as EMI and GPR, often applied in characterizing soil variability, are now deployed more frequently on archaeological sites. EMI in particular adds to the understanding of these rural environments as it enables a detailed and straightforward analysis of the pedological context (Rhoades et al., 1976; Sudduth et al., 2005)

An important asset for the knowledge of rural landscapes in Historic Flanders and also for the interpretation of geophysical data is a dataset of 70,000 aerial pictures, mostly of crop-marks, gathered since the 1970s and which is still being updated at the Department of Archaeology at Ghent University (Bourgeois et al., 2005; Bourgeois et al., 2002). This dataset offers a wide coverage of the north-west Flemish landscape, especially in the area between Ghent, Ypres and Bruges, the historic heart of medieval Flanders. Data from these photos as well as from different geophysical methods, historic sources (e.g. maps and written documents) and detailed fieldwalking will be gathered to develop a large-scale archaeogeophysical methodology stepping beyond previous small-scale or single-technique approaches. This will lead to a composed multi-layered image of the natural and human landscape, also allowing a comparison with excavated data and the evaluation of the methods used. In a further stage, trial trenching will be used for evaluation of the applied methods.

For our test-case, a region of some 50 ha was selected west of the village of Maldegem-Kleit, in the north-western part of Belgium (Fig. 35). The soil substrate in the area is made up from Eocene marine clay and is overlain with Quaternary aeolian sand deposits, which often are only a few centimetres thick.

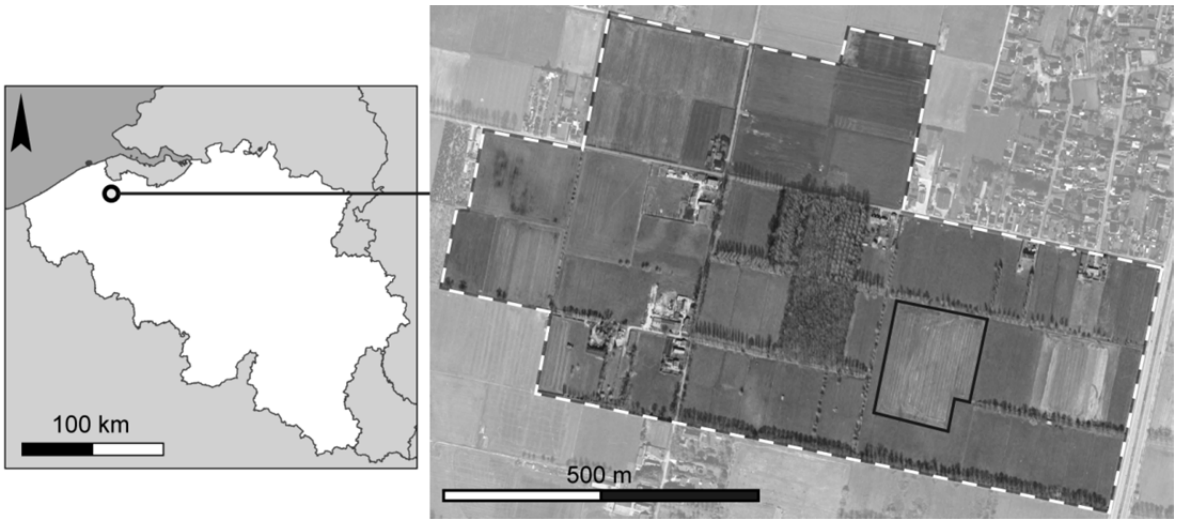

Fig. 35 Location of the study area in Belgium (left) and an orthophoto of the study area (AGIV, 2003). The white dashed line delineates the entire study area, the test field discussed here is delineated by the black line.

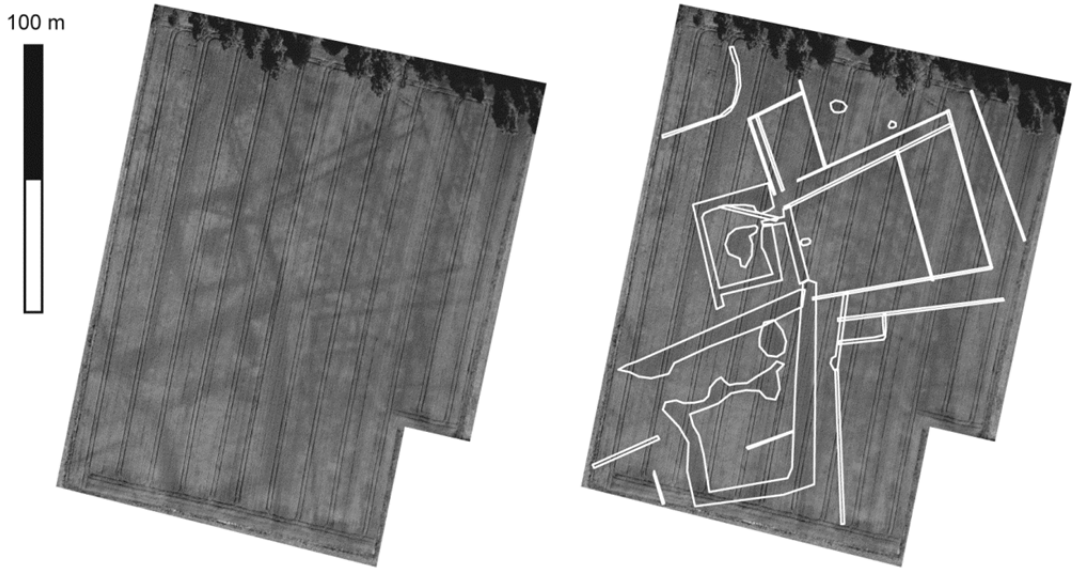

Fig. 36 Aerial photograph of the studied field, taken on June 4th 2010. In the picture on the right, the visible archaeological features are delineated by the white lines (Aerial photo n° 553546, Department of Archaeology, Ghent University).

The slightly undulating landscape was once part of the "Maldegemvelt", a large area of poor wasteland lying in between Ghent and Bruges, which was only definitively cultivated in the 18th century but contains important phases of reclamation during Roman and

Medieval times. The first archaeological features in this test-region were discovered in 1987 during an aerial photographic survey. A systematic follow-up of the site led to a dataset of 205 images taken under varying circumstances. These images revealed several enclosures, individual features and linear structures, visible as crop or soil marks, which were vectorised in a GIS-environment. One 3 ha field with a particularly high density of crop marks, revealing enclosures, ditches and possible pits and wells (Fig. 35 and Fig. 36), was selected as a primary test site to evaluate the use of different non-invasive survey methods. On this field, the topsoil has an overall larger sand content (nearly 80% of sand) while the underlying clay layers consist of some 65% of clay (Saey et al., 2013).

In a second stage, these data were compared to the results from two different geophysical methods (fluxgate gradiometer and EMI), to produce a broader insight into the detected features as well as to provide a mutual calibration of the observations made. An important objective is to gain insight into the landscape setting of the observed features and to examine the relationship between the pedology of the site and the visibility of features on aerial pictures.

Prior to the EMI survey, a magnetometer survey was performed by Peter Masters (Cranfield University) using a Bartington Grad 601-2 fluxgate gradiometer (De Clercq et al., 2012). The zigzag traverse method of survey was used with readings taken at 0.25 m intervals along 1 m wide spaced lines in grid squares of 30 m x 30 m. The data were then processed using Archeosurveyor v.2, and have been enhanced by clipping to remove extreme data point values, destriped to compensate for the directional effects that are inherent to vector magnetometer instruments, and interpolated in the X and Y direction with ordinary kriging.

Subsequently, detailed multi-receiver EMI survey was conducted using the Dualem-21s sensor in a mobile configuration. Measurements were taken along parallel lines, 0.75 m apart, with an in-line resolution of 0.25 m. In this section, the shallow σ_a measurements of the 1.1 m PRP coil pair, representative for a soil volume between 0 - 0.5 m, will be discussed. For the κ_a data, the focus will also be on the shallow measurements of the 1 m HCP coil pair (see section 4.3.2 and Simpson et al., 2010 for further information on the depth response of the IP signal component of this coil configuration). The κ_a values, expressed in dimensionless magnetic susceptibility units (msu), were calculated from the IP-response of each of the Dualem-21S coil pairs following equation 2.16 (section 2.1.4). All data were corrected for instrument drift and interpolated using ordinary kriging (see section 2.5.3).

4.2.3 Preliminary results

The fluxgate gradiometer survey revealed an overall low magnetic variability, ranging from -0.43 to +0.43 nT, and allowed for detecting a number of small ditches (Fig. 37A). The most prominent features in the magnetometer data could be related to the main enclosure seen on the aerial photographs (Fig. 36). However, based on these data it was not possible to further reconstruct the site's layout. The multi-receiver EMI data showed a clearer image of the features in the southern part of the field. The σ_a maps revealed the large structures visible on the aerial photographs (Fig. 37B). Furthermore, a number of different ditches and other features that did not show up on the aerial photographs were detected, indicating a different physical nature or varying depth of these anomalies. The observed contrast between the more resistive infilling and the sandy-to-clayey matrix, indicates a sandy infilling of the ditches. Saey et al. (2011) indicate that further processing, e.g. σ-slicing, may allow a clearer delineation of the archaeological features, which may facilitate a more detailed interpretation. This type of data analysis will be investigated in a later stage of the project. In addition to the archaeological anomalies that were detected, the σ_a data also revealed the pedological heterogeneity of the site. In the northern and eastern part of the field the 1.1 m PRP conductivity data show a strong increase in σ_a, indicating surfacing Eocene clay. On the other hand, the low conductive central part of the field indicates that a substantial amount sand was deposited on top of the Eocene clay (see Fig. 37 B and section 4.3.1). In the clayey environment, such more sandy locations offer a larger drainage capacity compared to the more impervious clay, making these locations more suited for human occupation.

The κ_a data (Fig. 37C) clearly show the structures and the main enclosure in the southern part of the site, visible as broad traces of increased susceptibility. These are likely caused by magnetic enhancement following the anthropogenic disturbance of the site based on the relatively low κ_a values and the less successful magnetometry results as, for example, attested by Linford (1994) at Yarnton, Oxfordshire (UK). On a number of locations where magnetometer survey also detected the magnetic ditch infilling, heating of soil might have further contributed to the magnetic signature of the features.

Apart from the enclosure ditches, a number of high κ_a zones could be distinguished that may be attributed to occupation zones, wells or pits. Furthermore, a large number of small anomalies with an elevated κ_a were detected scattered over the field, which most likely relate to magnetic rubble in the plough layer.

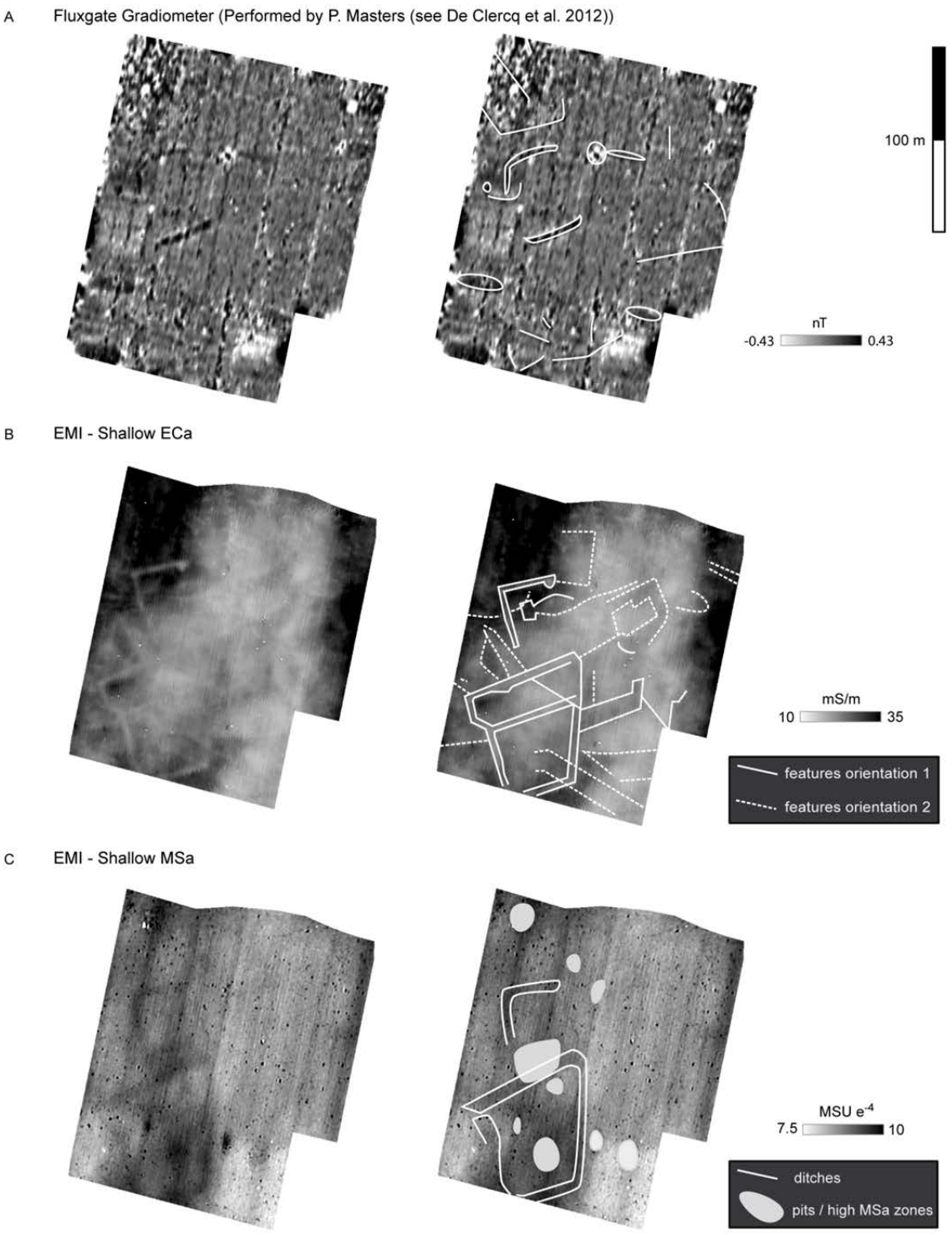

Fig. 37 Geophysical data of the field studied without (left) and with indication of the main anomalies and traces of the main enclosure (ME) seen in Figure 2 (right): (A) fluxgate gradiometer data, (B) shallow σ_a data (1.1 m PRP coil pair) and (C) shallow κ_a data (1 m HCP coil pair).

The clear visualization of the enclosure ditches in the κ_a data, illustrates the difference in detection potential between magnetic susceptibility measurements of the EMI sensor and the passive magnetometer survey. Whereas mainly abrupt changes in magnetization are recorded with the fluxgate gradiometer, the EMI based κ_a measurements allow detecting magnetic features with more diffuse boundaries (Dalan, 2008). Especially when dealing with subtle archaeological soil variability and not with, for example, stone architecture, κ_a measurements can be a valuable addition to the survey dataset.

4.2.4 Discussion

The first results of the visual analysis of the aerial photographs and geophysical surveys of the research area are promising. Geophysical methods affirm the high density of archaeological features seen on the aerial imagery, and add information on the composition of the detected anomalies. Although magnetometer survey did not provide significant insight, the EMI data suggested different occupation phases, based on the differing orientation of the detected features. Moreover, these data revealed different features than those rendered by the crop and soil marks. Based on the different survey data, it can be concluded that no massive (e.g. brick) structures are present at the site, but only 'negative' anomalies, which were excavated in the soil. In addition, a strong natural soil variation was recorded at the site that must have contributed to the selection of the site location.

A preliminary interpretation of the features suggests the presence of a multi-period settlement area. The complex structure of the site, combining at least three large enclosures is unknown in the region, which makes it hard to interpret the site functionally and chronologically solely based on aerial photographs or geophysical data (i.e. on the morphology of the detected archaeological traces). Therefore, it inquires a comprehensive approach to understand its role in the rural exploitation of the landscape. Based on recently excavated sites in the wider region, a High Medieval date can be suggested for the large enclosure. However, the rectilinear narrow ditches, shaping a trapezoidal enclosed area, suggest a Roman date as known from other regions (e.g. Northern France: Agache, 1978). To aid in obtaining a clearer chronological framework for the site, a first step will exist in analysing the material collected during the on-going fieldwalking campaigns (see also section 4.3).

The comparison of the first non-invasive prospection data shows that the aerial photography data offer the most straightforward insight into the archaeological variation and layout of the study site. It should, however, be noted that the presented

orthophotograph is the product of multiple aerial surveys taken through the course of the past three years. On the other hand, the geophysical data were gathered during one survey run per method. To conduct a more integral reconstruction of the site, starting from – and primarily based on – non-invasive survey data, the integration of various prospection data is of paramount importance. The complementarity of these different data types is demonstrated by this case study. However, following the poor interpretability of the magnetometry data, evaluating the full potential of magnetometer survey in the research area requires and for these specific archaeological contexts requires additional prospection over a larger area.

To allow a detailed archaeological reconstruction, the integration of excavation data remains pivotal. Without such data, composing a robust chronological framework is impossible, especially without the availability of detailed historical information. Furthermore, and among other things, an accurate functional site interpretation and the validation of non-invasive survey data requires true ground information, which is why based on the collected prospection data only a preliminary archaeological interpretation can be made.

In the following section, a more elaborate interpretation of the κ_a data will be taken on, along with an evaluation of the potential of the EMI derived κ_a data for discriminating subtle magnetic soil variations. In Chapter 5, the integration of true ground (excavation) data and geophysical survey results will discussed further.

4.3 Mapping subtle magnetic soil variations with multi-receiver EMI

4.3.1 Research objectives

In addition to the geophysical survey and aerial photography presented in 4.2, two fieldwalking campaigns were conducted on the Maldegem test site along with a more detailed analysis of the palaeotopographical variations based on the EMI data and the depth modelling procedure presented in the previous chapter (Saey et al., 2013). The fieldwalking rendered a large amount of surface finds related to the different enclosures (Fig. 38A). Apart from the large amount of archaeological features of the site, the EMI survey revealed a significant palaeotopographical variation, which was instrumental in the choice of settlement location (see also section 4.2.3). In the northern and central parts of the field, a depression was detected in the Eocene clay, which was filled up with a 1.5 m thick layer of aeolian quaternary sand (Fig. 38B).

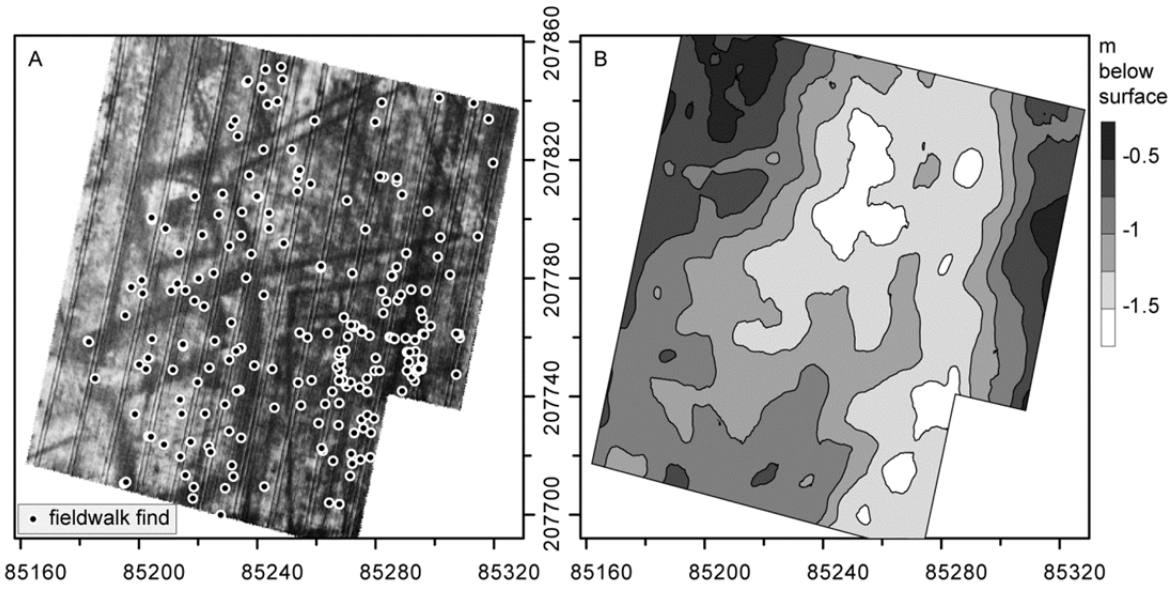

Fig. 38 Aerial orthophotograph of the study field, taken on the 4th of June, 2010 (Aerial photo n° 553546, Department of Archaeology, Ghent University) with indication of the fieldwalk finds (A), and palaeotopography of the site: depth to the Eocene clay below the sand (Saey et al., 2013) (B).

As a continuation of the research presented in 4.2, the detailed interpretation of the EMI κ_a measurements is taken on here. While EMI survey showed that the average σ_a of the test site was relatively high (57 mS/m for the 1 m HCP coil configuration and 88 mS/m for the 2 m HCP coil configuration), the required conditions for effective EMI surveying

were met, as these accord with the LIN conditions (Callegary et al., 2007 and McNeill, 1980) described in section 2.1.4. This indicates that the IP and QP signal components should accurately represent κ_a and σ_a variations, respectively. Through comparison with detailed magnetic susceptibility survey, fieldwalking results and lithological information, the lateral and vertical and lateral discrimination potential of the EMI κ_a measurements will be evaluated. More specifically, the representation of the IP EMI signal response for actual variations in soil magnetic susceptibility will be investigated.

4.3.2 Multi-volume κ_a measurements

For the IP signal response of the Dualem 21-S coil pairs, the cumulative depth responses vary from approximately 1 m to 1.5 m below the sensor for the HCP coil pairs, and from 0.6 m to 1.2 m below the sensor for the PRP coil pairs, based on the theoretical response functions (Simpson et al., 2010) and experimental observations. These soil volumes encompass the depth range of archaeological features in most archaeological surveys (exceptions include sedimentation areas). Furthermore, a multi-volume survey enables differentiating between topsoil κ_a and the κ_a of deeper soil layers.

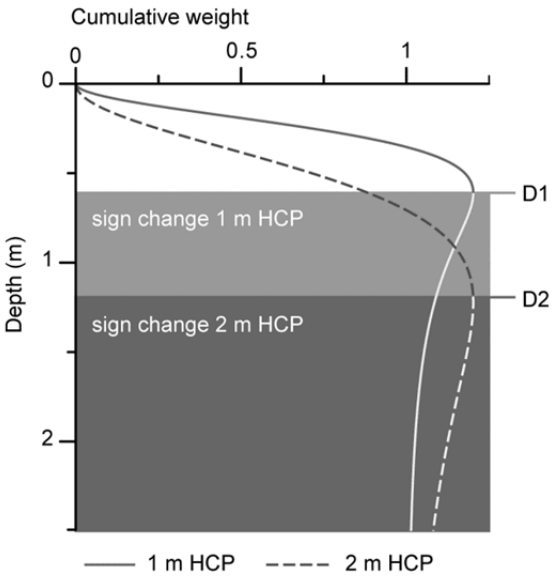

Fig. 39 Cumulative depth response of in-phase response of the 1 m and 2 m HCP coil pairs. D1 and D2 represent the critical depth for the 1 m and 2 m HCP configuration respectively, where the signal response inverts.

There are a number of downsides inherent to the HCP and PRP coil configurations. Whereas HCP coil pairs enable very stable IP measurements, the cumulative response of these configurations has a signal change below a certain depth (Fig. 39). As a consequence, highly magnetic anomalies that are below this critical depth, but still fall within the detectable range of the coil pair, appear as anomalies with a reduced κ_a within the surrounding area and vice-versa (Simpson et al., 2010). For the Dualem-21S sensor, this critical depth is approximately 0.6 m for the 1 m HCP coil pair (D1 on Fig. 39) and 1.2 m for the 2 m HCP coil pair (D2 on Fig. 39). Based on these critical depths, it can be concluded that all detected archaeological features presented in this case study occur at shallow depths (i.e. above the 1 m HCP critical depth of 0.6 m). When an anomaly is

situated deeper below the soil surface, and given the relative susceptibility (i.e. high or low) of the measured anomaly, further analysis of the HCP κ_a data can to a certain extent allow qualitatively interpreting the feature's depth when taking the critical depths of multiple HCP coil pairs into account. An example of such a qualitative depth interpretation is presented in the Appendix.

In PRP orientation, the IP response suffers less from signal change (Simpson et al., 2010), but in field conditions these measurements are often unstable, which makes them less suited for visualising archaeological features. For example, when the magnetic contrast between features is low, and in environments with a lot of magnetic background variations (such as heterogeneous soil mineralogy or the presence of ferrous utility pipes) the interpretation of the PRP IP response can be hampered by instrument-induced noise.

At the test site, the PRP data suffered from a poor signal to noise ratio. Apart from a number of linear features that were attributed to recent agricultural activities, interpretation of all PRP datasets was hindered by a distinct salt-and-pepper noise (Fig. 40A). Results for the 1 m and 2 m HCP coil configurations (Fig. 40B, C), on the other hand, proved the discrimination potential of the EMI κ_a measurements. Comparison of these data to a magnetometry survey at the site showed that the κ_a measurements allowed a more straightforward interpretation of the detected archaeological features (see section 4.2). The magnetometry results did not allow for a reconstruction of the layout of the site. With EMI, two large enclosures could be discerned on the 1 m HCP κ_a data along with a number of pits and ditches. However, a discrepancy remained between the geophysical results and the aerial photographs as nearly 50% of the archaeological features seen from the air did not show up in the magnetometry or the κ_a data. In the 2 m HCP κ_a data, only few archaeological traces were visible, indicating the shallow depth extent of the features. Here, more background variation, i.e. a larger underlying trend in κ_a, was observed, coinciding with the pedological and palaeotopographical variation witnessed in the σ_a measurements (Fig. 37B and Fig. 40B). Apart from the apparently deeper parts of the detected enclosures, the detected magnetic anomalies were weak; rendering a maximum κ_a of 0.0016 msu for the 1 m HCP coil pair and of 0.0041 msu for the 2 m HCP coil pair in the EMI data.

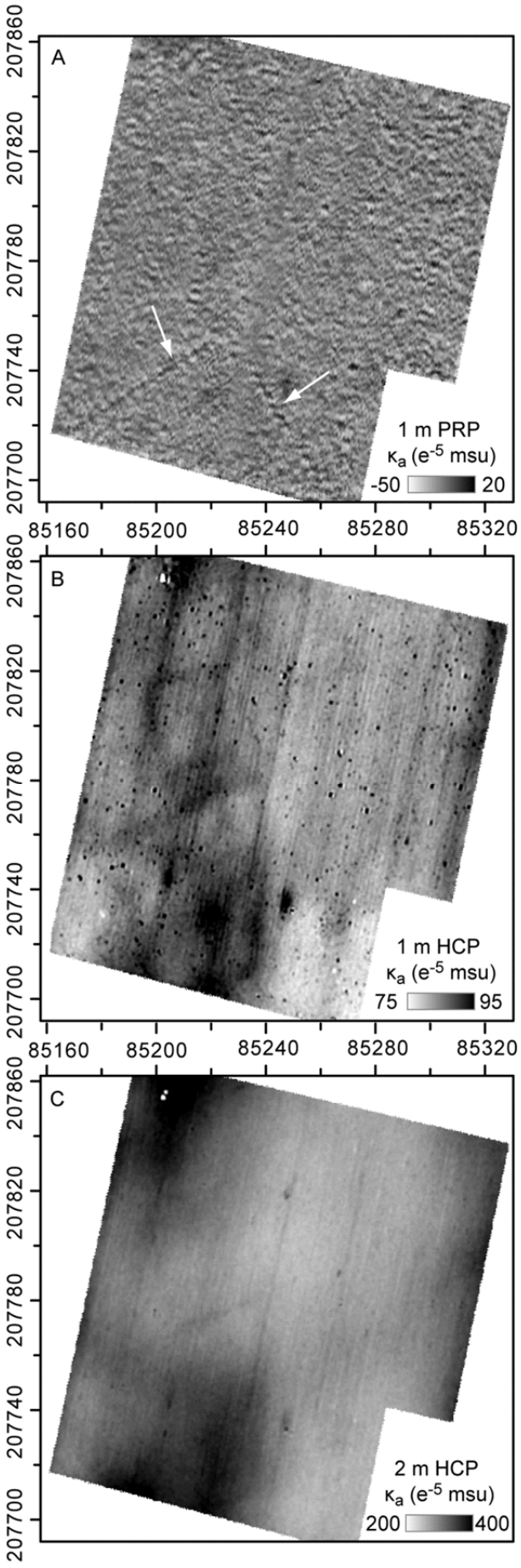

Fig. 40 κ_a-data from the 1 m PRP (A), 1 m HCP (B) and 2 m HCP (C) coil configurations. In (A) the traces related to ploughing of the field are indicated by white arrows.

4.3.3 Magnetic susceptibility measurements with the Bartington MS2 system

To complement the EMI derived κ_a data, and to account for differences between these and other available survey data, a Bartington MS2 magnetic susceptibility system was used together with a MS2H sub-surface probe and a MS2D loop sensor. The MS2 sensors operate on the principle of AC induction, which is similar to Slingram EMI instruments such as the Dualem-21S. However, the MS2 measurements have the advantage that these are fairly insensitive to the electrical conductivity of the measured medium, whereas in certain conditions, e.g. in saline environments, the κ_a or IP-response of an EMI sensor can be influenced by the soil electrical conductivity or QP-response (Callegary et al., 2007). This way, the MS2 sensors can be used to evaluate the possible interference between IP and QP signal components of EMI measurements.

	Dualem 21-S		Bartington MS2	
	1 m HCP	2 m HCP	MS2D	MS2H
Average	86	315	9	9
Minimum	29	130	4	0
Maximum	185	452	17.9	34*
standard deviation	5	25	2	13

Table 2 Descriptive statistics of the different κ_a and κ measurements. κ_a and κ-values are expressed in e-5 msu SI. (*excluding one outlier of 160 e-5 msu for profile 6)

In a first step, topsoil κ_a was measured with the MS2D loop sensor. The effective penetration depth of the MS2D, which corresponds to 90% of the recorded signal, is considered to be 6 cm (Lecoanet et al., 1999) whereby 50% of the signal response is obtained at 1.5 cm below the sensor as described in the Bartington instrument specifications. In total, 225 measurements were taken in a 10 m by 10 m grid with the 1.0 measurement range, i.e. an accuracy of 1×10^{-5} SI units, whereby the instrument was zeroed between each measurement. These measurements were then interpolated to a 2.5 m × 2.5 m grid using ordinary kriging (see Chapter 2 and Goovaerts, 1997). Apart from a general comparison between the MS2D data and the EMI survey, we wanted to evaluate if the MS2D measurements would reveal shallower archaeological traces that could not be discerned in the EMI κ_a data.

To investigate the relationship between the archaeological and geophysical data further, 15 locations were selected for κ-profiling with the MS2H probe. The MS2H probe

has a 0.5 cm horizontal signal depth penetration around its tip and a vertical resolution of 1.25 cm (Bartington instrument specifications). At each location, a borehole was prepared with a 2.5 cm gouge auger and lithological descriptions were made. The κ-measurement were taken in 5 cm intervals, starting at a depth of 10 cm and down to a minimum depth of 50 cm depending on the depth of the undisturbed substrate. Along with the κ_a-measurements, the lithology of the profiles was described. To allow a straightforward comparison of the different data types, all values are displayed in the 10^{-5} range (Table 2).

4.3.4 Topsoil magnetic susceptibility: MS2D

The MS2D measurements were compared to the 1 m HCP Dualem-21S data (Fig. 34A, B), as the latter are influenced more by topsoil variations than the 2 m HCP measurements. The difference in measured soil volume between both datasets results in a mean κ_a for the MS2D data that is nearly ten times lower than the results from the 1 m HCP κ_a-measurements (Table 2). This can be explained by the larger soil volume that is taken into account in the 1 m HCP measurements. However, the standard deviations of both datasets lie more closely together and vary only 3 e^{-5} msu, indicating that while the MS2D survey resulted in a broad data range, the 1 m HCP κ_a-measurements are closely clustered around the mean. Again, this can be attributed to the volumetric difference between both survey datasets. The shallow depth penetration of the loop sensor gives a high local resolution, whereas the 1 m HCP coil pair takes into account a much larger soil volume, which has a smoothing effect on the individual measurements. As a result, each measurement is slightly smoothed by taking into account more of the background variation within the measured soil volume. In other words, the MS2D offers sharper κ_a-contrasts than the 1 m HCP data.

A similar spatial trend could be observed between the MS2D and the 1 m HCP κ_a-data (Fig. 41B); most of the magnetic variation is present in the south to south-western part of the field. In the MS2D data, the most dominant magnetic anomaly was detected around the small enclosure. On the other hand, the most southern and largest enclosure had a much smaller influence on the measurements than in the 1 m HCP data. In the north-eastern part of the field, a larger κ_a-variation was attested in the MS2D dataset. This could indicate that the archaeological features seen on the aerial photograph in this part of the field represent very shallow κ_a anomalies.

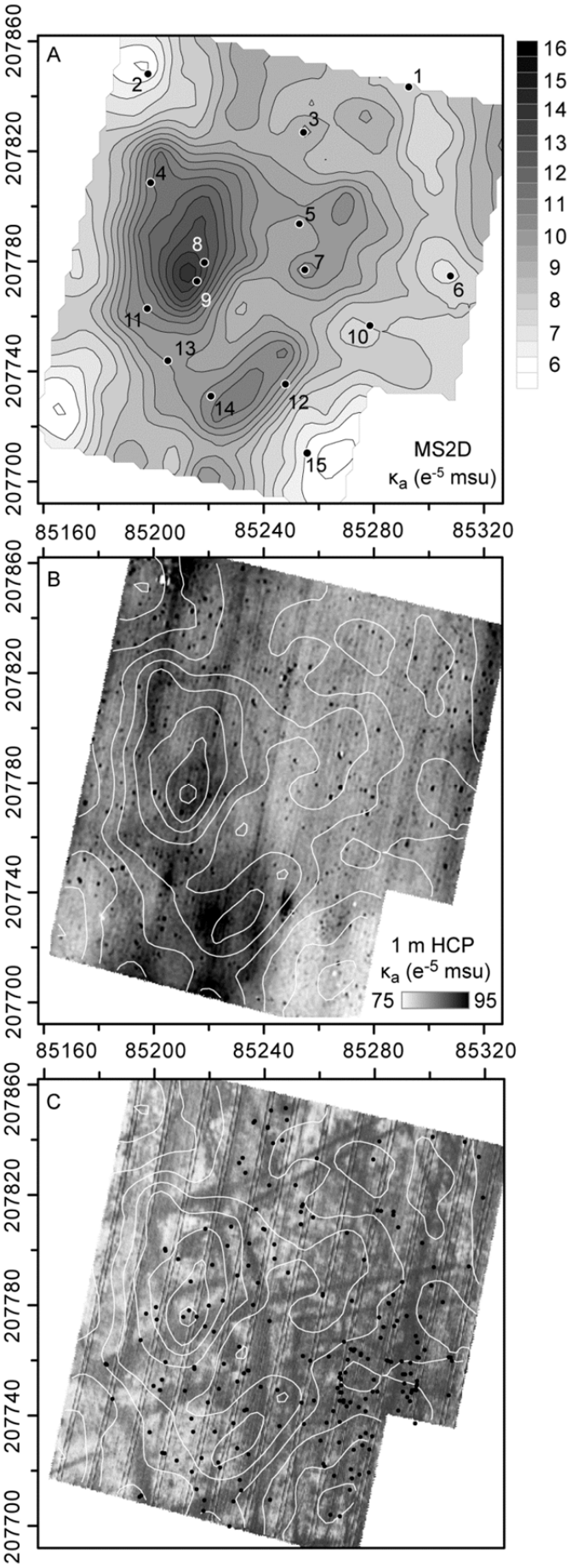

Fig. 41 κ_a-data from the MS2D survey with indication of the MS2H probing locations (A), MS2D κ_a-data contours plotted on the 1 m HCP κ_a-measurements (B), MS2D κ_a-data contours plotted on the aerial photograph (C).

To evaluate the MS2D potential for detecting the spread of archaeological activity areas, these data were compared to aerial photograph and the fieldwalking results (Fig. 41C). Most of the assembled finds are located within the enclosures seen on the aerial photograph. Still, the correlation between the fieldwalking data and the MS2D results remains the strongest for the enclosures that can also be discerned in the EMI data. The spatial distribution of the finds in the eastern and south-eastern part of the field shows a different pattern than observed in the MS2D plot. This was most apparent in the south-eastern part of the field where the highest concentration of surface material was found, but no enhanced κ_a could be detected with the MS2D loop sensor.

4.3.5 Magnetic susceptibility profiling: MS2H

The MS2H-profiles showed that overall, the plough layer had the strongest influence on the κ-measurements (Fig. 42). However, only at four locations (8, 9, 12 and 13 on Fig. 42A and Fig. 41) an unusual increase of κ was attested in the plough layer, coinciding with observed magnetic variations in the 1 m HCP and MS2D data.

The average κ of the deeper layers was 4.6 e^{-5} msu. Here, a distinction could be made between the susceptibility of the undisturbed soil and the buried archaeological deposits. At nine locations (1, 3, 4, 8, 9, 10, 11, 13 and 14) black organic sand was present, often with traces of brick, burnt material and oxidation, which was identified as an archaeological layer. However, only in a few cases a slight increase in κ was observed in this layer (locations 4, 8, 9, 11 and 14). At these locations, the enhanced susceptibility of the archaeological deposits was also observed in the 2 m HCP κ_a-measurements, showing the potential of the deeper EMI measurements to discriminate small variations in κ_a. The MS2H-profiles further showed a significant contribution of the undisturbed soil to the overall κ of the site. While the sand and sandy clay layers had a generally low κ (between 0 to 1 e^{-5} msu), the mineralogy of the Eocene clay caused a significant increase in κ (mainly between 1 and 2 e^{-5} msu). Only at one location, a ferrous horizon caused higher κ in the sand (profile 5 on Fig. 41). This increased κ of the Eocene clay was also attested in the 2 m HCP measurements where particularly in the north-western, eastern and south-western part of the field, large areas with increased κ_a were observed. The contribution of the Eocene clay to the 2 m HCP κ_a-measurements was most clearly attested at location 2, where the depth to the clay layer was only 40 cm. However, at locations 9, 11 and 13 the contribution of the Eocene clay to the 2 m HCP data was negligible. Here, the depth to clay was below 120 cm, i.e. below the critical depth of the 2 m HCP coil configuration for detecting κ-

variations, and only more shallow features could be discriminated. As an example, we refer to location 9 where the 2 m HCP measurements allowed discriminating the elevated κ from the archaeological layer, but influence from the underlying clay layer could not be observed.

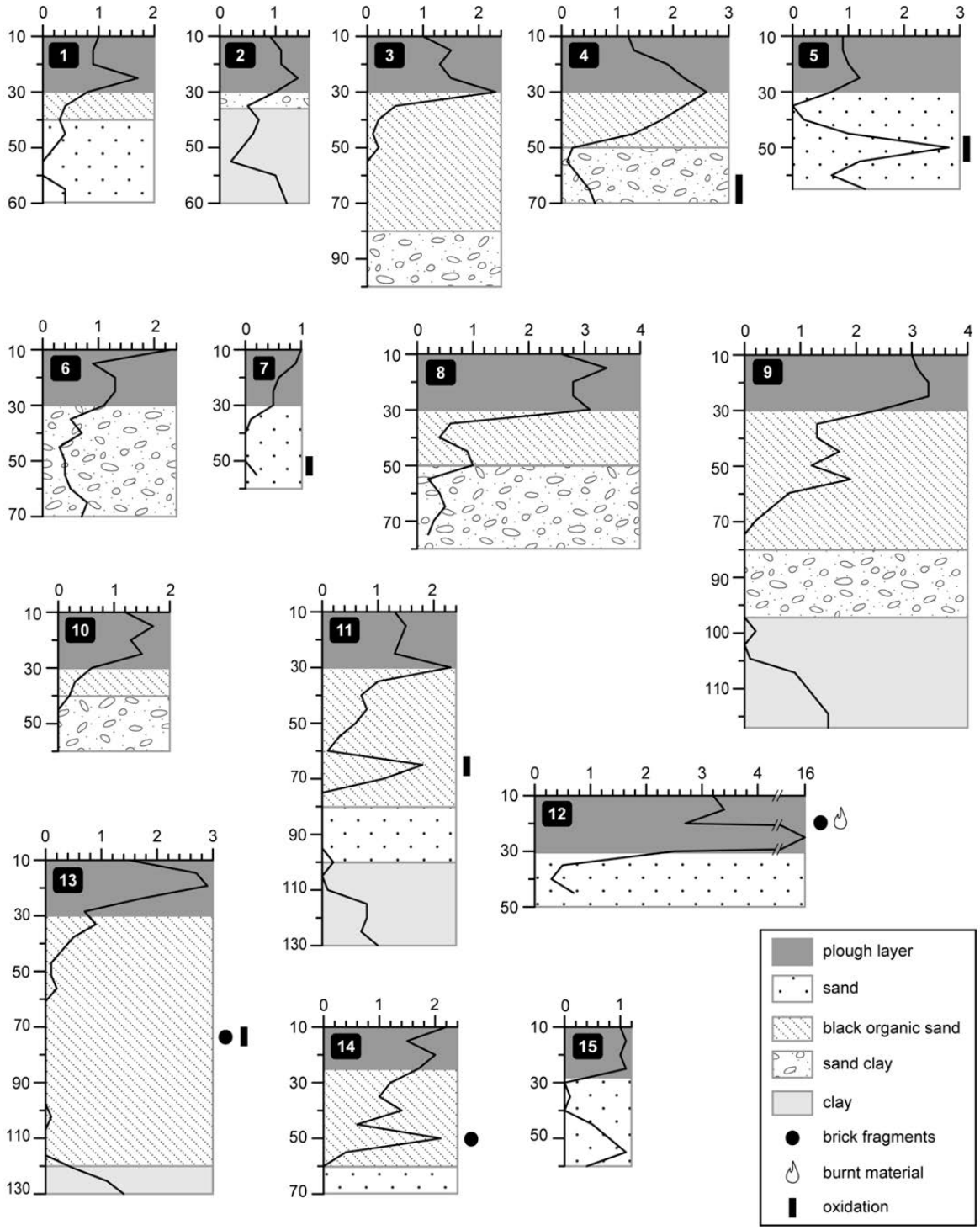

Fig. 42 MS2H κ-profiles with indication of the observed stratigraphy.

4.3.6 Discussion and conclusion

Overall the κ-profiles show that where archaeological deposits were encountered, the susceptibility of the plough layer increased significantly (i.e. between 1 and 2 e^{-5} msu instead of >1 e^{-5} msu where no archaeological features were detected). The resulting enhanced topsoil susceptibility caused the variations that were detected with the MS2D survey. In nearly all cases, the same magnetic variations were recorded in the 1 m HCP κ_a-measurements. Only at locations 1 and 3 the slight κ_a increases were not reflected in the EMI data. The 2 m HCP measurements were also proven to be representative for the elevated κ_a of the archaeological deposits for depths surpassing 0.5 m below the surface. In addition, κ-profiling allowed correlating the large-scale κ-trend observed in the 2 m HCP data to the higher susceptibility of the Eocene clay layer. Combined with comparison to the observed σ_a variations at the site, this shows the independence of the IP response of the HCP coil configurations of the soil conductivity or QP signal response. The detected κ_a variations can therefore be considered a reliable representation of the magnetic variations of the study site.

While, as presented in the previous chapter, the vertical analysis of σ_a data can be performed quite easily through basic inversion protocols, the vertical analysis (or depth inversion) of κ_a data has not been successfully implemented. As a result, it was not possible to conduct a quantitative comparison between the magnetic profiles and the κ_a data. However, through qualitatively comparing different measurements of soil κ, clearer insight was obtained into the influence of archaeological and pedological features on multi-receiver EMI κ_a-measurements. Even when the archaeological anomalies only displayed small κ contrasts, and despite the natural magnetic variation related to the Eocene clay, it was possible to clearly discriminate such features in the EMI κ_a data. Furthermore, the integration of multiple simultaneous κ_a-measurements of different soil volumes, allows accurately discriminating between topsoil κ and magnetic variations of deeper soil layers.

The complex nature of the HCP IP signal response prohibits a straightforward definition of the depth of investigation of this coil based on the 70% response depth, as is possible with other (e.g. VCP) coil configurations and the QP signal response (see section 2.4). However, through comparing multiple HCP κ_a datasets, gathered with HCP coil pairs with different intercoil separations, a depth estimate can be made of detected features when the top of these features is situated between the critical depths of two such coil pairs (an example of such a qualitative depth interpretation is presented in the Appendix). As all

features discussed in Chapter 4 were situated above the critical depths of the applied HCP coil pairs, such an evaluation could not be performed for the Maldegem study site.

At the study site, mapping soil susceptibility through the multi-receiver EMI sensor and the Bartington MS2 system allowed for the most accurate magnetic mapping of the anthropogenic soil disturbances, taking the features discriminated on the aerial photograph as a reference. It remains, however, difficult to explain the discrepancies that exist between the geophysical data and the aerial photograph. The contrast between the anthropogenically modified infilling of the shallow ditches in the north-eastern part of the field and the undisturbed soil influence the vegetation in a way detectable through aerial photography. On the other hand, this difference in soil composition has not left a contrast distinguishable in the EMI and magnetometer survey data. While for the magnetometry data the failure to detect these features cannot be attributed to the shallow depth of these features, this might not be the case for the EMI survey. The slight contrast discerned in κ-profiles 1 and 3 could indicate that the use of different coil configurations might allow visualizing these features. However, while the PRP coil configuration is more sensitive to variations in the upper soil layers, the poor signal to noise ratio rendered these data useless. Here, EMI survey with VCP coil configurations could potentially offer a solution, but to date such a survey has not been conducted at the test site.

Chapter 5

The integrated reconstruction of past human environments

The content of this chapter is based on:

> De Smedt et al., 2013. The 3-D reconstruction of medieval wetland reclamation through electromagnetic induction survey. *Scientific Reports*, 3, 1517 (pp. 5).

5.1 Introduction

Geophysical techniques are often used to produce palaeolandscape reconstructions and archaeological landscape reconstructions are common in earth and archaeological sciences, the integrated reconstruction of human-landscape interactions with these methods has not been taken on. Archaeologists mostly perceive archaeological landscapes as the geographical (or spatial) distribution of archaeological features and environments constructed or altered by humans, and their interconnectivity. Although the current topography, in the form of DEM's, is a common starting point in archaeological landscape analysis, the integration of spatially continuous information on past natural landscape variations remains rare. DEM's do incorporate indirect information about the palaeotopography, but especially in sedimentation areas (e.g. alluvial environments) the correlation between current elevation data and past landforms is restricted.

A number of conventional survey methods, discussed in Chapter 3, allow adding point and transect-wise pedological and geomorphological information, but these datasets do not

offer spatial continuity across the studied areas. As with other environmental data (e.g. pollen diagrams), information on past landforms and stratigraphy is mostly derived from type sections.

In landscape archaeology, geophysical methods are increasingly being applied to conduct large area surveys (Gaffney et al., 2012; Kvamme, 2003; Trinks et al., 2010). These techniques allow for bridging the gap between point finds and the surrounding landscape, and especially by combining these data with DEM's detailed reconstructions of archaeological landscapes can be produced. Although these techniques allow obtaining high-resolution archaeological information at a landscape-scale, they often neglect natural landscape variations. Studies of past human-landscape, however, interactions rely upon the integration of archaeological, biological and geological information within their geographical context.

In Chapter 3, a methodology was presented to reconstruct past landscapes with σ_a-data from multi-receiver EMI survey in 3-D. In Chapter 4, the potential of multi-receiver EMI instruments for mapping minute magnetic anomalies was discussed. Here we show how simultaneous mapping of multiple physical soil properties with such instruments permits an integrated reconstruction of past human landscape interactions.

As in the previous chapters, the Dualem-21S sensor was used, which allows recording σ_a and κ_a of four different soil volumes simultaneously (Simpson et al., 2009b). Whereas in non-saline environments σ_a can be directly related to soil texture (clay, silt, sand), and is influenced by soil organic matter and water content (Rhoades et al., 1976; Sudduth et al., 2005), κ_a anomalies are often the result from ferrimagnetic soil enrichment (Fassbinder et al., 1990; Le Borgne, 1955), the anthropogenic disturbance (Gaffney and Gater, 2003) of top soils (e.g. ditches), or the heating of soil (Le Borgne, 1960) (e.g. hearths, bricks) (see also Chapter 2). This contrasts to other geophysical survey techniques, such as magnetometry (Aspinall et al., 2008) and ground penetrating radar (Jol, 2009), that each target only one specific variable and are inadequate to appreciate the full range of soil textural variability of surveyed sites. However, integrating electrical and magnetic soil properties in a single EMI survey allows targeting the pedological, geomorphological and archaeological variations jointly. Through combining the inversion protocol presented in Chapter 3, with detailed κ_a data from multiple soil volumes an integrated reconstruction is targeted of the anthropogenic and natural soil variations of the studied areas.

In this chapter, the proposed methodology is applied to reconstruct the 3-D layout and pedological setting of a medieval reclaimed landscape in Flanders (Belgium). Combined

with limited and directed excavations, the results offer a unique insight into the way such marginal landscapes were reclaimed and occupied during the Middle Ages.

5.2 Study area and survey strategy

The reclaimed wetland presented in this chapter was discovered during an EMI survey conducted within the framework of the geoarchaeological research project (see section 3.2) in the eastern extension of the Moervaart palaeolake (Fig. 43). As part of the palaeotopographical mapping campaign, an area starting from within the palaeolake and onto the adjacent sand ridge was surveyed at the 2 m × 0.25 m resolution (see sections 2.5.1 and 3.4). After detection of the wetland site, the designed landscape was resurveyed with the Dualem-21s at a sampling resolution of 0.75 m × 0.25 m.

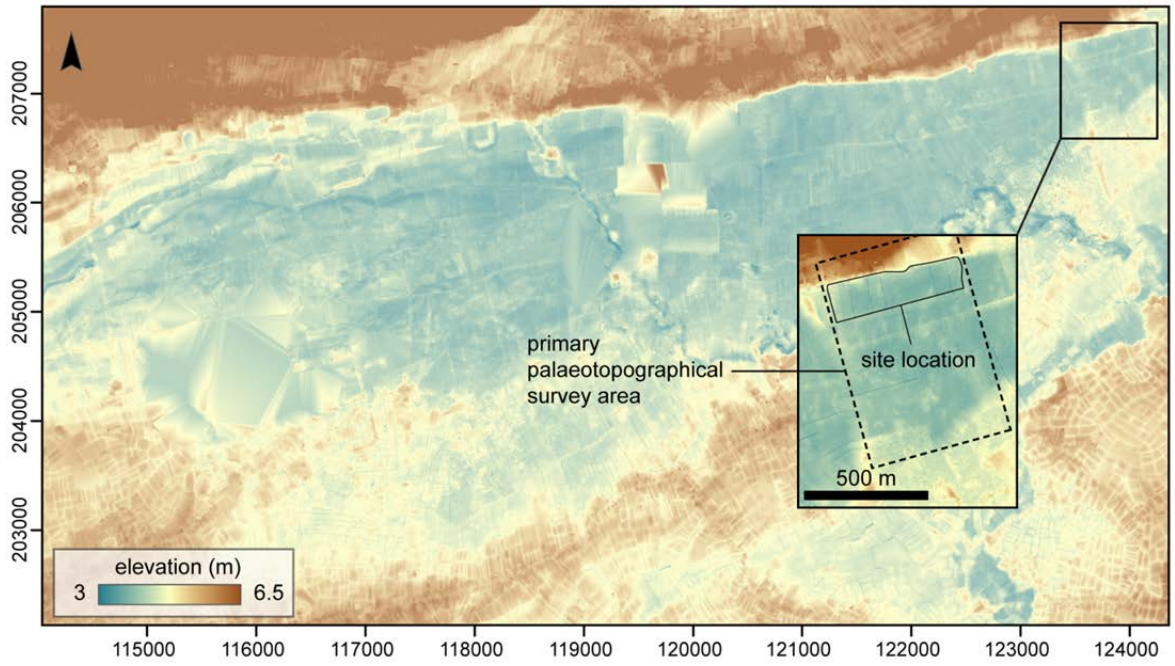

Fig. 43 DEM of the Moervaart palaeolake with indication of the study area in the eastern extension of the palaeolake (rectangle). The inset zooms in on the study area and shows the location of the palaeotopographical survey area and the wetland site location (black line).

5.3 The 3-D reconstruction of a medieval reclaimed wetland through multi-receiver EMI survey

5.3.1 Historical setting and research context

In Europe, one of the most characteristic examples of past human-landscape interaction, is the reclamation of wetlands and forest that followed the urbanisation of the historical County of Flanders (Fig. 44b). During Medieval periods, these lowlands experienced a considerable population growth, making the County one of the most densely populated areas in Europe between the 11th and the 15th centuries (Prevenier, 1983). To meet the demands of emerging cities, such as Ghent, Bruges and Ypres (Verhulst, 1999), entire natural landscapes were reclaimed, transforming these into a landscape of dynamic exploitation (Brenner, 2001). The ruling Counts of Flanders spearheaded this evolution by endowing feudal lords with lands, while abbeys were deliberately installed on marginal land all over Flanders.

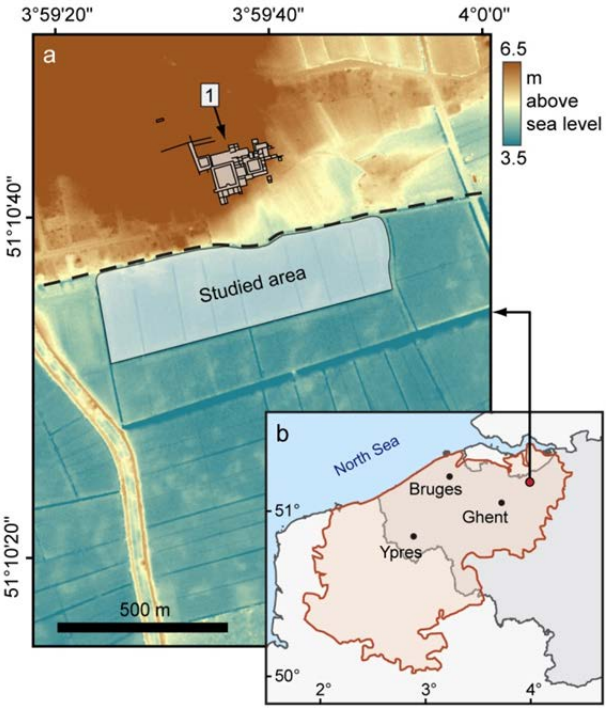

Fig. 44 a, The location and elevation (AGIV, 2004) of the study area with indication of the excavated Abbey of Boudelo (De Belie, 1997) (1). The dashed line represents the boundary between the palaeolake (to its south) and the coversand ridge (to its north). b, Location of the studied area (red dot) within the late medieval County of Flanders (orange boundary) and the current state boundary of Belgium.

More recently, natural processes (e.g. flooding) and modernisation have altered the cultural landscape of medieval Flanders, leaving the nature and exact layout of these designed landscapes largely unknown (De Clercq et al., 2012). Although social formation and economic exploitation of reclaimed landscapes during the High Middle Ages is, to some extent, documented in historical and cartographical sources, archaeological evidence remains scarce. One of the main reasons for this scarcity is that traditional investigations have focused on recovering architectural remains rather than situating the structures within their broader environmental contexts. By focusing on elite residences and monastic buildings, archaeological investigations have contributed to the biased image of medieval settlement landscapes that still prevails.

The situation was no different for the Cistercian abbey of Boudelo located in the north of the County of Flanders (Fig. 44). In 1197, a small religious community settled in this area (Ghent State Archives: Abdij van Boudelo rec.8 sheet 80), which at that time was an outback of the County, dominated by marshes and wetlands. Early historical accounts, such as those by monks from the Abbey of Clairvaux in Bourgogne (France), give testament to the harsh environmental conditions. They describe life at Boudelo as *pauper* and *misserimus*: poor and full of misery (Ghent State Archives: Abdij van Boudelo rec.6,50). However, the community improved its property by cultivating the surrounding land. Between the 13th and 16th centuries, the monastic estate expanded to over 1000 ha, making the community one of the leading cultivators in the County. After religious as well as military struggles and successive floods, the monks were forced to abandon their grounds in Boudelo in 1578. They found refuge in Ghent and the monastic buildings were sold and dismantled.

Although the extensive reclamation strategy of the abbey is attested in historical records mentioning embankment, drainage, stockbreeding, extraction of peat and clay, and the production of building ceramics, it remains hidden in the archaeological record. Excavations in the 1970s revealed the remnants of the cloister range and the abbey church, leading archaeologists to interpret the abbey grounds as limited to the coversand ridge (De Belie, 1997) (Fig. 37a). The border of the monastic precinct was believed to coincide with the edge of a Late Glacial palaeolake, which was, and remains, a waterlogged environment dominated by peat and lime-rich lacustrine deposits (Fig. 20). However, in 2011 an EMI survey of this wetland area drastically altered this interpretation, as it unveiled traces of the abbey's outer court that once was part of the monastic precinct; a previously unknown designed landscape from which the monks directed their cultivation of the surrounding area.

5.3.2 Results

a. EMI survey

The σ_a data revealed a complex environment with alternations of highly conductive lake deposits and peat accumulations (Fig. 45a).

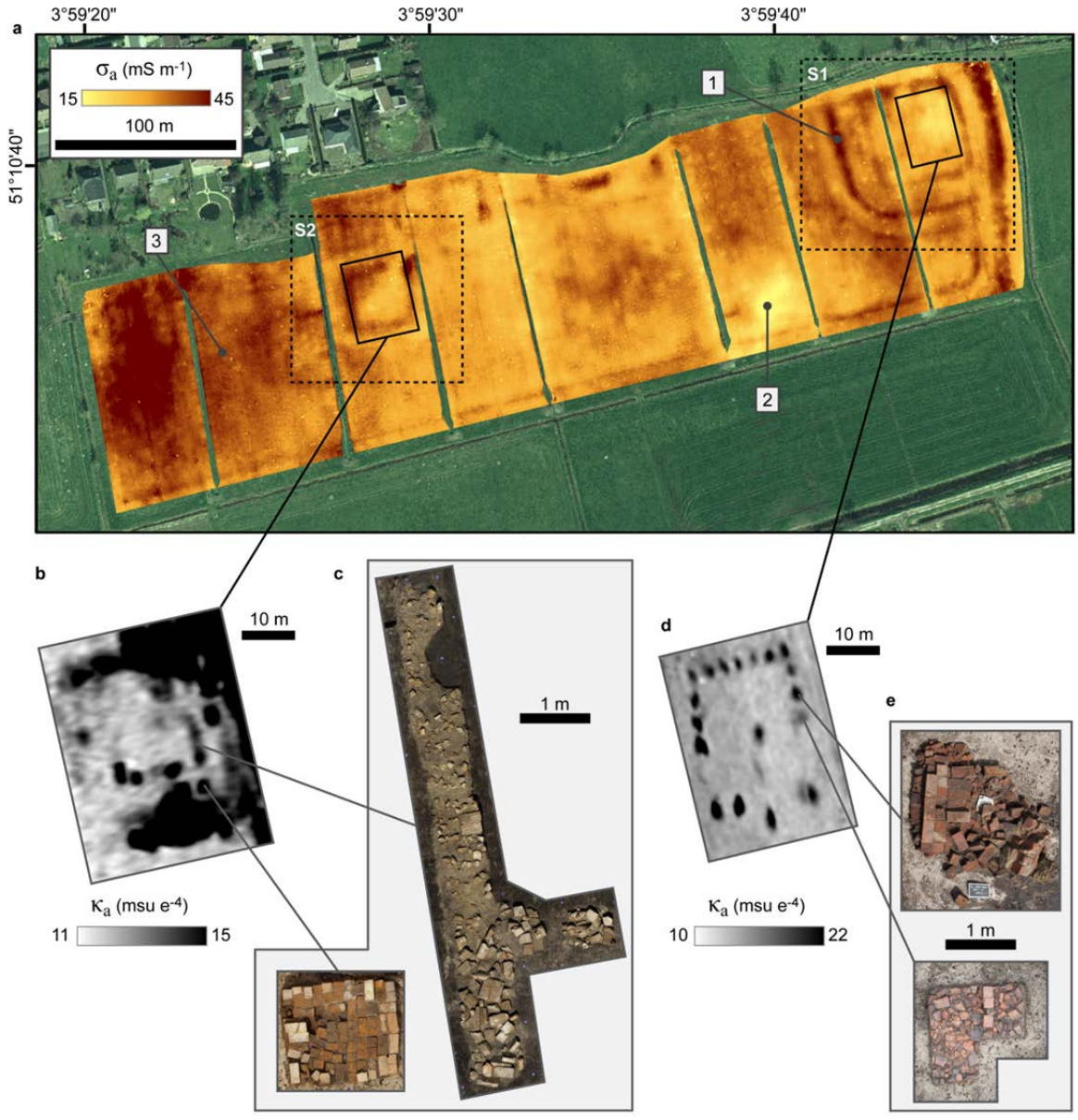

Fig. 45 a, 1 m HCP σ_a data and orthophotograph (AGIV, 2003b) of the study area with indication of a man-made ditch (1), a sandy outcrop (2) and an area with accumulated peat and lacustrine deposits (3). The dashed lines indicate both moated sites S1 and S2. b, 2 m HCP κ_a data of the platform of S2, showing the central building and the magnetic disturbances caused by rubble in the ditches and leading towards the north (Supplementary Fig. 2). c, e, Orthophotos of the brick foundations as revealed by the excavations at S2 (c) and S1 (e). d, 2 m HCP κ_a data showing traces of 18 brick block foundations on the platform in S1.

Apart from scarce sandy outcrops the measurements indicate a buried marshland influenced by long lasting, saturated conditions. Several ditches were revealed as highly conductive anomalies surrounding the entire survey area and enclosing two smaller zones (Fig. 45-47).

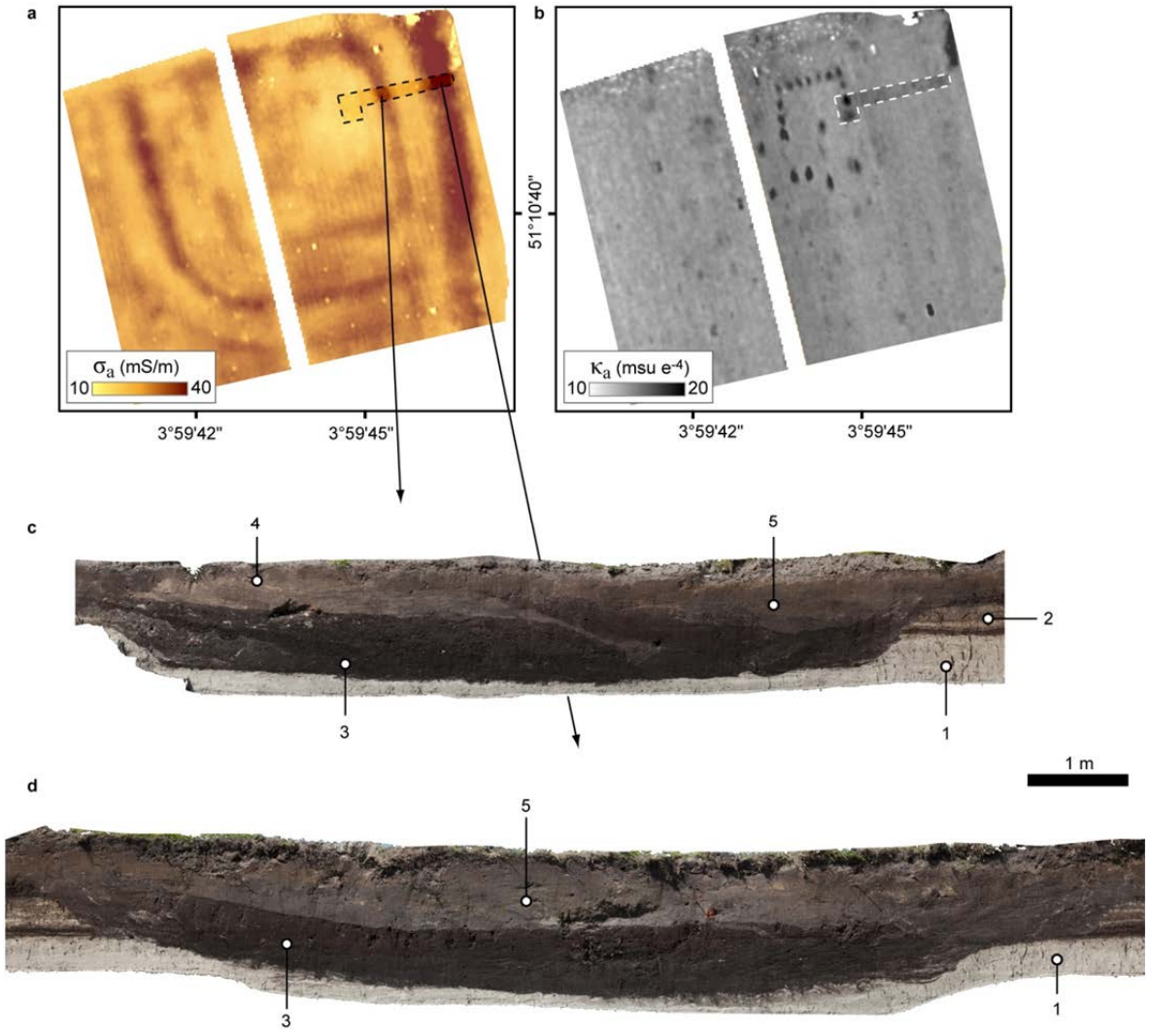

Fig. 46 a–b, Location of the excavation trench plotted on 1 m HCP σ_a data (a) and 2 m HCP κ_a measurements (b), targeting the two moat ditches visible on the σ_a plot and two of the brick block foundations seen in the κ_a measurements. c–d, geometrical profiles of the two sectioned moat ditches showing the pleniglacial sand substrate (1), palaeolake deposits (2), peat infilling of the bottom of the ditches (3) and sandy (4) and clayey (5) top infilling of the ditches.

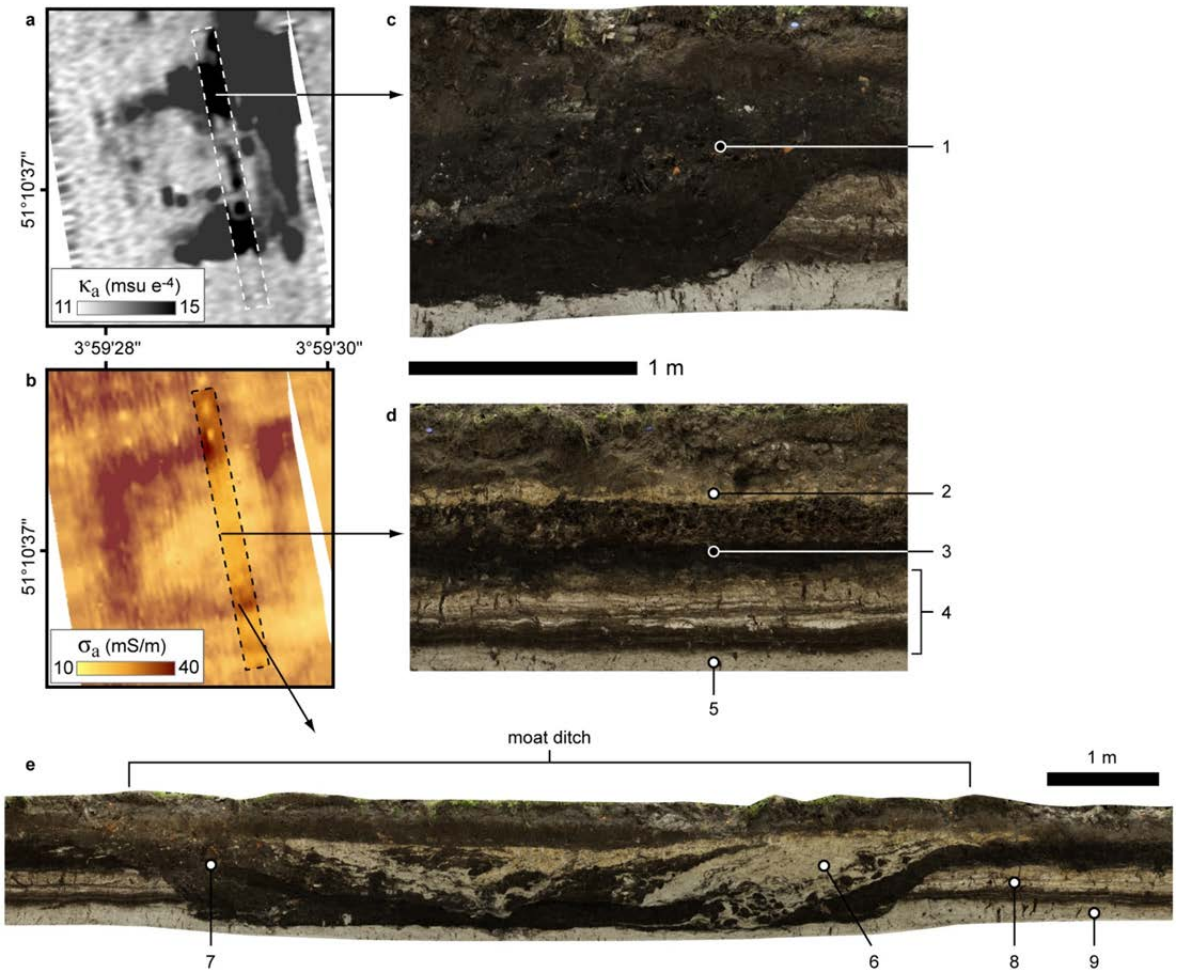

Fig. 47 Location of the excavation trench plotted on 2 m HCP κ_a measurements (a) and 1.1 m PRP σ_a data (b), targeting the moat ditches on the σ_a plot and the central brick structure and magnetic anomalies in the ditches visible in the κ_a measurements. c, Geometrical profile detail showing the magnetic rubble in the moat ditch (1), mainly brick debris and metal slags. d, Geometrical profile detail showing traces of the medieval terrain levelling (2) underlying peat (3), palaeolake deposits (4) and pleniglacial sand substrate (5). e, Geometrical profile of the southern moat ditch showing traces of the thrown-in moat embankment (6) brick rubble (7), palaeolake deposits (8) and pleniglacial sand substrate (9).

To interpret and complement the geophysical data excavation trenches were laid out across the ditches and the central structure of each site (Fig. 46 and Fig. 47). At S1, the excavation targeted both moat ditches and two of the large magnetic anomalies. We selected these two anomalies as they appear differently in the 1 m HCP and 2 m HCP κa data (Fig. 48). While one anomaly was most present in the 1 m HCP data (anomaly A2 on Fig. 48), the other was most apparent in the 2 m HCP dataset (anomaly A1 on Fig. 41). Furthermore, anomaly A2 was the only of the 18 large magnetic features that was nearly indistinguishable on the 2 m HCP data plot. A transect-wise comparison of the κ_a signature

of A1 and A2 further shows the difference between both features. While these measurements indicate that A1 is present in the uppermost soil layers, A2 appears to be most prominent in the deeper soil layers.

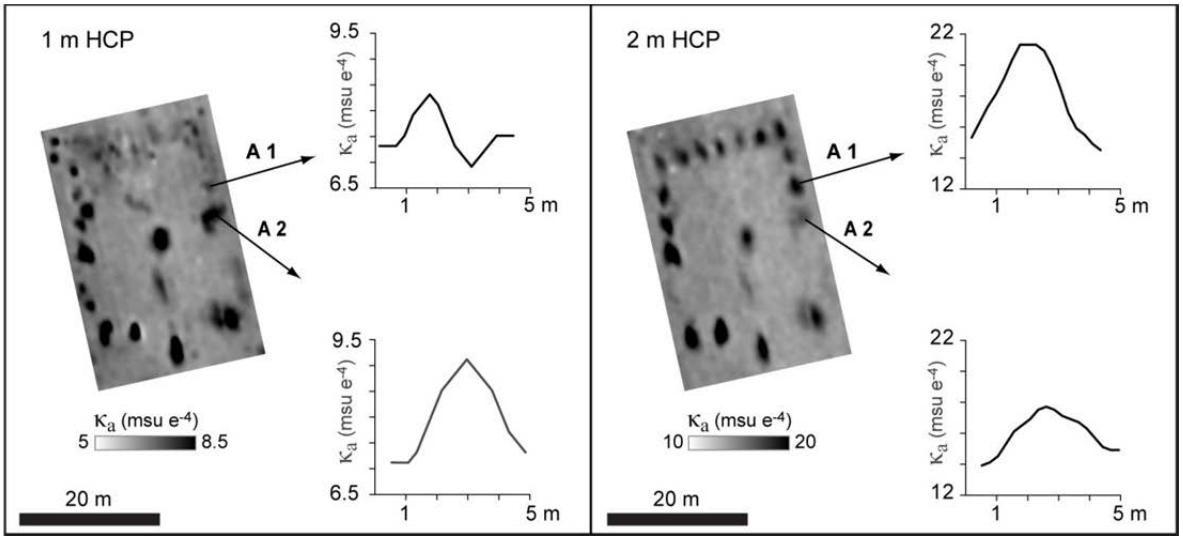

Fig. 48 κ_a data-plots from the 1 m HCP (left) and 2 m HCP coil pairs (right) with indication of the two anomalies (A1 and A2) targeted in the excavation trench across S1 (see Fig. 46). Two transects, extracted from the EMI κ_a data, are presented, showing the different signature of A1 and A2 in the 1 m and 2 m HCP data.

Prior to excavation, the structure at S1 was resurveyed with a fluxgate gradiometer array by David Simpson (Geosurveys Ltd, Portugal) (see De Smedt et al., 2011b). The array was composed of four Foerster Ferex 4.032 DLG probes, which were mounted on a hand-pushed cart, 0.25 m apart. The results of the magnetometer survey showed similar traces as detected by the EMI survey, but with a finer resolution. When we look in detail to anomalies A1 and A2, as indicated on Fig. 48 and Fig. 49, a difference between these two features can also be discerned on the magnetometry data. While A1 displays a strong thermoremanent signature, A2 has a less pronounced magnetic signature. However, unlike with the multi-layered κ_a-data from the EMI survey, a straightforward qualitative interpretation of the depth extent these two features is not possible based on the magnetometry plot. Furthermore, these fluxgate

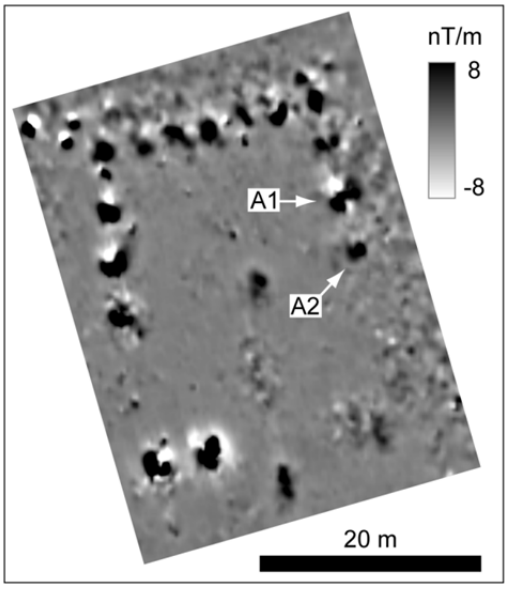

Fig. 49 Fluxgate gradiometer data of the structure at S1 (courtesy of David Simpson (De Smedt et al. 2011b)).

gradiometer data did not allow for the detection any other features than those discerned in the EMI κ_a-data.

b. Excavation results

At both sites, brick structures were found, as indicated by the κ_a measurements (Fig. 45b–e). These were identified as block foundations used to support a larger, most likely wooden, structure and to keep it away from the saturated soil. At S1, the different κ_a signature of anomalies A1 and A2 could be related to the level of preservation of the brick structures (Fig. 50). Anomaly A1 was the best preserved foundation with most of the brick present in situ below the plough layer, causing the strong response in the 2 m HCP κ_a measurements (A1 in Fig. 50). On the other hand, anomaly A2 had been severely disturbed whereby the bricks were scattered through the plough layer, leaving only little material in situ in the deeper soil layers. Therefore, A2 was detected mainly with the 1 m HCP coil configuration, while it could be less discerned in the 2 m HCP data (A2 in Fig. 50).

Extrapolating these findings to the remaining, non-excavated, magnetic anomalies of the structure at S1 indicates a good level of preservation for most of the brick foundations. All of the remaining anomalies are strongly present in the 2 m HCP data, indicating a

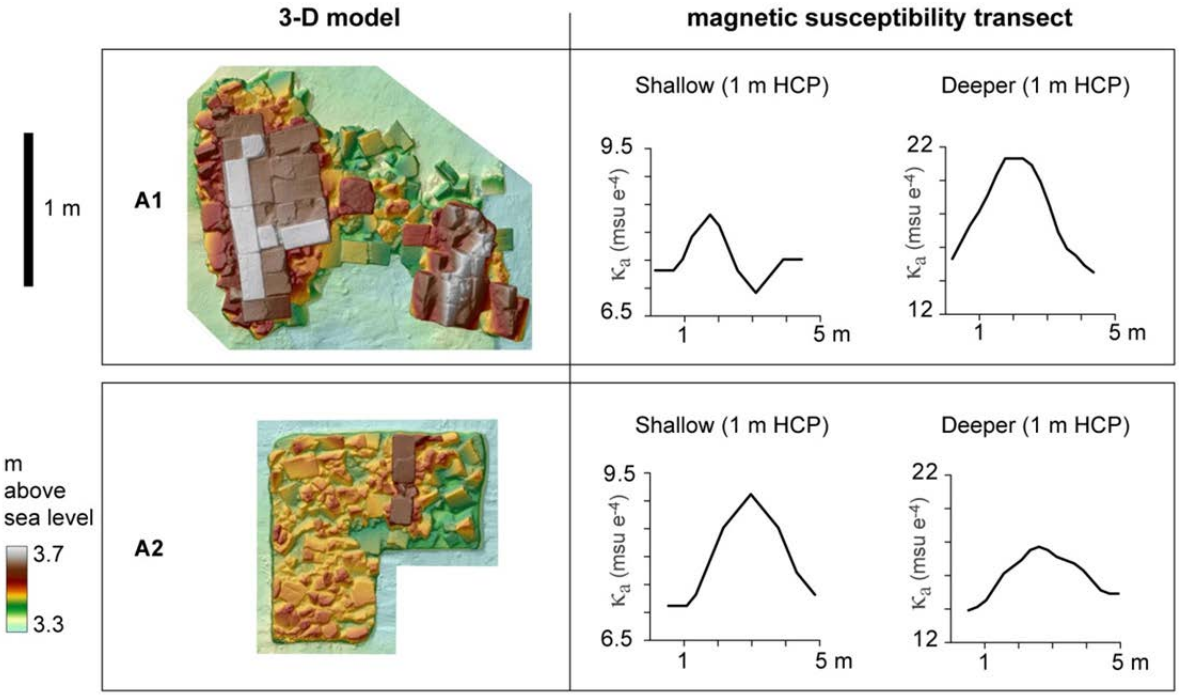

Fig. 50 3-D elevation models of the excavated brick foundations at S1 (De Reu et al., 2013), seen as anomalies A1 (top) and A2 (bottom) on the κ_a data presented in Fig. 48, and transect-wise representation of the 1 m HCP and 2 m HCP κ_a measurements over these structures.

substantial amount of *in situ* brick material. Nevertheless, the 1 m HCP data show that there is substantial scattering of material in the upper soil layers for at least 7 of the separate building foundations. Although these results indicate a good level of preservation for this structure, further validation of this hypothesis is needed, and would require additional excavations or inversion of the κ_a data.

Whereas a functional interpretation of S2 has been hampered by the poor conservation of the excavated building remains, the central structure at S1 has been interpreted as a large monastic barn. The morphology of the sandy outcrop, combined with elevated ground water levels caused instability of the foundations leading to the collapse of the building. The excavated material culture and construction materials indicate that both sites were occupied between the 13th and the early 14th centuries. This links their abandonment to a period of documented increased flooding in the region (Buisman, 1995).

c. Integrated 3-D modelling

Based on the σ_a and excavation data, we modelled the relative medieval topography of the site (De Smedt et al., 2013b; Saey et al., 2008). Although the heterogeneity of the ditch infillings, the peat layers and the targeted sandy layers limited the precision of this modelling procedure, an accurate model of the medieval surface was obtained. At 84 validation locations in the excavation trench at S2 a RMSE of 0.37 cm and a Spearman correlation coefficient of 0.80 was obtained between the observed (Fig. 51a) and modelled (Fig. 51b) depths to the archaeological layers.

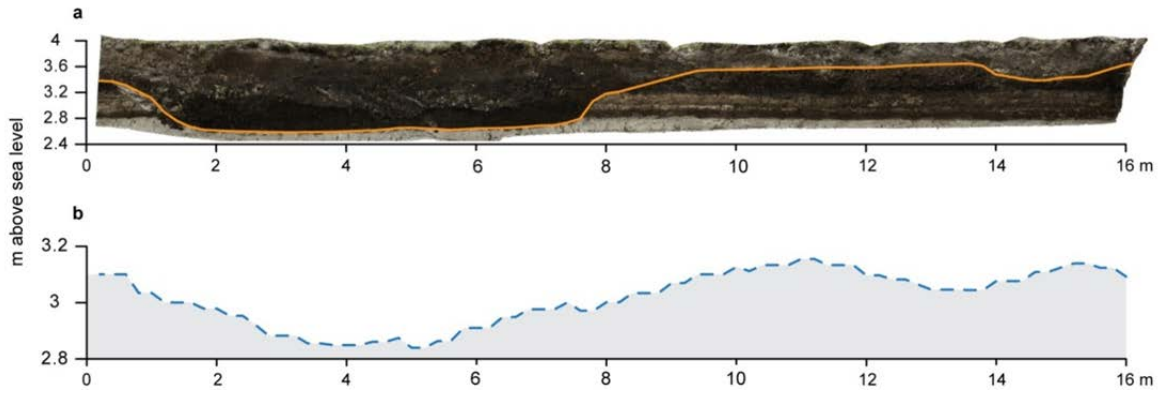

Fig. 51 a, Geometrically correct visualisation of the western profile of the northern moat ditch in S2 (Supplementary Fig. 2b). 84 calibration points, 0.2 m apart, along the targeted archaeological surface (orange line), were used to validate the surface model. b, modelled medieval surface . Note the difference in y-scale between (a) and (b), which indicates the smaller standard deviation of the modelled depths (standard deviation = 0.10 m) compared to the observed surface levels (standard deviation = 0.43 m).

Although the selection of the validation observations was not statistically random, the results confirmed the relative model correspondence to the medieval topography. A comparison of the modelled data to the observed surface along the validation transect (Fig. 51), shows the smoothing effect on the modelled data, but confirms the accurate representation of the targeted archaeological layers.

By integrating the κ_a data into the model, a comprehensive reconstruction of the reclaimed landscape was obtained (Fig. 52). Both S1 and S2 are located on prominently higher and sandier locations, which are connected to the bordering sand ridge in the north. However, while the barn (at S1) was built on an existing sandy outcrop, excavations showed that S2 was artificially raised (Fig. 47d) by removing sand from the ditches and the adjacent sand ridge. The design of both sites confirms a link to the nearby abbey buildings as their topographic position was chosen or altered in order to allow easy access to the sand ridge. The ditch enclosing the area was largest east of S1 with a width of up to 10 m and a depth of 1.5 m below the surface (Fig. 46). Here, a larger drainage capacity was needed, as the ditch was part of the complex-wide drainage system. This large ditch also expressed a separation between the inside and outside worlds; a symbolic reminder of the separation between religious and secular life (Cassidy-Welch, 2001). The ditches circling S2 and the remainder of S1 rarely surpassed a depth of 1 m and had a width ranging from 2 m to 8 m (Fig. 46d and Fig. 47e). These wide ditches did not only supply additional drainage for the enclosed zones, but also formed a physical boundary that embodied aspects of identity and status (Verhaeghe, 1981). Individual compounds, such as S1 and S2, with an (artificially) raised platform and enclosed by ditches, can be defined as late-medieval moated sites (Verhaeghe, 1981). In addition, the surface model shows dykes neighbouring the ditches that add to the embankment and visibility of both moated sites. Remnants of these earthworks were attested in the excavation trenches, either still in situ or thrown into the moat ditches (Fig. 47).

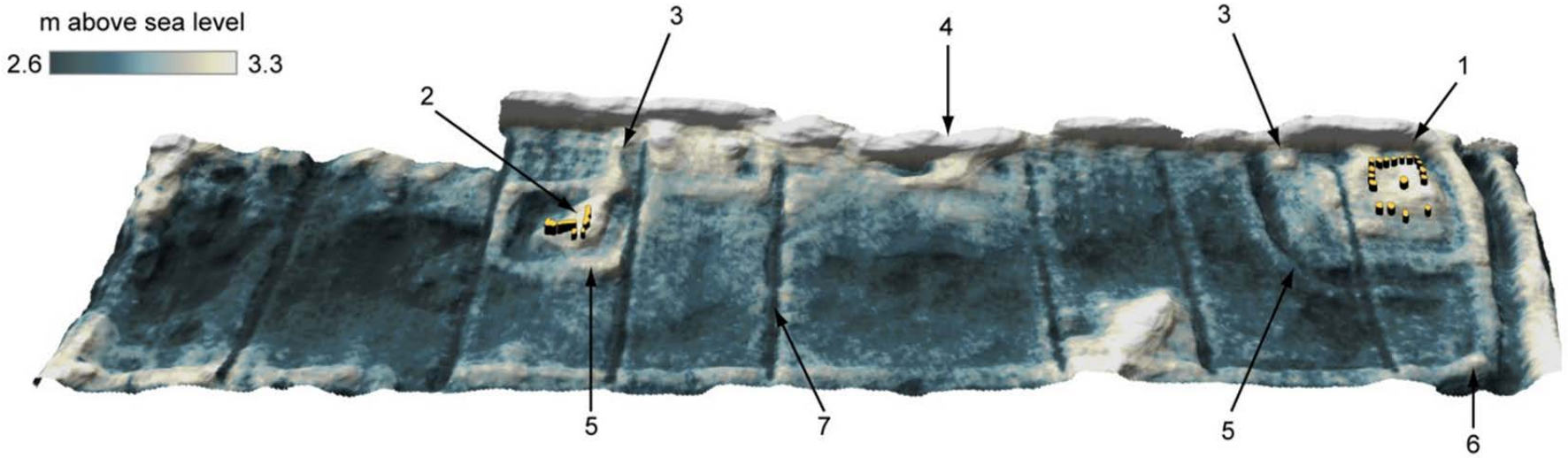

Fig. 52 Three-dimensional model of the depth to the medieval surface and schematic representation of the barn and central building remains at S1 and S2, derived from the κ_a data (Fig. 45). The topographical model shows the sandy outcrop bearing structure S1 (1) and the artificially raised terrain forming the platform at S2 (2). At both sites, a pathway to the coversand ridge can be seen (3). In the north of the site, the edge of the coversand ridge itself is visible (4). Moat embankments are present around both S1 and S2 (5) and a large enclosure embankment (6) surrounds the entire area. Present-day parcel ditches separate the different agricultural fields in the area (7).

5.3.3 Discussion and conclusion

Supported only by very limited invasive research, the presented reconstruction gives a comprehensive and unique insight into a designed medieval environment and shows, despite its transient nature, the amount of effort that was put into it. Through calibrating the geophysical inversion procedure with 3-D excavation data, we obtained accurate insight into the medieval topography. Along with palaeotopographical variations, i.e. the morphology of the palaeolake floor, the human alterations to the wetland could be visualized in three dimensions. However, whereas the relative morphology of the medieval surface was accurately predicted, additional information on the genesis of the modeled topographical variations was mainly deduced from the excavations. Most strikingly, the different origin between the topography of S1 and S2, the former being a natural sandy outcrop while the latter was artificially raised, could only be witnessed in the excavation.

The combination of electrical and magnetic subsurface variations rendered a detailed and accurate image of the geoarchaeological variations at the site. Nevertheless, a full integration of the σ_a and κ_a data was not yet accomplished. While the inversion of σ_a data utilizes all recorded QP EMI measurements, the κ_a data is merely plotted. Here, additional research into the quantitative combination of the multiple κ_a measurements could allow incorporating more of the vertical κ_a variations in the final model. Still, through comparing the magnetic signature of the detected magnetic anomalies insight was gained into the scatter of magnetic material in the shallow and more deeper soil layers. Comparison of the obtained IP response for anomalies A1 and A2 to excavation data, allowed correlating the different magnetic signature in the 1 m HCP and 2 m HCP IP data to the preservation level of these features. Although this correlation could not be quantified, extrapolation of this ascertainment to the remainder of the anomalies at S1 indicates a good level of preservation of the central structure.

The results show how 3-D mapping of multiple soil properties with multi-receiver EMI, combined with limited and directed invasive research, provides a broad foundation for further geoarchaeological research. These results also underline the discrepancies that can exist between historical information and uncovered archaeological realities, and can contribute to understanding the response of past societies to social and environmental changes.

In the future, the presented methodology could be optimized by integrating additional physical soil properties with the σ_a and κ_a data. Integrating GPR data, thus taking into account the dielectric permittivity of the soil, could, for example, add detailed information

on the morphology of the preserved structures. Furthermore, the extraction of depth information from GPR profiles, could allow for a more detailed calibration of inverted EMI data.

With the incorporation of the presented approach into different studies and environments, our knowledge of past human-landscape interactions can be significantly improved.

Chapter 6

Final conclusions and perspectives

6.1 Final discussion and conclusions

The general aim of this thesis was to investigate the use of multi-receiver EMI survey for the integrated reconstruction of past human landscapes, with particular focus on the interaction between past societies and their environment. The general conclusions of the thesis are formulated with reference to the general objectives stated in the introduction (section 1.2).

6.1.1 The 3-D reconstruction of buried landscapes

In Chapter 3, the 3-D reconstruction of past natural landscapes with multi-receiver EMI was taken on. Specific focus of this chapter was on the reconstruction of the palaeolandscape of a lacustrine environment with a complex pedology. Firstly, a 1-D inversion procedure for predicting the depth of palaeochannel deposits was evaluated. In this modelling procedure, augering data were included through a calibration procedure that steered the inversion. By comparing the resulting depth model to lithological data, and to the results of an additional geophysical survey method; ERT, this inversion procedure was proven accurate along two transects. Subsequently, the morphology of the deposits underlying a section of a palaeochannel was accurately modelled in 3-D over an area of 0.45 ha. The main limitation of this approach was related to the depth sensitivity of the EMI instrument, and to the heterogeneity of the palaeochannel deposits. While the depth sensitivity of the EMI sensor restricted accurate depth predictions below 3 m below the surface, the complex stratigraphy imposed a smoothing effect on the modelled depths. Despite these drawbacks, an accurate modelling of the palaeochannel depth was obtained

in 2-D and 3-D. It was concluded that the 1-D inversion procedure allowed for an accurate modelling of the depth to a predefined soil horizon in an environment with a complex pedology. The comparison with ERT showed that the presented method was not only faster, but facilitated the composition of a straightforward 3-D model of the targeted soil layer.

In a second phase, the tested modelling procedure was applied to a 60 ha multi-receiver EMI dataset with known prehistoric sites, dated to the Late Glacial and the Early Holocene. The targeted palaeotopographical model was then to serve as a basis for an integrated reconstruction of the prehistoric landscape of the studied area. Although the heterogeneity of the alluvial and lacustrine deposits present within the study area imposed anticipated limitations on the models interpretability, the palaeotopography of the area was accurately predicted by combining multi-receiver EMI data with limited calibration augerings into the inversion procedure. A total RMSE of 0.57 m was considered acceptable for modelled depths ranging between 0 – 4 m below the surface, particularly in combination with a correlation coefficient of 0.77. The obtained 3-D surface model showed a palaeohydrological system with varying morphology, indicating a two-phased river system, surrounding the known prehistoric site locations. Based on this depth model, sampling locations were selected in the deepest parts of the reconstructed palaeochannels to couple the active phases of these channels to the prehistoric occupation of the landscape. ^{14}C dating confirmed two distinct active phases of the palaeoriver system, dating to the Late Glacial and the Early Holocene, proving the parallels between the prehistoric occupation and the palaeohydrological evolution. Whereas the river system showed a distinct morphological variation that could be linked to the different chronology between the two phases, it was more challenging to deduce channel flow direction from the palaeotopographical model. Although based on the depth model a flow direction could be attributed to the Early Holocene channel, this was not possible for the Late Glacial channels. Here, the genesis of the palaeochannel deposits hampered determining flow direction purely based on the depth to the sand underlying the more silty and organic palaeochannel deposits. This indicates the limitations of EMI derived depth models, as the applied methodology only allows discriminating between soil layers with different electrical conductivities. This also shows the importance of integrating detailed lithological information through coring or type sections when interpreting the palaeolandscape variations. Nevertheless, through the inversion of multi-receiver EMI data, a high-resolution 3-D model could be constructed of the palaeotopography over an area of 60 ha.

The lateral resolution that was obtained in reconstructing the morphology of the targeted soil layer, is unprecedented in palaeolandscape reconstruction.

As a final conclusion, it was found that multi-receiver EMI allows for reconstructing past landscapes in 3-D over wide areas. Through using a mobile survey setup, it was possible to gather the required the required data efficiently. Integrating calibration data, further allowed increasing model accuracy, even in areas with a complex pedology.

6.1.2 Mapping weak magnetic anomalies with multi-receiver EMI

The evaluation of multi-receiver EMI for mapping minute archaeological features was taken on in Chapter 4. Within the framework on a comparative study of non-invasive methods for detecting the ephemeral traces of historical rural occupation, the sensitivity of multi-receiver EMI for such features was investigated. Comparison to magnetometry data showed the sensitivity of the IP-signal response of an EMI instrument in detecting slightly ferrimagnetic archaeological features. Whereas a fluxgate gradiometer survey did not allow for a straightforward reconstruction of the archaeological features present in the test site, EMI proved more efficient in mapping minute variations in magnetic susceptibility. Still, while aerial photography of the test site revealed archaeological traces throughout the entire field, none of the applied geophysical techniques allowed detected all of these archaeological features. This shows that even though the soil composition within the most shallow archaeological features has an effect on the vegetation, making these visible on aerial photographs taken under ideal circumstances, these minute variations did not cause a significant alteration to the physical characteristics of the soil considered in the geophysical surveys. However, the combined input of σ_a and κ_a data gather with a multi-receiver EMI instrument, revealed additional natural and anthropogenic soil variation indicating a more complex occupation history than suggested by the aerial photographs. Furthermore, the σ_a data allowed reconstructing the palaeotopography of the site, which revealed a close link between the soil morphology and the choice of settlement location.

In a second step, the validity of the IP-signal response of the different EMI coil pairs for reconstructing lateral and vertical variations in soil magnetic susceptibility was investigated. Comparison of the multi-receiver EMI data to magnetic susceptibility profiling and topsoil magnetic susceptibility measurements, showed that the IP-response can be considered representative for κ_a variations, within the boundary conditions described in the LIN-conditions (2.3.4), irrespective of the soil σ_a variability. Through combining multiple coil pairs, it was also possible to discriminate between natural and

archaeological magnetic variations. While the former were present most in the largest volumetric measurements (2 m HCP), the latter could be distinguished best in the more shallow κ_a data (1 m HCP). There remains, however, a downside to some coil pairs for mapping κ_a. Although on several occasions (e.g. Simpson, 2009; Tabbagh, 1986b), the PRP orientation has been pointed out as one of the most suited coil configurations for archaeological surveying, it was concluded that in certain field conditions the IP-response of this configuration is most susceptible to instrumental noise. Particularly in environments with a heterogeneous background κ, such as the presented test site, obtaining stable κ_a-measurements is not always possible. On the other hand, the HCP coil configurations were proven to allow a very stable measurement of the κ_a. Furthermore, the combination of multiple HCP coil pairs with a different intercoil separation (i.e. 1 m and 2 m), enabled interpreting the vertical κ_a variations. It was thus concluded that overall, and of the tested coil configurations, the combination of 1 m and 2 m HCP coil pairs allowed the most efficient mapping of κ_a variability. In addition, even though quantitative analysis of the depth of detected anomalies could was not achieved, a quantitative estimation was considered possible based on 1 m and 2 m HCP IP data and 1.1 m PRP IP data (as presented in the example in the appendix).

At the Maldegem test site, an important difference remains between the aerial photograph and the EMI data. Although the latter offered detailed insight into the palaeotopography of the site, the aerial photograph was most effective in visualising the archaeological variations. Susceptibility profiling indicated a slight magnetic enhancement of the plough layer on anomalies discerned on the aerial photograph, which were invisible in the EMI data. This could indicate that the failure to detect these features through EMI survey is related to depth sensitivity of the applied coil configurations. Apart from additional surveys with VCP coil pairs, excavation and detailed magnetic analysis of these shallow features might offer insight into the absence of these features in the geophysical survey data.

6.1.3 Reconstructing human-landscape interactions in 3-D

In Chapter 5, multi-receiver EMI survey was used to compose an integrated, 3-D reconstruction of the natural morphology of, and the human intervention into, a past landscape. As a test case, the reconstruction of a medieval reclaimed wetland was attempted. Based on the magnetic and electrical variations detected with multi-receiver EMI, excavation trenches were laid out to validate and interpret the obtained geophysical

data. By combining the excavation data with the EMI measurements, it was possible to model the 3-D layout of the buried historical landscape. The RMSE of 0.37 m was considered acceptable as, analogous to the modelling validation presented in Chapter 3, the procedure allowed for reconstructing the depth variations of the targeted soil layer. Furthermore, through validating the reconstruction along an excavated section, the correlation between the modelled and observed depths to the targeted soil layer, which was verified by a Spearman correlation coefficient of 0.80, could be visually tested.

Through integrating κ_a into the landscape reconstruction, a full image of the buried wetland environment was obtained. However, the inversion of κ_a data was not taken on as up to date, a reliable depth modelling procedure has not been developed based on multiple κ_a datasets, simultaneously collected with a multi-receiver EMI sensor. Nevertheless, vertical information about the magnetic features visible in the κ_a was obtained by comparing the data-layers representative for different soil volumes. This way, the difference between disturbed and *in situ* features of one of the detected buildings could be estimated, offering insights into the level of preservation of this archaeological structure.

It was concluded that multi-receiver EMI offers the potential to create accurate models of the natural and anthropogenic variations of past landscapes. As with the reconstruction of buried landforms, the integration of true ground information increases the scientific value of the reconstructions. By incorporating limited excavation data, guided by the geophysical data, the reliability of such models can be evaluated and enhanced significantly.

The use of mobile multi-receiver EMI can help unveil traces of past human-landscape interactions in an exhaustive manner, and at a landscape scale. Through combining multiple physical soil variables in one survey, the natural and anthropogenic soil variations can be reconstructed simultaneously. The vertical discrimination potential added by the use of multiple coil pairs then leads the way to 3-D reconstructions of these variations.

6.1.4 Future perspectives

In this thesis, the large potential of multi-receiver EMI instruments for reconstructing past human-landscape was shown. However, a large part of this potential still remains unexplored. While the inversion of σ_a data already allows accurate modelling of the depth and σ of predefined soil layers, the vertical discrimination potential of multiple κ_a measurements has been less investigated. Although it was proven throughout the previous chapters that depth information can be deduced from these datasets, such analyses were not

combined into modelling sequences within the framework of this thesis. Another discrepancy between the use of σ_a and κ_a data from EMI survey is the correlation of these physical variables to specific soil properties. While advances in soil science have furthered the use of σ_a to determine, for example, soil texture variations, straightforward pedological interpretation of detected κ_a-variations is not possible. Here, the plethora of variables underlying magnetic soil variations is an evident limitation. However, until today no significant research effort has been invested to improve the interpretability of κ_a data from EMI sensors. To achieve a better understanding of the relationship between the IP response of Slingram EMI instruments and specific soil properties, the integration of additional magnetic soil properties alongside these data seems needed. The research from the group of Prof. Alain Tabbagh has already led the way for such an approach, by integrating measurements of magnetic viscosity in the EMI survey dataset, but the efficient implementation of these analyses on a large scale has not yet been realized. Along with the integration of detailed information on the magnetic mineralogy of study sites, as for example indicated by the results of dr. Neil Linford (1994 and 1996), a more efficient usage of the available coil configurations in multi-receiver EMI instruments has to be pursued. The unstable character of the IP-response of PRP coil pairs needs to be further examined together with instrument developers, as this remains an coil geometry that has been proved highly valuable in detecting shallow soil variations (e.g. Tabbagh, 1986). The combination of additional HCP coil configurations could also provide a solution, as this coil configuration was proven to be the most efficient, and most reliable, throughout the presented studies. Nevertheless, to accurately interpret HCP IP data, having additional, unambiguous information on the magnetic susceptibility of the detected anomalies (i.e. for example from coil pairs free from sign change) facilitates a more direct interpretation of the observed variations. In addition, combined analysis of IP-data from the VCP coil pair, which was not deployed within the framework of this thesis, alongside κ_a-data from HCP and PRP coil pairs can further vertical interpretation and inversion of these datasets (see also Saey et al., Submitted).

In respect to the inversion of multi-receiver EMI data, we have only taken the first steps. Although alternative EMI inversion algorithms have been proposed (e.g. Monteiro Santos et al., 2010), the 1-D inversion procedure as developed by Saey (2011), and built upon throughout this thesis, is to the authors opinion the most efficient depth inversion procedure for large area, high-resolution EMI datasets. A better understanding and revision of the LIN-approximations and EMI instrument signal responses as formulated by Wait

(1962) and McNeill (1980b) can hopefully improve the accuracy and reliability of this procedure in the future, and make way for 2- and maybe even 3-D inversion algorithms.

Lastly, implementation of multi-sensor surveys (or platforms) can form a basis for joint interpretation and fusion of the different resulting datasets. Although hinted on in many occasions in soil survey, environmental research and archaeology, a true integration of multi-sensor data still needs to be tackled at a field scale. The incorporation of non-invasive geophysical such as sensors that record magnetic viscosity, magnetometer instruments and GPR sensors alongside multi-receiver EMI sensors is already taking place. Data fusion, however, remains a gap to bridge.

Appendix

The qualitative depth estimation of a magnetic anomaly through multi-receiver EMI data.

In this appendix an example is presented of how the use of multiple, simultaneous κ_a measurements with HCP coil pairs with varying intercoil separation can aid in estimating the depth of a magnetic anomaly. The presented measurements were obtained during one survey run with the Dualem-21 sensor, at a survey resolution of 0.85 cm between survey lines and an in-line resolution of approximately 0.25 cm.

The survey was conducted in the framework of an archaeological study guided by the RAAP Archaeological Consultancy and commissioned by the Flemish Heritage service (Onroerend Erfgoed) in Spiere (Belgium), aimed at determining the extent of a known Neolithic settlement. The pedology of the area is mainly made up of loess, resulting in very low magnetic background variations. The EMI survey revealed a number of highly magnetic circular anomalies. A number of these anomalies rendered different responses in the 1 m and 2 HCP IP-data.

The anomaly presented in Fig. A1 shows up positive in the 1.1 m PRP κ_a data (Fig. A1A) and in the 2 m HCP κ_a data (Fig. A1B), while it can be seen as a negative magnetic anomaly in the 1 m HCP coil pair. As PRP coil pairs do not suffer from a sign change, the contrast (highly susceptible anomaly – low susceptible background) can be taken as representative. With this knowledge, the depth of the feature can be qualitatively determined by taking the HCP response functions (Fig. A1D) into account.

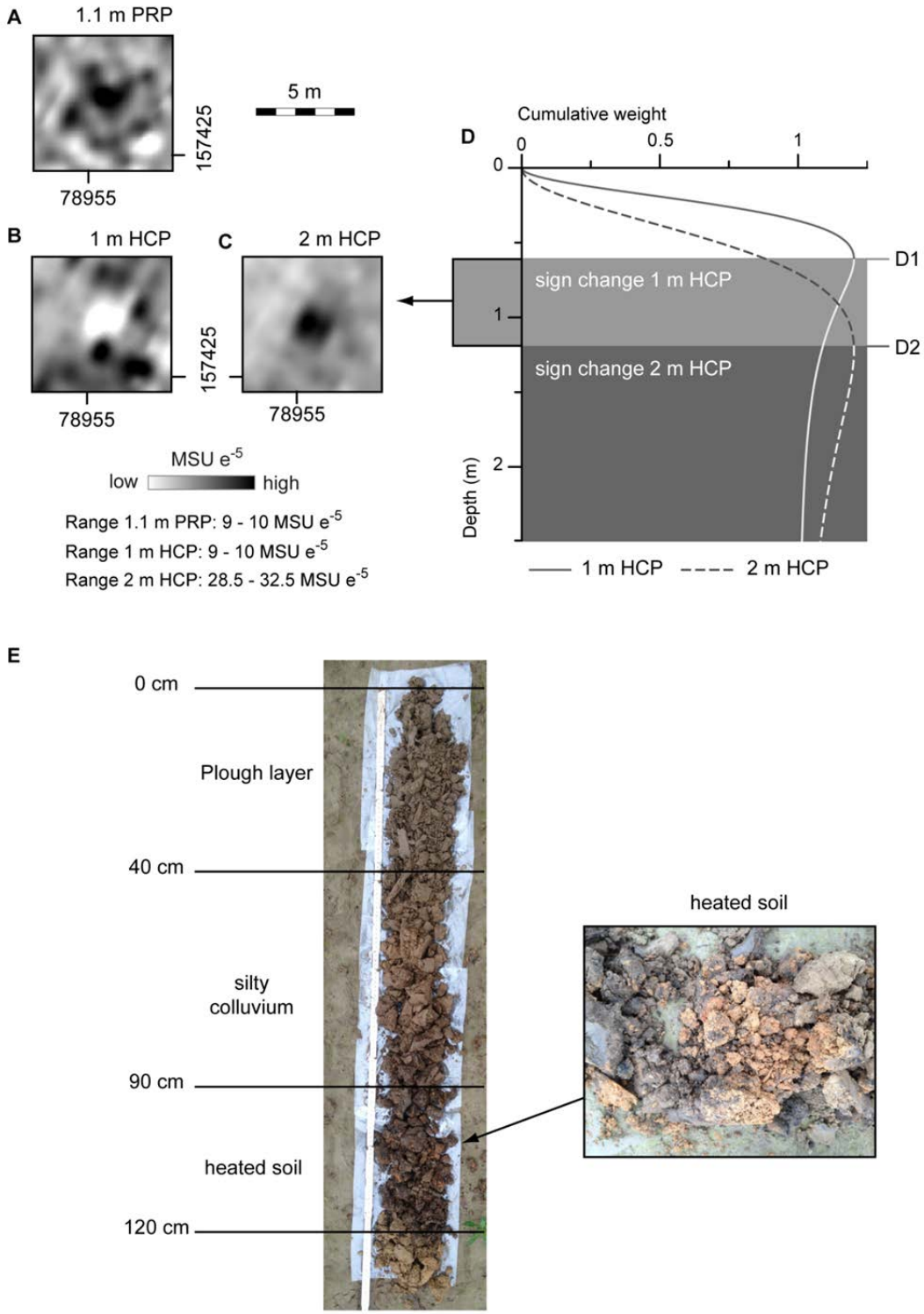

Fig. A1 Simultaneously obtained κ_a data from the 1.1 m PRP (A), 1 m HCP (B), and 2 m HCP (C) coil pairs of the Dualem-21S of an anomaly with a higher magnetic susceptibility than the surrounding soil. D shows the cumulative response depths with indication of the position of the top of the anomaly, based on the positive response in the 1.1 m PRP and 2 m HCP data, and the negative response in the 1 m HCP data. E shows a soil profile obtained by augering in the anomaly, which revealed a layer of heated soil and ceramics between 0.9 m – 1.2 m below the surface

The sign change in the 1 m HCP measurements, and the direct representation of the higher susceptibility of the feature in the 2 m HCP data, places the feature between the two critical depths of these coil pairs, i.e. between 0.6 and 1.2 m below the sensor. With a sensor height of 0.16 m above the surface, the depth of the feature can therefore be placed between approximately 0.5 and 1.1 m below the surface.

To validate this interpretation, coring was performed with a 5 cm dutch auger (Fig A1E). Below the silty plough layer and a silty colluvium, heated soil was attested between 0.90 – 1.20 m below the surface (i.e. 1.06 m and 1.36 m below the sensor), confirming the qualitative interpretation of the feature depth based on the theoretical response functions. The feature was composed of heated soil, ceramic fragments and burnt flint chips. Although no further magnetic analysis of the feature was performed, it can be assumed that the heating of the soil caused a magnetic enhancement of the low natural soil magnetism in the area, resulting in the measured increase in κ_a.

Although quantitative analysis of the HCP signal response to extract depth information has not been successfully performed, the presented case study shows how the specific IP signal response of HCP coil pairs can aid in evaluating the depth of detected anomalies when the relative magnetic susceptibility (i.e. high or low) of the investigated feature is known.

References

Abdij van Boudelo, record 6, *sub no.* 50. Ghent State Archives.

Abdij van Boudelo, record 8, sheet 80 r°-v°, Ghent State Archives.

Abdu, H., Robinson, D.A., Jones, S.B., 2007. Comparing bulk soil electrical conductivity determination using the DUALEM-1S and EM38-DD electromagnetic induction instruments. *Soil Science Society of America Journal* **71**: 189-196.

Agache, R., 1978. *La somme pré-romaine et romaine*. Mémoires de la Société des Antiquaires de Picardie, Amiens.

AGIV, 2003a. Digitaal Hoogtemodel Vlaanderen. *Nieuwsbrief GIS Vlaanderen*.

AGIV, 2003b. Orthofoto's, middenschalig, kleur (2002), provincie Oost-Vlaanderen (CD-ROM). Ondersteunend centrum GIS-Vlaanderen.

AGIV, 2004. DHM-Vlaanderen (2001-2004): Digitaal Hoogtemodel Vlaanderen (CD-ROM). Ondersteunend centrum GIS-Vlaanderen.

Allred, B.J., Reza Ehsani, M., Saraswat, D., 2006. Comparison of Electromagnetic Induction, Capacitively-Coupled Resistivity, and Galvanic Contact Resistivity Methods for Soil Electrical Conductivity Measurement, *Applied Engineering in Agriculture* **22**: 215-230.

Aspinall, A., Gaffney, C., Schmidt, A., 2008. *Magnetometry for archaeologists*. Altamira Press, Lanham.

Baines, D., Smith, D.G., Froese, D.G., Bauman, P., Nimeck, G., 2002. Electrical resistivity ground imaging (ERGI): a new tool for mapping the lithology and geometry of channel-belts and valley-fills. *Sedimentology* **49**: 441-449.

Bates, M.R., Barham, A.J., Pine, C.A., Williamson, V.D., 2000. Evaluation strategies for deeply stratified alluvial areas: the use of borehole stratigraphic logs. In: S. Roskams (Ed.), *Interpreting stratigraphy. Site evaluation recording procedures and stratigraphic analysis.* BAR International Series. Archaeopress, Oxford, pp. 49-69.

Bates, M.R., Bates, C.R., 2000. Multidisciplinary Approaches to the Geoarchaeological Evaluation of Deeply Stratified Sedimentary Sequences: Examples from Pleistocene and Holocene Deposits in Southern England, United Kingdom. *Journal of Archaeological Science* **27**: 845–858.

Bates, M.R., Bates, C.R., Whittaker, J.E., 2007. Mixed Method Approaches to the Investigation and Mapping of Buried Quaternary Deposits: Examples from Southern England. *Archaeological Prospection* **14**: 104-129.

Bats, M., De Reu, J., De Smedt, P., Antrop, M., Bourgeois, J., Court-Picon, M., De Maeyer, P., Finke, P., Van Meirvenne, M., Verniers, J., Werbrouck, I., Zwertvaegher, A., Crombé, P., 2009a. Geoarchaeological research of the large palaeolake of the Moervaart (municipalities of Wachtebeke and Moerbeke-Waas, East-Flanders, Belgium). From Late Glacial to Early Holocene. *Notae Praehistoricae* **29**: 105-112.

Bats, M., De Reu, J., De Smedt, P., Antrop, M., Bourgeois, J., Court-Picon, M., De Maeyer, P., Finke, P., Van Meirvenne, M., Verniers, J., Werbrouck, I., Zwertvaegher, A., Crombé, P., 2009b. Geoarchaeological research of the large palaeolake of the Moervaart (municipalities of Wachtebeke and Moerbeke-Waas, East Flanders, Belgium): from Late Glacial to Early Holocene. *Notae Praehistoricae* **29**: 105-112.

Bats, M., De Smedt, P., De Reu, J., Gelorini, V., Zwertvaegher, A., Antrop, M., Bourgeois, J., De Maeyer, P., Finke, P., Van Meirvenne, M., Verniers, J., Crombé, P., 2011. Continued geoarchaeological research at the Moervaart palaeolake area (East Flanders, B): field campaign 2011. *Notae Praehistoricae* **31**: 201-211.

Bats, M., De Smedt, P., Werbrouck, I., Zwertvaegher, A., Court-Picon, M., De Reu, J., Serbruyns, L., Demiddele, H., Antrop, M., Bourgeois, J., De Maeyer, P., Finke, P., Van M[e]irvenne, M., Verniers, J., Crombé, P., 2010. Continued geoarchaeological research at the Moervaart palaeolake area (East Flanders, Belgium): preliminary results. *Notae Praehistoricae* **30**: 55-61.

Beamish, D., 2011. Low induction number, ground conductivity meters: A correction procedure in the absence of magnetic effects, *Journal of Applied Geophysics* **75**: 244-253.

Beck, A.E., 1981. Physical Principles of Exploration Methods: An Introductory Text for Geology and Geophysics Students. John Wiley, New York.

Benech, C., Marmet, E., 1999. Optimum depth of investigation and conductivity response rejection of the different electromagnetic devices measuring apparent magnetic susceptibility, *Archaeological Prospection* **6**: 31-45.

Binford, L.R., 1983. In pursuit of the past: decoding the archaeological record. University of California Press.

Bockheim, J.G., Gennadiyev, A.N., Hammer, R.D., Tandarich, J.P., 2005. Historical development of key concepts in pedology. *Geoderma* **124**: 23-36.

Bourgeois, J., Meganck, M., Semey, J., 2005. Almost a century of aerial photography in Belgium. An overview. In: J. Bourgeois, M. Meganck (Eds.), *Aerial Photography and Archaeology 2003. A Century of Information.* Academia, Gent, pp. 37-48.

Bourgeois, J., Roovers, I., Meganck, M., Semey, J., Pelegrin, R., Lodewijckx, M., 2002. Flemish aerial archaeology in the last 20 years: past and future perspectives. In: R. Bewley, W. Raczkowski (Eds.), *Aerial Archaeology*. Developing Future Practice. . NATO Science Series, pp. 76-83.

Brenner, R., 2001. The Low Countries in the transition to capitalism. In: P. Hoppenbrouwers, J.L. Van Zanden (Eds.), From peasants to farmers? The transformation of the rural economy and society in the Low Countries (middle ages-beginning 20th century) in the light of the Brenner Debate. Brepols, Turnhout, pp. 275-338.

Brevik, E., Fenton, T., Lazari, A., 2006. Soil electrical conductivity as a function of soil water content and implications for soil mapping, Precision Agriculture **7**, 393-404.

Bronk, R.C., 2009. Bayesian analysis of radiocarbon dates. *Radiocarbon* **51**: 337-360.

Buisman, J., 1995. Duizend jaar weer, wind en water in de Lage Landen, 1: tot 1300. Van Wijnen.

Butler, D.K. (Ed.), 2005. *Near-surface geophysics. Investigations in geophysics*. Society of Exploration Geophysicists.

Callegary, J.B., Ferre, T.P.A., Groom, R.W., 2007. Vertical spatial sensitivity and exploration depth of low-induction-number electromagnetic-induction instruments. *Vadose Zone Journal* **6**: 158-167.

Cassidy-Welch, M., 2001. Monastic Spaces and their Meanings: Thirteenth-Century English Cistercian Monasteries. Medieval Church Studies. Brepols, Turnhout.

Challis, K., Howard, A.J., 2006. A Review of Trends within Archaeological Remote Sensing in Alluvial Environments. *Archaeological Prospection* **13**: 231-240.

Conyers, L.B., Ernenwein, E.G., Grealy, M., Lowe, K.M., 2008. Electromagnetic conductivity mapping for site prediction in meandering river floodplains. *Archaeological Prospection* **15**: 81-91.

Crombé, P., Sergant, J., Robinson, E., De Reu, J., 2011. Hunter–gatherer responses to environmental change during the Pleistocene–Holocene transition in the southern North Sea basin: Final Palaeolithic–Final Mesolithic land use in northwest Belgium. *Journal of Anthropological Archaeology* **30**: 454-471.

Crombé, P., Van Strydonck, M., Boudin, M., Van den Brande, T., Derese, C., Vandenberghe, D.A.G., Van den haute, P., Court-Picon, M., Verniers, J., Bos, J.A.A., Verbruggen, C., Antrop, M., Bats, M., Bourgeois, J., De Reu, J., De Maeyer, P., De Smedt, P., Finke, P.A., van Meirvenne, M., Zwertvaegher, A., 2012. Absolute dating (14C and OSL) of the formation of coversand ridges occupied by prehistoric man in NW Belgium. *Radiocarbon* **54**: 715-726.

Crombé, P., Verbruggen, C., 2002. The Late Glacial and Early Post Glacial occupation of northern Belgium: the evidence from Sandy Flanders. In: B.V. Eriksen, Bratlund, B. (Ed.), *Proceedings of a U.I.S.P.P. Symposium Recent studies in the Final Palaeolithic of the European plain*. Stockholm, pp. 165-180.

Dalan, R.A., 2008. A review of the role of magnetic susceptibility in archaeogeophysical studies in the USA: recent developments and prospects. *Archaeological Prospection* **15**: 1-31.

De Belie, A., 1997. *De Boudelo abdij archeologisch onderzocht*, Belsele. De Belie, Alfons.

De Clercq, W., 2011. Roman rural settlements in Flanders. Perspectives on a 'non-villa' landscapes in extrema Galliarum. In: N. Roymans, T. Derks (Eds.), *Villa Landscapes in the Roman North*. Amsterdam University Press, Amsterdam, pp. 235-258. .

De Clercq, W., Bats, M., Laloo, P., Sergant, J., Crombé, P., 2011. Beware of the known. Methodological issues in the detection of low density rural occupation in larg^{e-}surface archaeological landscape-assessment in Northern-Flanders (Belgium). In: G. Blanquaert, F. Malain, H. Stäube, J. Vanmoerkerke (Eds.), *Understanding the past: a matter of surface-area. Acts of the XIIIth session of the EAA congress, Zadar 2007*. British Archaeological Reports, International Series. Archaeopress, Oxford, pp. 73-89.

De Clercq, W., De Smedt, P., De Reu, J., Herremans, D., Masters, P., Saey, T., Stichelbaut, B., Van Meirvenne, M., 2012. Towards an Integrated Methodology for Assessing Rural Settlement Landscapes in the Belgian Lowlands. *Archaeological Prospection* **19**: 141-145.

De Moor, G., Heyse, I., 1974. Lithostratigrafie van de Kwartaire afzettingen in de overgangszone tussen de kustvlakte en de Vlaamse Vallei in Noordwest België. *Natuurwetenschappelijk Tijdschrift* **56**: 85-109.

De Reu, J., Bats, M., De Smedt, P., Bourgeois, J., Antrop, M., Court-Picon, M., De Maeyer, P., Finke, P., Van Meirvenne, M., Verniers, J., Werbrouck, I., Zwertvaegher, A., Crombé, P., 2010. Bronze and Iron Age landscapes in Sandy Flanders (NW-Belgium): a geoarchaeological approach. *LUNULA (BRUSSEL)* **18**: 17-22.

De Smedt, P., Saey, T., Lehouck, A., Stichelbaut, B., Meerschman, E., Islam, M.M., Van De Vijver, E., Van Meirvenne, M., 2013a. Exploring the potential of multi-receiver EMI survey for geoarchaeological prospection: a 90 ha dataset. *Geoderma* **40**: 1260–1267.

De Smedt, P., Van Meirvenne, M., Davies, N.S., Bats, M., Saey, T., De Reu, J., Meerschman, E., Gelorini, V., Zwertvaegher, A., Antrop, M., Bourgeois, J., De Maeyer, P., Finke, P.A., Verniers, J., Crombé, P., 2013b. A multidisciplinary approach to reconstructing Late Glacial and Early Holocene landscapes. *Journal of Archaeological Science* **40**: 1260-1267.

De Smedt, P., Van Meirvenne, M., Meerschman, E., Saey, T., Bats, M., Court-Picon, M., De Reu, J., Zwertvaegher, A., Antrop, M., Bourgeois, J., De Maeyer, P., Finke, P.A., Verniers, J., Crombé, P., 2011a. Reconstructing palaeochannel morphology with a mobile multicoil electromagnetic induction sensor. *Geomorphology* **130**: 136-141.

De Smedt, P., Van Meirvenne, M., Simpson, D., 2011b. Multi-signal EMI and geoarchaeology – Evaluating integrated magnetic susceptibility measurements for archaeological prospection. *9th international conference on archaeological prospection, September 19 – 24, 2011*.

Dearing, J.A., 1999. Magnetic susceptibility. In: J. Walden, F. Oldfield, J. Smith (Eds.), *Environmental magnetism. A practical guide.* Technical Guide. Quaternary Research Association, London.

Dearing, J.A., Hay, K.L., Baban, S.M.J., Huddleston, A.S., Wellington, E.M.H., Loveland, P.J., 1996. Magnetic susceptibility of soil: an evaluation of conflicting theories using a national data set. *Geophysical Journal International* **127**: 728-734.

Derese, C., Vandenberghe, D.A.G., Zwertvaegher, A., Court-Picon, M., Crombé, P., Verniers, J., Van den haute, P., 2010. The timing of aeolian events near archaeological settlements around Heidebos (Moervaart area, N Belgium). *Netherlands Journal of Geosciences* **89**: 173-186.

Dualem, I., 2007. *Dualem-21S User's Manual*. Dualem, Inc., Milton.

Evans, M.E., Heller, F., 2003. *Environmental Magnetism. Principles and Applications of Enviromagnetics*. International Geophysics Series. Academic Press, California.

Fassbinder, J.W.E., Stanjekt, H., Vali, H., 1990. Occurrence of magnetic bacteria in soil. *Nature* **343**: 161-163.

Fassbinder, J.W.E. 1994. Die magnetischen Eigenschaften und die Genese ferrimagnetischer Minerale in Böden im Hinblick auf die magnetische Prospektion archäologischer Bodendenkmäler. PhD Thesis, Ludwig-Maximilians-Universität, München.

Fraser, D., 1972. A new multicoil aerial electromagnetic prospecting system. *Geophysics* **37**: 518-537.

French, C., 2010. People, Societies, and Landscapes. *Science* **328**: 443-444.

Gaffney, C., 2008. Detecting trends in the prediction of the buried past: a review of geophysical techniques in archaeology. *Archaeometry* **50**: 313-336.

Gaffney, C., Gaffney, V., Neubauer, W., Baldwin, E., Chapman, H., Garwood, P., Moulden, H., Sparrow, T., Bates, R., Löcker, K., Hinterleitner, A., Trinks, I., Nau, E., Zitz, T., Floery, S., Verhoeven, G., Doneus, M., 2012. The Stonehenge Hidden Landscapes Project. *Archaeological Prospection* **19**: 147-155.

Gaffney, C., Gater, J., 2003. *Revealing the buried past. Geophysics for archaeologists*. Tempus, Gloucestershire.

Gavin, H., 2011. The Levenberg-Marquardt method for nonlinear least squares curve-fitting problems. Duke University, North-Carolina.

Goldberg, P., Macphail, R.I., 2006. *Practical and theoretical geoarchaeology*. Blackwell Publishing, Oxford.

Goovaerts, P., 1997. *Geostatistics for natural resources evaluation*. Applied Geostatistics Series. Oxford University Press, New York, USA.

Gourry, J.-C., Vermeersch, F., Garcin, M., Giot, D., 2003. Contribution of geophysics to the study of alluvial deposits: a case study in the Val d'Avaray area of the River Loire, France. *Journal of Applied Geophysics* **54**: 35-49.

Henry, E.R., 2011. A multistage geophysical approach to detecting and interpreting archaeological features at the LeBus Circle, Bourbon County, Kentucky. *Archaeological Prospection* **18**: 231-244.

Howard, A.J., Brown, A.G., Carey, C.J., Challis, K., Cooper, L.P., Kincey, M., Toms, P., 2008. Archaeological resource modelling in temperate river valleys: a case study from the Trent Valley (UK). *Antiquity* **318**: 1040-1054.

Howell, M., 1966. A soil conductivity meter. *Archaeometry* **9**: 20-23.

Islam, M., Meerschman, E., Saey, T., De Smedt, P., Van De Vijver, E., Van Meirvenne, M., 2011. *Comparing apparent electrical conductivity measurements on a paddy field under flooded and drained conditions.* Precision Agriculture **13**, 384 - 392.

Jenny, H., 1994. Factors of soil formation: a system of quantitative pedology. Dover Publications, New York.

Joffe, J.S., 1936. *Pedology*. Rutgers University Press, New Brunswick.

Jol, H.M., 2009. Ground penetrating radar: theory and applications. Elsevier, Oxford.

Jordan, D., 2009. How effective is geophysical survey? A regional review. *Archaeological Prospection* **16**: 77-90.

Keay, S., Earl, G., Hay, S., Kay, S., Ogden, J., Strutt, K.D., 2009. The role of integrated geophysical survey methods in the assessment of archaeological landscapes: the case of Portus. *Archaeological Prospection* **16**: 154-166.

Keller, G.V., Frischknecht, F.C., 1966. *Electrical Methods in Geophysical Prospection.* International Series of Monographs in Electromagnetic Waves Volume 10. Pergamon Press, London.

Kvamme, K.L., 2003. Geophysical surveys as landscape archaeology. *American Antiquity* **68**: 435-457.

Le Borgne, E., 1955. Susceptibilité magnetique anormale du sol superficial. *Annales de Géophysique* **11**: 399-419.

Le Borgne, E., 1960. Influence du feu sur les propriétés magnétiques du sol et sur celles du schiste et du granite. *Annales de Géophysique* **16**: 159-195.

Lecoanet, H., Lévêque, F., Segura, S., 1999. Magnetic susceptibility in environmental applications: comparison of field probes. *Physics of the Earth and Planetary Interiors* **115**: 191-204.

Linford, N.T., 1994. Mineral magnetic profiling of archaeological sediments. *Archaeological Prospection* **1**: 37-52.

Linford, N.T., 1998. Geophysical survey at Bodem Vean Cornwall, including an assessment of the microgravity technique for the location of suspected archaeological void features, *Archaeometry* **40**: 187-216.

Loke, M.H., Barker, R.D., 1996. Rapid least-squares inversion of apparent resistivity pseudosections by a quasi-Newton method. *Geophysical Prospecting* **44**: 131-152.

Matheron, G., 1962. Traité de Géostatistique Appliqué, Tome 1. Technip, Paris.

Minasny, B., McBratney, A.B., 2010. Conditioned Latin Hypercube Sampling for Calibrating Soil Sensor Data to Soil Properties. In: R.A. Viscarra Rossel, A.B. McBratney, B. Minasny (Eds.), *Proximal Soil Sensing*. `Progress in Soil Science. Springer, New York, pp. 111-120.

McNeill, J.D., 1980a. Electrical conductivity of soils and rocks. Technical Note 5, Geonics Limited, Ontario.

McNeill, J.D., 1980b. Electromagnetic terrain conductivity measurement at low induction numbers. Technical Note 6, Geonics Limited, Ontario.

McNeill, J.D., 1996. Why doesn't Geonics Limited build a multi-frequency EM31 or EM38. Technical Note 30, Geonics Limited, Ontario.

Minasny, B., McBratney, A.B., 2006. A conditioned Latin hypercube method for sampling in the presence of ancillary information. *Computers & Geosciences* **32**: 1378-1388.

Monteiro Santos, F.A., Triantafilis, J., Bruzgulis, K.E., Roe, J.A.E., 2010. Inversion of multiconfiguration electromagnetic (DUALEM-421) profiling data using a one-dimensional laterally constrained algorithm. *Vadose Zone Journal* **9**: 117-125.

Moorman, B.J., 1990. Assessing the ability of ground penetrating radar to delineate subsurface fluvial lithofacies. M.Sc. Thesis, The University of Calgary, Calgary, 124 pp.

Nabighian, M.N. (Ed.), 1991. *Electromagnetic methods in applied geophysics.* Investigations in Geophysics, 2 Society of Exploration Geophysicists.

Nanson, G.C., Knighton, A.D., 1996. Anabranching rivers: their cause, character and classification. *Earth Surf. Process. Landf.* **21**: 217-239.

Neubauer, W., Eder-Hinterleitner, A., Seren, S., Melichar, P., 2002. Georadar in the Roman Civil Town Carnuntum, Austria: an Approach for Archaeological Interpretation of GPR Data. *Archaeological Prospection* **9**: 135-156.

Prevenier, W., 1983. La démographie des villes du comté de Flandre aux XIVe et XVe siècles. *Revue du Nord* **65**: 255-275.

Reimer, P.J., Baillie, M.G.L., Bard, E., Bayliss, A., Beck, J.W., Blackwell, P.G., Bronk, R.C., Buck, C.E., Burr, G.S., Edwards, R.L., Friedrich, M., Grootes, P.M., Guilderson, T.P., Hajdas, I., Heaton, T.J., Hogg, A.G., Hughen, K.A., Kaiser, K.F., Kromer, B., McCormac, F.G., Manning, S.W., Reimer, R.W., Richards, D.A., Southon, J.R., Talamo, S., Turney, C.S.M., van der Plicht, J., Weyhenmeyer, C.E., 2009. IntCal09 and Marine09 radiocarbon age calibration curves, 0-50,000 years cal BP. *Radiocarbon* **51**: 1111-1150.

Renfew, C., Bahn, P., 2004. *Archaeology: Theories, Methods, and Practice*. Thames & Hudson.

Reynolds, J.M., 1997. An introduction to applied and environmental geophysics. Wiley & Sons, New York.

Rhoades, J.D., Raats, P.A.C., Prather, R.J., 1976. Effects of Liquid-phase Electrical Conductivity, Water Content, and Surface Conductivity on Bulk Soil Electrical Conductivity. *Soil Science Society of America Journal* **40**: 651-655.

Richards, K., Chandra, S., Friend, P., 1993. Avulsive channel systems: characteristics and examples. *Geological Society, London, Special Publications* **75**: 195-203.

Saey, T., 2011. Fusing multiple signals of an electromagnetic induction sensor to characterize contrasting soil layers and buried features. PhD Thesis, Ghent University, Ghent, 163 pp.

Saey, T., De Smedt, P., De Clercq, W., Meerschman, E., Islam, M.M., Van Meirvenne, M., 2013. Identifying Soil Patterns at Different Spatial Scales with a Multi-Receiver EMI sensor. *Soil Science Society of America Journal* **77**: 382 - 390

Saey, T., De Smedt, P., Meerschman, E., Islam, M.M., Meeuws, F., Van De Vijver, E., Lehouck, A., Van Meirvenne, M., 2011. Electrical conductivity depth modelling with a multireceiver EMI sensor for prospecting archaeological features. *Archaeological Prospection* **19**: 21-30.

Saey, T., Islam, M.M., De Smedt, P., Meerschman, E., Van De Vijver, E., Lehouck, A., Van Meirvenne, M., 2012. Using a multi-receiver survey of apparent electrical

conductivity to reconstruct a Holocene tidal channel in a polder area. *Catena* **95**: 104-111.

Saey, T., Simpson, D., Vermeersch, H., Cockx, L., Van Meirvenne, M., 2009. Comparing the EM38DD and Dualem-21S sensors for depth-to-clay mapping. *Soil Science Society of America Journal* **73**: 7-12.

Saey, T., Simpson, D., Vitharana, U.W.A., Vermeersch, H., Vermang, J., Van Meirvenne, M., 2008. Reconstrucing the paleotopography beneath the loess cover with the aid of an electromagnetic induction sensor. *Catena* **74**: 58-64.

Saey, T., Van Meirvenne, M., Trinks, I., De Smedt, P., Verhoeven, G., Neubauer, W., Integrating multi-receiver EMI measurements to interpret the soil landscape around the school of gladiatiors, Carnuntum. *Submitted*

Schrott, L., Sass, O., 2008. Application of field geophysics in geomorphology: advances and limitations exemplified by case studies. *Geomorphology* **93**: 55-73.

Scollar, I., 1962. Electromagnetic prospecting methods in archaeology. *Archaeometry* **5**: 146-156.

Scollar, I., 1990. *Archaeological Prospecting and Remote Sensing*. Topics in Remote Sensing. Cambridge University Press, Cambridge.

Sheets, K.R., Hendrickx, J.M.H., 1995. Noninvasive Soil Water Content Measurement Using Electromagnetic Induction, *Water Resources Research* **31**: 2401-2409.

Sheriff, R.E., 1991. *Encyclopedic Dictionary of Exploration Geophysics*. Geophysical references, 13. Geophysical references, Tulsa.

Simpson, D., 2009. Geoarchaeological prospection with multi-coil electromagnetic induction sensors. PhD Thesis, Ghent University, Ghent 154 pp.

Simpson, D., Lehouck, A., Van Meirvenne, M., Bourgeois, J., Thoen, E., Vervloet, J., 2008. Geoarchaeological prospection of a medieval manor in the Dutch Polders using an electromagnetic induction sensor in combination with soil augerings. *Geoarchaeology* **23**: 1-14.

Simpson, D., Lehouck, A., Verdonck, L., Vermeersch, H., Van Meirvenne, M., Bourgeois, J., Thoen, E., Docter, R., 2009a. Comparison between electromagnetic induction and fluxgate gradiometer measurements on the buried remains of a 17th century castle. *Journal of Applied Geophysics* **68**: 294-300.

Simpson, D., Van Meirvenne, M., Lück, E., Rühlmann, J., Saey, T., Bourgeois, J., 2010. Sensitivity of multi-coil frequency domain electromagnetic induction sensors to map soil magnetic susceptibility. *European Journal of Soil Science* **61**: 469-478.

Simpson, D., Van Meirvenne, M., Saey, T., Vermeersch, H., Bourgeois, J., Lehouck, A., Cockx, L., Vitharana, U.W.A., 2009b. Evaluating the multiple coil configurations of the EM38DD and DUALEM-21S sensors to detect archaeological anomalies. *Archaeological Prospection* **16**: 91-102.

Slavich, P., Petterson, G., 1990. Estimating average rootzone salinity from electromagnetic induction (EM-38) measurements. *Australian Journal of Soil Research* **28**: 453-463.

Smith, J., 1999. An introduction to the magnetic properties of natural materials. In: J. Walden, F. Oldfield, J. Smith (Eds.), *Environmental magnetism: a practical guide.* QRA Technical Guides. Quaternary Research Association, London, pp. 5-25.

Sudduth, K.A., Kitchen, N.R., Wiebold, W.J., Batchelor, W.D., Bollero, G.A., Bullock, D.G., Clay, D.E., Palm, H.L., Pierce, F.J., Schuler, R.T., Thelen, K.D., 2005. Relating apparent electrical conductivity to soil properties across the north-central USA. *Computers and Electronics in Agriculture* **46**: 263-283.

Tabbagh, A., 1984. Interest in the slingram EM method for archaeological prospecting, *SEG Technical Program Expanded Abstracts*, pp. 206-208.

Tabbagh, A., 1985. The response of a three-dimensional magnetic and conductive body in shallow depth electromagnetic prospecting. *Geophysical Journal of the Royal Astronomical Society* **81**: 215-230.

Tabbagh, A., 1986a. Applications and advantages of the Slingram electromagnetic method for archaeological prospecting. *Geophysics* **51**: 576-584.

Tabbagh, A., 1986b. What is the best coil orientation in the Slingram electromagnetic prospecting method? *Archaeometry* **28**: 185-196.

Tite, M.S., Mullins, C., 1970. Electromagnetic prospecting on archaeological sites using a soil conductivity meter. *Archaeometry* **12**: 97-104.

Trinks, I., Johansson, B., Gustafsson, J., Emilsson, J., Friborg, J., Gustafsson, C., Nissen, J., Hinterleitner, A., 2010. Efficient, large-scale archaeological prospection using a true three-dimensional ground-penetrating Radar Array system. *Archaeological Prospection* **17**: 175-186.

Van Dam, R.L., 2012. Landform characterization using geophysics—Recent advances, applications, and emerging tools. *Geomorphology* **137**: 57-73.

Van Vlaenderen, L., Sergant, J., De Bock, H., De Meireleir, M., 2006. *Steentijdvondsten in de Moervaartdepressie (Oost-Vlaanderen, België). Inventaris en geografische analyse*. Archeologische Inventaris Vlaanderen. Buitengewone reeks. Arch. I.V., Gent.

Verhaeghe, F., 1981. Medieval Moated Sites in Coastal Flanders. In: F.A. Aberg, A.E. Brown (Eds.), *Medieval Moated Sites in North-West Europe.* BAR International Series. Archaeopress, Oxford, pp. 127-172.

Verhulst, A., 1995. *Landschap en landbouw in Middeleeuws Vlaanderen*. Gemeentekrediet, Brussels.

Verhulst, A., 1999. *The rise of cities in North-Western Europe*. Cambridge University Press, Cambridge.

Wait, J., 1982. *Geo-electromagnetism*. Academic Press, Inc., New York.

Wait, J.R., 1962. A note on the electromagnetic response of a stratified earth. *Geophysics* **27**: 382-385.

Webster, R., Oliver, M.A., 2001. *Geostatistics for environmental scientists*. Statistics in practice. John Wiley & Sons, West Sussex.

Werbrouck, I., Antrop, M., Van Eetvelde, V., Stal, C., De Maeyer, P., Bats, M., Bourgeois, J., Court-Picon, M., Crombé, P., De Reu, J., De Smedt, P., Finke, P.A., Van Meirvenne, M., Verniers, J., Zwertvaegher, A., 2011. Digital elevation model generation for historical landscape analysis based on LiDAR data, a case study in Flanders (Belgium). *Expert Systems with Applications* **38**.

West, G.F., Macnae, J.C., 1991. Physics of the elecromagnetic induction method. In: M.N. Nabighian (Ed.), *Electromagnetic methods in applied geophysics – Volume 2, Application parts A and B.* Investigations in Geophysics. Society of Exploration Geophysicists, Oklahoma, pp. 5-46.

Williams, M., Dunkerley, D., De Deckker, P., Kershaw, P., Chappell, J., 1993. *Quaternary Environments*. Arnold, London.

Curriculum vitae

1 Personal information

Name:	Philippe De Smedt	Email:	Philippe.DeSmedt@UGent.be
Date of birth:	May 31st, 1984	Tel.:	0032(0)478.516.007
Address:	Ganzendries 82		
	9000 Gent, Belgium		

2 Education

2009-2013	PhD research in Bioscience Engineering: Land and Forest Management
	Ghent University, Belgium
2005-2008	Master in Archaeology
	Ghent University, Belgium
2002-2005	Candidate in Archaeology
	Ghent University, Belgium

3 Professional experience

a. Research

2009-2013	Doctoral researcher
	Department of Soil Management
	Ghent University, Belgium
2008-2009	Field archaeologist and research intern
	Department of Archaeology
	Ghent University, Belgium

b. Taught courses and workshops

June 2012	Geophysical soil sensors for archaeological prospection
	Theoretical and practical applications of EMI sensors
	Practical course on processing and visualizing geophysical data
	Ghent University, Belgium

May 2012 — 1st MAC international workshop of archaeological geophysics
Introduction to the principles and applications of EMI survey for archaeologists: theory and practice
Archaeological Museum of Cataluña, Ullastret, Spain

c. Geophysical research campaigns (not included in the thesis)

2012 — Geophysical research 'Spiere-Helkijn" (Spiere, Belgium)
Mapping the extent of a Neolithic settlement
RAAP Archaeological Consultancy

2011 — Geophysical research 'Fort Sint-Frederik' (Knokke-Heist, Belgium)
Detailed archaeological mapping of a 17th century Spanish fortress
Raakvlak, intercommunal heritage service for the Bruges region

2010 — Geophysical research 'Moervaart-Noord' (Sint-Kruis-Winkel, Belgium)
Palaeotopographical mapping prior to archaeological evaluation
VIOE, Flemish Institute for Heritage Management

2009 — Geophysical research 'Golf Hof ter Hille' (Koksijde, Belgium)
Archaeological mapping for the evaluation of a 90 ha development area
Municipality of Koksijde

4 Scientific publications

4.1 Publications in ISI-annoted journals (A1)

a. In press.

25. Meerschman, E.; Van Meirvenne, M.; Mariethoz, G.; Islam, M.M.; **De Smedt, P.**; Van De Vijver, E.; Saey, T. In Press. Using bivariate multiple-point statistics and proximal soil sensor data to map fossil ice-wedge polygons. *Geoderma*.

24. Saey, T.; **De Smedt, P.**; De Clercq, W.; Meerschman, E.; Islam, M.M.; Van Meirvenne, M. 2013. In Press. Identifying soil patterns at different spatial scales with a multi-receiver EMI sensor. *Soil Science Society of America Journal*.

23. Meerschman, E.; Van Meirvenne, M.; Van De Vijver, E.; **De Smedt, P.**; Islam, M.M.; Saey, T. 2013. In Press Mapping complex soil patterns with multiple-point geostatistics. *European Journal of Soil Science*.

22. De Reu, J.; Bourgeois, J; Bats, M.; Zwertvaegher, A.; Gelorini, V.; **De Smedt, P.**; Chu, W.; Antrop, M.; De Maeyer, P.; Finke, P.; Van Meirvenne, M.; Verniers, J.; Crombé, P. In Press. Application of the topographic position index to heterogeneous landscapes. *Geomorphology*.

21. **De Smedt, P.**; Saey, T.; Lehouck, A.; Stichelbaut, B.; Meerschman, E.; Islam, M.M.; Van De Vijver, E.; Van Meirvenne, M. In Press. Exploring the potential of multi-receiver EMI survey for geoarchaeological prospection: A 90 ha dataset. *Geoderma*.

20. Van Meirvenne, M.; Islam, M.M.; **De Smedt, P.**; Meerschman, E.; Van De Vijver, E.; Saey, T. In Press. Key variables for the identification of soil management classes in the aeolian landscapes of north–west Europe. *Geoderma*.

b. Published

19*. **De Smedt, P.**; Van Meirvenne, M.; Herremans, D.; De Reu, J.; Saey, T.; Meerschman, E.; Crombé, P.; De Clercq, W. 2013. The 3-D reconstruction of medieval wetland reclamation through electromagnetic induction survey. *Scientific Reports*, 3, 1517, (5 pp)

18. De Reu, J.; Bourgeois, J.; Bats, M.; **De Smedt, P.**; Gelorini, V.; Zwertvaegher, A.; Antrop, M.; De Maeyer, P.; Finke, P.A.; Van Meirvenne, M.; Verniers, J.; Crombé, P. 2013. Beyond the unknown, understanding prehistoric patterns in the urbanised landscape of Flanders. *Journal of Historical Geography*, 40, 1-15.

17*. **De Smedt, P.**; Van Meirvenne, M.; Davies, N.S.; Bats, M.; Saey, T.; De Reu, J.; Meerschman, E.; Gelorini, V.; Zwertvaegher, A.; Antrop, M.; Bourgeois, J.; De Maeyer, P.; Finke, P.A.; Verniers, J.; Crombé, P. 2013. A multidisciplinary approach to reconstructing Late Glacial and Early Holocene landscapes. *Journal of Archaeological Science*, 40, 1260-1267.

16. De Reu, J.; Plets, G.; Verhoeven, G.; **De Smedt, P.**; Bats, M.; Cherretté, B.; De Maeyer, W.; Deconynck, J.; Herremans, D.; Laloo, P.; Van Meirvenne, M.; De Clercq, W. 2013. Towards a three-dimensional cost-effective registration of the archaeological heritage. *Journal of Archaeological Science*, 40, 1108-1121.

15. Crombé, P.; Van Strydonck, M.; Boudin, M.; Van den Brande, T.; Derese, C.; Vandenberghe, D. A. G.; Van den Haute, P.; Court-Picon, M.; Verniers, J.; Gelorini, V.; Bos, J.A.A.; Verbruggen, F.; Antrop, M.; Bats, M.; Bourgeois, J.; De Reu, J.; De Maeyer, P.; **De Smedt, P.**; Finke, P. A.; Van Meirvenne, M; Zwertvaegher, A. 2012. Absolute Dating (14C and OSL) of the Formation of Coversand Ridges Occupied by Prehistoric Hunter-Gatherers in NW Belgium. *Radiocarbon*, 54, 715-726.

14. Saey, T.; Islam, M.M.; **De Smedt, P.**; Meerschman, E.; Van De Vijver, E.; Lehouck, A.; Van Meirvenne, M. 2012. Using a multi-receiver survey of apparent electrical conductivity to reconstruct a Holocene tidal channel in a polder area. *Catena*, 95, 104-111.

* Included in this thesis

13. Islam, M.M.; Meerschman, E.; Saey, T.; **De Smedt, P.**; Van De Vijver, E.; Van Meirvenne, M. 2012. Comparing apparent electrical conductivity measurements on a paddy field under flooded and drained conditions. *Precision Agriculture*, 13, 384-392.

12*. De Clercq, W.; **De Smedt, P.**; De Reu, J.; Herremans, D.; Masters, P.; Saey, T.; Stichelbaut, B.; Van Meirvenne, M. 2012. Towards an Integrated Methodology for Assessing Rural Settlement Landscapes in the Belgian Lowlands. *Archaeological Prospection*, 19, 141-145.

11. Saey, T.; **De Smedt P.**; Meerschman, E.; Islam, M.M.; Meeuws, F.; Van De Vijver, E.; Lehouck, A.; Van Meirvenne, M. 2012. Electrical Conductivity Depth Modelling with a Multireceiver EMI Sensor for Prospecting Archaeological Features. *Archaeological Prospection*, 19, 21-30.

10. Islam, M.M.; Saey, T.; Meerschman, E.; **De Smedt, P.**; Meeuws, F.; Van De Vijver, E.; Van Meirvenne, M. 2011. Delineating water management zones in a paddy rice field using a Floating Soil Sensing System. *Agricultural Water Management*, 102, 8-12.

9. De Reu, J.; Bourgeois, J.; **De Smedt, P.**; Zwertvaegher, A.; Antrop, M.; Bats, M.; De Maeyer, P.; Finke, P.; Van Meirvenne, M.; Verniers, J.; Crombé, P. Measuring the relative topographic position of archaeological sites in the landscape, a case study on the Bronze Age barrows in northwest Belgium. *Journal of Archaeological Science*, 38, 3435-3446.

8. Islam, M.M.; Cockx, L.; Meerschman, E.; **De Smedt, P.**; Meeuws, F.; Van Meirvenne, M. 2011. A floating sensing system to evaluate soil and crop variability within flooded paddy rice fields. *Precision Agriculture*, 12, 850-859.

7. Meerschman, E.; Van Meirvenne, M.; **De Smedt, P.**; Saey, T.; Islam, M.M.; Meeuws, F.; Van De Vijver, E.; Ghysels, G. 2011. Imaging a Polygonal Network of Ice-Wedge Casts with an Electromagnetic Incution Sensor. *Soil Science Society of America Journal*, 75, 2095-2100.

6. Saey, T.; Van Meirvenne, M.; Dewilde, M.; Wyffels, F.; **De Smedt, P.**; Meerschman, E.; Islam, M.M.; Meeuws, F.; Cockx, L. 2011. Combining multiple signals of an

electromagnetic induction sensor to prospect land for metal objects. *Near Surface Geophysics*, 9, 309-317.

5*. **De Smedt P.**; Van Meirvenne, M.; Meerschman, E.; Saey, T.; Bats, M.; Court-Picon, M.; De Reu., J.; Zwertvaegher, A.; Antrop, M.; Bourgeois, J.; De Maeyer, P.; Finke, P.A.; Verniers, J.; Crombé, P. 2011. Reconstructing palaeochannel morphology with a mobile multicoil electromagnetic induction sensor. *Geomorphology*, 130, 136-141.

4. Werbrouck, I.; Antrop, M.; Van Eetvelde, V.; Stal, C.; De Maeyer, P.; Bats, M.; Bourgeois, J.; Court-Picon, M.; Crombé, P.; De Reu, J.; **De Smedt, P.**; Finke, P.A.; Van Meirvenne, M.; Verniers, J.; Zwertvaegher, A. 2010. Digital Elevation Model generation for historical landscape analysis based on LiDAR data, a case study in Flanders (Belgium). *Expert Systems with Applications*, 38, 8178-8185.

3. Saey, T.; Van Meirvenne, M.; **De Smedt, P.**; Cockx, L.; Meerschman, E.; Islam, M.M.; Meeuws, F. 2011 Mapping depth-to-clay using fitted multiple depth response curves of a proximal EMI sensor. *Geoderma*, 162, 151-158.

2. De Reu, J.; Deweirdt, E.; Crombé, P.; Bats, M.; Antrop, M.; De Maeyer, P.; **De Smedt, P.**; Finke, P.A.; Van Meirvenne, M.; Verniers, J.; Zwertvaegher, A.; Bourgeois, J. 2011. Les tombelles de l'âge du bronze en Flandre sablonneuse (nord-ouest de la Belgique): un status quaestionis. *Archaologisches Korrespondenzblatt*, 41, 491-505.

1. Zwertvaegher, A.; Werbrouck, I.; Finke, P.A.; De Reu, J.; Crombé, P.; Bats, M.; Antrop, M.; Bourgeois, J.; Court-Picon, M.; De Maeyer, P.; **De Smedt, P.**; Sergant, J.; Van Meirvenne, M.; Verniers, J.2010 On the Use of Integrated Process Models to Reconstruct Prehistoric Occupation, with Examples from Sandy Flanders, Belgium. *Geoarchaeology*, 25, 784-814.

4.2 Publications in non-ISI indexed, peer reviewed journals (A2)

8. Crombé ,P.; **De Smedt, P.**; De Reu, J.; Herremans, D.; Lombaert, L.; Linseele, V.; de Clercq, W. 2012. De vondst van een benen artefact in de Moervaart depressie te Klein-Sinaai (provincie Oost-Vlaanderen, B). Notae Praehistoricae, 32, 115–20.

7. Meylemans, E.; **De Smedt, P.**; Storme, A.; Bastiaens, J.; Deforce, K.; Desloover, D.; Van Meirvenne, M. 2011. A multi-diciplinary palaeoenvironmental survey in the western Moervaart-depression (East Flanders, B). Notae Praehistoricae, 31, 7–15.

6. Bats, M.; **De Smedt, P.**; De Reu, J.; Gelorini, V.; Zwertvaegher, A.; Antrop, M. Bourgeois, J.; De Maeyer, P.; Finke, P. A.; Van Meirvenne, M.; Verniers, J.; Crombé, P. 2011. Continued geoarchaeological research at the Moervaart palaeolake area (East Flanders, B) : field campaign. Notae Praehistoricae, 31, 201–11.

5. De Reu, J.; Bats, M.; Crombé, P.; Antrop, M.; Court-Picon, M.; De Maeyer, P.; **De Smedt, P.**; Finke, P. A.; Van Meirvenne, M.; Verniers, J.; Werbrouck, I.; Zwertvaegher, A.; Bourgeois, J. 2011. Een GIS benadering van de bronstijdgrafheuvel in Zandig-Vlaanderen : enkele voorlopige resultaten (België). Lunula (Brussel), 19, 3–8.

4. Bats, M.; **De Smedt, P.**; Werbrouck, I.; Zwertvaegher, A.; Court-Picon, M.; De Reu, J.; Serbruyns, L.; Demiddele, H.; Antrop, M.; Bourgeois, J.; De Maeyer, P.; Finke, P.A.; Van Meirvenne, M.; Verniers, J.; Crombé, P. 2011. Continued geoarchaeological research at the Moervaart palaeolake area (East Flanders, Belgium) : preliminary results. Notae Praehistoricae, 30, 55–61.

3. De Reu, J.; Bats, M.; **De Smedt, P.**; Bourgeois, J.; Antrop, M.; Court-Picon, M.; De Maeyer, P.; Finke, P.A.; Van Meirvenne, M.; Verniers, J.; Werbrouck, I.; Zwertvaegher, A.; Crombé, P. 2010. Bronze and Iron Age landscapes in Sandy Flanders (NW-Belgium) : a geoarchaeological approach. Lunula (Brussel), 18, 17–22.

2. De Reu, J.; Bats, M.; Bourgeois, J.; Antrop, M.; Court-Picon, M.; De Maeyer, P.; **De Smedt, P.**; Finke, P.A.; Van Meirvenne, M.; Verniers, J.; Werbrouck, I.; Zwertvaegher, A.; Crombé, P. 2010. Digitizing, inventorying, reviewing and analyzing the “Bronze Age barrows database” of East and West Flanders (Belgium). Lunula (Brussel), 18, 43–7.

1. Bats, M.; De Reu, J.; **De Smedt, P.**; Antrop, M.; Bourgeois, J.; Court-Picon, M.; De Maeyer, P.; Finke, P.A.; Van Meirvenne, M.; Verniers, J.; Werbrouck, I.; Zwertvaegher, A.; Crombé, P. 2009. Geoarchaeological research of the large palaeolake of the Moervaart (municipalities of Wachtebeke and Moerbeke-Waas, East Flanders, Belgium) : from Late Glacial to Early Holocene. Notae Praehistoricae, 29, 105–12.

4.3 Conference proceedings

4. **De Smedt, P.**; Bats, M.; Van Meirvenne, M. 2011. Unravelling palaeohydrology: revealing prehistoric landscapes with integrated near surface geophysics. In: *Palaeolithic Mesolithic conference, The British Museum, London (UK), 17th-18th November 2011*. 5-6.

3. **De Smedt, P.**; Van Meirvenne, M.; Simpson, D. 2011. Multi-signal EMI and geoarchaeology: evaluating integrated magnetic susceptibility measurements for archaeological prospection. In: *9th international conference on Archaeological Prospection, Izmir, Turkey, 2011-09-19*. Drahor, M.G. & Berge, M. eds. Archaeology and Art Publications. 54-57.

2. **De Smedt, P.**; Saey, T.; Lehouck, A.; Van Meirvenne, M. 2011 Continuous multi-signal EMI survey in geoarchaeological research: a 90 ha dataset. In: *2nd Global workshop on Proximal Soil Sensing, Montréal, QU, Canada, 2011-05-15*. 40-43.

1. Islam, M.M., Van Meirvenne, M., Loonstra, E., **De Smedt, P.**, Meeuws, F., Van De Vijver, E.; Saey, T. 2011. Key properties for delineating soil management zones. In: *2nd Global workshop on Proximal Soil Sensing, Montréal, QU, Canada, 2011-05-15*. 52-55.